DISSERTATION

MEMBRANE ADSORBERS AND NOVEL AFFINITY PEPTIDES FOR RECOMBINANT PROTEIN PURIFICATION

Submitted by

Justin Weaver

Department of Chemical and Biological Engineering

In partial fulfillment of the requirements

For the Degree of Doctor of Philosophy

Colorado State University

Fort Collins, Colorado

Spring 2015

Doctoral Committee:

Advisor: S. Ranil Wickramasinghe

Xianghong Qian
Jon O. Carlson
Travis S. Bailey

ABSTRACT

MEMBRANE ADSORBERS AND NOVEL AFFINITY PEPTIDES FOR RECOMBINANT PROTEIN PURIFICATION

The purification of recombinant proteins for use as pharmaceutically active ingredients represents one of the largest costs of drug development and production. Of the different classes of recombinant protein therapeutics monoclonal antibodies represent the largest percentage of protein therapeutics currently on the market with even more in clinical development. The work presented in this thesis describes the evaluation of both commercial and newly designed anion exchange and hydrophobic interaction (HIC) membrane adsorbers as well as identification of novel affinity peptides for the purification of recombinant proteins, specifically monoclonal antibodies.

Commercially available anion-exchange membrane adsorbers were evaluated for their potential to remove impurities commonly present at low concentration in recombinant protein solutions expressed in mammalian cell culture. These so-called trace impurities include virus, host cell proteins, and DNA; these impurities are of particular concern because they are highly immunogenic at very low concentrations. Ionic strength and pH were shown to be the dominant factors affecting impurity binding on quaternary amine (Q) membranes indicating these ligands interact with the impurities primarily through electrostatic interactions. It is likely impurity interactions with primary amine ligands involved not only electrostatic but hydrogen bonding interactions which stabilized impurity-ligand interactions enabling greater removal at a broader range of solution pH and ionic strength conditions. Binding of host cell proteins with a broad

range of isoelectric points was also demonstrated using the primary amine ligand as compared to the Q ligands. The effect of solution pH, ionic strength, flow rate, and the presence of competing anionic species was investigated.

In addition to commercially available anion-exchange membrane adsorbers novel anion-exchange membranes, developed by Dr. Bharat Bhut and Prof. Scott Husson at Clemson University, were evaluated for binding capacity and virus removal. Regenerated cellulose microfiltration membranes were modified with a negatively-charged quaternary amine polymer, systematically varying the polymer chain density and length. IgG and DNA binding capacity, as well as minute virus of mice removal, was evaluated as a function of polymer chain density and length. It was shown that IgG binding capacity increased with polymer chain density indicating IgG access to binding sites was not a limiting factor. Similarly, high polymer chain density and longer polymerization time (translating to longer polymer chain length) resulted in higher DNA binding and virus removal again indicating ligand accessibility was not an issue even with large solutes such as virus.

Environmentally-responsive hydrophobic interaction membranes were also developed in the Wickramasinghe lab and evaluated for protein binding capacity and recovery. Three-dimensional polymer brushes were grafted from 0.45 μm pore size regenerated cellulose membrane surfaces. The dynamic binding capacity of human IgG was greater than current commercially available hydrophobic interaction membranes with comparable recoveries.

Affinity purification using novel small peptides was also explored as an antibody purification tool. Several heptapeptide affinity ligands were identified that bound specifically to the Fc region of IgG. These peptides have similar function to *Staphylococcus Aureus* Protein A, which is used extensively as an affinity purification ligand for monoclonal antibodies in the

pharmaceutical industry. A large library of seven amino acid-long peptides was screened via M13 Phage Display for specific binding to the Fc, or constant region, of human IgG antibody. After initial identification, specificity of binding only to IgG was demonstrated through subsequent competitive ELISA assays. Though the affinity peptides were initially screened against human IgG_4 Fc, binding to a larger subset of human and non-human antibodies was shown indicating the peptides were binding to highly conserved regions on the antibodies. Because Protein A has some limitations in industrial process applications, these novel heptapeptides may provide an alternative solution for affinity purification of monoclonal antibodies.

ACKNOWLEDGEMENTS

First of all, I wish to thank my advisor Dr. S. Ranil Wickramasinghe for his support and guidance throughout these past five years. His support of my various projects as well as his extraordinary amount of patience with an admittedly hard-headed and independent student was such a determining factor enabling me to finish this work. I would also like to thank the members of my committee Dr. Matt J. Kipper, Dr. Travis S. Bailey, Dr. Jon O. Carlson, and Dr. Xianghong Qian for their patience, guidance, ad hoc hallway discussions, and encouragement.

Several individuals played crucial roles at CSU in helping me to overcome numerous obstacles and also helped me maintain a positive attitude regarding my work. Though this list is far from inclusive I would like to specifically mention the members of the Geiss lab Dr. Brian Geiss, Jordan Steel, Bejan Saeedi, Dan April, Manooch Saeedi, and Brittney Henderson. Also a big thanks to the people within the Biochemistry department, especially the Protein Expression and Purification Facility, specifically Teri McLain, Dustin Noblitt, Hataichanok (Mam) Scherman, and Mark van der Woerd.

And of course a big thanks to my friends and fellow students within the Chemical and Biological Engineering department for all the good times. There are many of you, and I couldn't have done it without you.

Last but not least I would like to thanks my family: my parents George and Kay, as well as my sister, Heather, and brother, Adam. Without their support, especially in the final months of this work, I would not have made it. I love you all!

TABLE OF CONTENTS

LIST OF TABLES

LIST OF FIGURES

Chapter 1

Introduction

1.1 Research Motivation

Recombinant proteins represent a large and growing fraction of the overall pharmaceutical products on the current world market, 15% in 2007 (Aitken et al., 2009). The price to patients for these biologically-derived products is substantially higher than conventional, chemical-based pharmaceutical agents (McNeil, 2007). The high price of biologics can be attributed to the more expensive drug discovery process and increased timeframe and costs associated with process development and commercial production (Petigara and Anderson, 2008). In 2011 monoclonal antibodies (mAbs) represented 25% of all approved biologics and are projected to remain a high proportion of approved biopharmaceutical drug products in the near future (Rader, 2011). Reducing the costs of these products such as Rituxan® (Non-Hodgkin Lymphoma), Remicade® (Rheumatoid Arthritis), Herceptin® (Breast Cancer) as well as future products will directly benefit patients through lower prices and insurance co-pays. Therefore the work presented in this thesis was focused on developing and evaluating purification technologies which have the potential to lower the cost of development and production of protein biologics, specifically monoclonal antibodies.

1.2 Monoclonal Antibody Purification

Up until the mid-2000's the main production bottleneck lay with the upstream side of biologic processes; that is, during the production of the protein itself, usually within a mechanical bioreactor (Holzer, 2011). Protein titers, in bacterial and especially mammalian expression systems, have increased dramatically during the last decade, more than 10-fold in many cases (Dinnis and James, 2005). Downstream processes, of which purification is the major part, have been identified as the current major production bottleneck for mAbs and other biologics (Antoniou et al., 2011; Holzer, 2011; Langer, 2011). Currently mAb purification processes are somewhat similar across most biotech companies with most adopting a flexible generic, or platform, process in an effort to minimize both costs and time to clinic/market (Davies, 2009; Liu et al., 2010; Shire et al., 2010; Shukla et al., 2007b).

An example mAb platform process is presented in Figure 1.1. After production in a bioreactor the mAb supernatant is clarified, or separated from all solids and cell debris, via depth filtration or continuous centrifugation. The clarified supernatant containing the mAb is then processed through several chromatography unit operations. The great majority of mAb chromatography processes begin with a Protein A affinity step because of the high purity and product concentration realized. An intermediate chromatography step follows (cation exchange, hydrophobic interaction, or other) to remove product-related impurities such as aggregates and/or truncated species. The final chromatography unit operation is the polishing step (typically anion exchange), so called because it is designed to remove harmful impurities present at much lower concentration than the mAb itself. Dedicated virus inactivation and removal steps are also included in most processes for added safety (Berthold et al., 1992; Gottschalk, 2011). Finally, a tangential flow filtration step is employed to exchange the buffer to optimize long-term product

stability and concentrate the mAb before it is filled. Several unit operations within the mAb purification process have been identified as bottlenecks including the Protein A step, and the polishing step (labeled as Anion Exchange Chromatography in Figure 1.1) (DePalma, 2012).

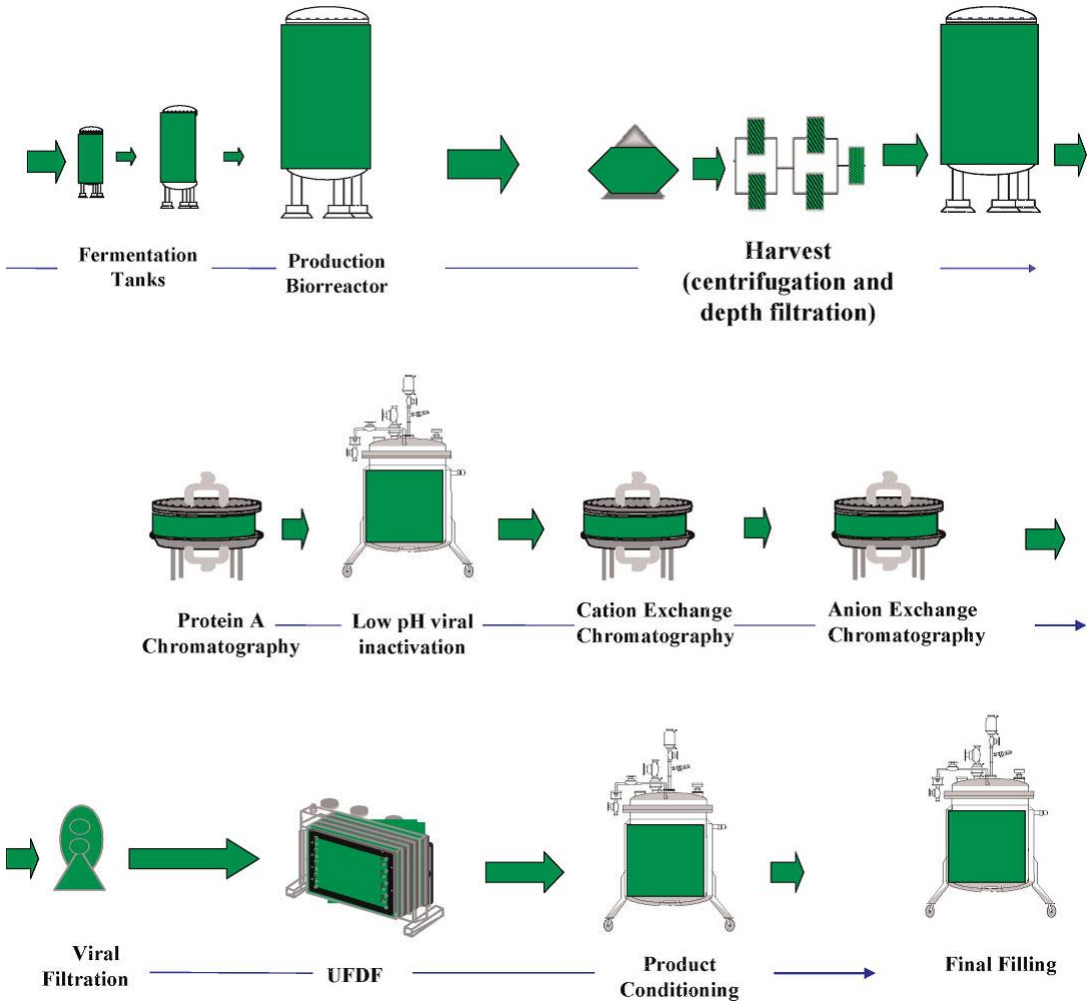

Figure 1.1: Generic "Platform" mAb purification process (Vázquez-Rey and Lang, 2011).

Protein A, a protein originally derived from *S. aureus* that specifically binds the Fc-region of various IgGs and other immunoglobulins, is used extensively as an affinity ligand for mAb purification. Typically mAb is secreted into the supernatant in the bioreactor by the production cell line, usually Chinese Hamster Ovary (CHO), NS/0 (mouse), or some other

mammalian cell line, with resulting very low purity (Chartrain and Chu, 2008). Example impurities present in the supernatant along with secreted mAb include cell byproducts (host cell proteins, lipids, DNA), possible viral contaminants, and growth media components (small molecules, growth factors, and BSA) (Necina et al., 1998). Protein A affinity chromatography is therefore an ideal first step; consistently delivering high purity through specific binding (Cromwell et al., 2006). However, there are several problems with the protein A ligand (and its derivatives) that limit the utility in commercial mAb production such as binding capacity, stability, and elution conditions (Cromwell et al., 2006; Pakiman et al., 2012; Shukla et al., 2007a). The disadvantages of Protein A and the need for an affinity alternative to protein A is discussed further in section 1.5 of this thesis.

The polishing chromatography step has also been implicated as a major mAb production bottleneck (Li et al., 2005). Very large diameter columns and column volumes which are optimized for high flow rates leads to gross underutilization of conventional packed bead columns as polishing steps. The flow rates are necessarily slow for a packed bead column polishing step when considering the residence time required to achieve sufficient impurity binding capacity. This is due to the diffusion-limited transport of impurities (host cell proteins, DNA, virus, etc.) into the pore interiors of the packed beads. The resin pores, small in diameter to maximize surface area, represent a significant mass transfer limitation for binding solutes. Transport of impurities to binding sites in the pore interiors (the vast majority of binding sites) is limited by pore diffusion from the bead surface inwards (Al-Rubeai, 2011; Curling and Gottschalk, 2007). Therefore either the flow rate must be sufficiently slow or the column must be sufficiently wide to provide a long enough residence time to allow impurity diffusion into the pores. Since slower flow rates would entail unacceptably long unit operation oversized columns

have been used leading to significant underutilization of the bed. Therefore alternatives to packed bead columns for polishing applications, such as macroporous membrane adsorbers, are gaining notoriety but require further evaluation.

1.3 Membrane Adsorbers

An alternative to adsorptive packed beads with pores large enough to permit convective transport of impurities to all binding sites would be advantageous to current and future mAb purification processes, decreasing both processing time and resources (Phillips et al., 2005; Zhou and Tressel, 2006). Membrane adsorbers fulfill this criterion with interconnected porous structures with average pore diameters much larger than packed bead resins. Membrane adsorbers created for the purpose of protein purification have pore sizes of 0.22 μm or larger (Fraud et al., 2009; Roper and Lightfoot, 1995; Varadaraju et al., 2011; Weaver et al., 2013). The larger pore size is responsible for several advantages of the membrane adsorbers when compared to porous bead resins. The membrane acts as a support structure permitting the binding species to adsorb onto ligands attached to the inner pore surface.

The large pore diameter allows convective transport of all impurity species to all binding ligands on both the external and internal pore surfaces. Ideally binding is limited by binding kinetics only. Therefore binding capacity is theoretically independent of flow rate in convectively-driven binding processes like within membrane adsorbers, at least at flow rates useful to protein purification. Figure 1.2 provides a visual illustration of this point showing electron micrographs of both a porous bead and membrane adsorber with icons showing transport of impurities to binding sites (Curling and Gottschalk, 2007).

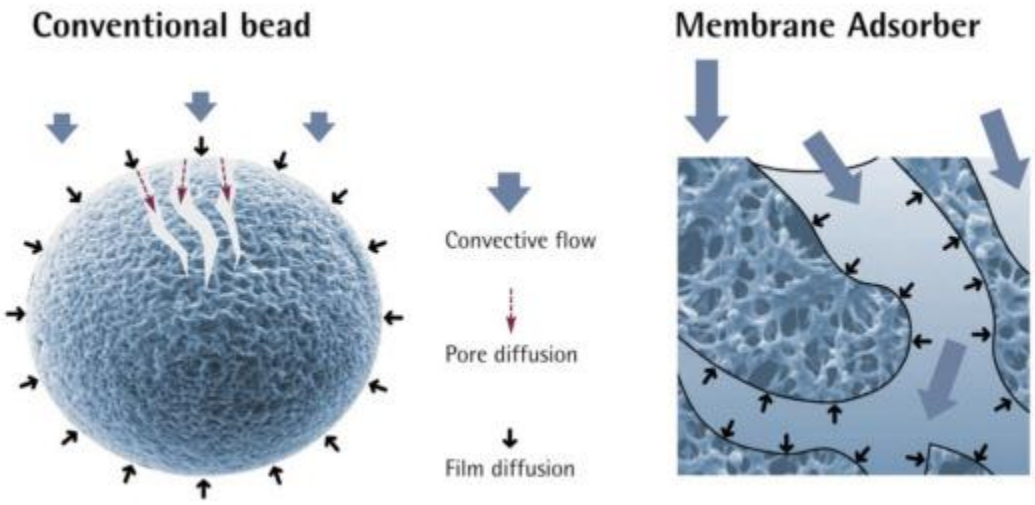

Figure 1.2: Comparison of conventional porous bead and macroporous membrane adsorber binding mechanisms (Curling and Gottschalk, 2007).

Back pressure is another parameter in which membrane adsorbers provide a clear advantage over porous beads during mAb purification. For a given flow rate the back pressure is much lower through a macroporous membrane compared to a packed bead column due to the larger pores and open structure. Thus faster flow rates can be utilized without, due to convective impurity transport to all binding sites, any loss in binding capacity. This translates to decreased processing time during manufacturing which results in substantial cost savings (Zhou et al., 2006).

Membrane adsorbers are also commercially available as pre-sterilized, ready–to-go units which don't require any pre-use cleaning. This allows for much lower buffer usage (and WFI usage), also a cost saving measure (Allen, 2008; Fraud et al., 2010). Cleaning validation is also not required with pre-sterilized membranes leading to additional cost savings. It is however still not clear if economic benefits may be realized using membrane adsorbers as pre-sterilized,

single-use units or using a single membrane for many cycles as has been traditionally done with packed bead columns (Warner and Nochumson, 2003).

1.3.1 Anion-Exchange Membrane Adsorbers

Though membrane adsorbers have been developed with different binding mechanisms such as hydrophobic interaction, affinity, or cation-exchange, anion-exchange packed bead columns and membranes are used in the majority of mAb processes for polishing applications (Ghosh and Wang, 2006; Giovannoni et al., 2009; Kuczewski et al., 2010; Teeters et al., 2002). Anion-exchange is appropriate given most trace impurities are very or somewhat negatively-charged at neutral pH. Most model viruses approved by the FDA for removal studies are negatively charged (Porter, 1980; Strauss et al., 2010). Host Cell Proteins (HCP), no matter the expression system, are a broad population of negative- and positively-charged impurities. DNA of course is negatively-charged all along its backbone due to the phosphate groups. Other trace impurities such as leached protein A are also negatively charged at neutral pH increasing the utility of anion-exchange as a polishing mechanism (Liu et al., 2010). Therefore the membrane adsorber work presented in this thesis focuses exclusively on anion-exchange membranes.

1.3.2 Hydrophobic Interaction Chromatography (HIC) Membrane Adsorbers

Among the different modes of chromatography Hydrophobic Interaction Chromatography (HIC) may be one of the most useful while being the most under-used for mAb purification. HIC has been shown to be an effective product aggregate removal step which is a major focus of industrial mAb purification processes (Ebert and Fischer-Frühholz, 2011; Lu et al., 2009; Yoo and Ghosh, 2012). HIC has also been shown to be a good viral clearance process operation; another crucial aspect of biologics and mAb purification (Kelley et al., 2008).

However, traditional HIC ligands suffer from two limitations compared with other methods of chromatography: lower binding capacity and lower protein recovery (Chen et al., 2008; Müller et al., 2011).

The driving force for binding to hydrophobic media is typically high salt concentration (Frau et al., 2009) and many proteins "salt out" of solution below the optimal binding salt concentration (Gagnon et al., 1997). This leads to binding capacities much lower than the > 50 g/L capacities typically realized over ion-exchange media. The other limitation lies in desorption of bound protein from the hydrophobic media. Elution of proteins from HIC media is accomplished either through decreased salt concentration and/or introduction of chemicals, such as organics or chaotropes, which disrupt hydrophobic interactions (Tsumoto et al., 2007). Organics and chaotropes, such as Urea or Guanidine HCl, have detrimental effects on protein stability and folding and are therefore unsuited for use in industrial protein HIC processing. Many proteins, monoclonal antibodies included, do not fully desorb from hydrophobic media with no salt alone, leading to lower recovery (Chen et al., 2008).

One method which may increase desorption of protein using low or no salt may be the use of hydrophobic ligands that become more hydrophilic in lower salt solutions. Chapter 6 of this thesis discusses work with polymerized N-vinylcaprolactam, an environmentally responsive polymer that is hydrophobic in high ionic strength solutions and hydrophilic in low ionic strength solutions.

1.4 Viral Quantification

Viral clearance during biologic purification, of which anion-exchange polishing is a critical step, must be demonstrated to ensure safety of the final product. Therefore an assay for

viral quantification is required. The traditional assay most commonly found in academic and industrial literature is the cell-based plaque assay. The cell line will necessarily be different for each virus type due to most viruses having a very specific cellular tropism (Itah et al., 2004). For example the virus used during the work in this thesis, Minute Virus of Mice prototype strain, forms lytic plaques on mouse fibroblast cell lines such as A9 only (Ball-Goodrich et al., 1991). However, cell-based plaque assays suffer from several limitations: assay time (up to six days), assay throughput, and subjective result interpretation (Edelman and Barletta, 2003). Several serial dilutions per sample are required to ensure a well with a countable number of plaques is obtained. The cell culture must be at a certain confluence as well as within a given number of passages in order to obtain reliable and reproducible virus titer data. Therefore a more rapid assay was preferred for the work described herein; the assay chosen was quantitative polymerase chain reaction (QPCR).

QPCR is a more complex version of standard PCR; template DNA is amplified exponentially over successive cycles during which a reporter dye or probe binds to double-stranded DNA as it is created. The fluorescence signal, which is below detectability until a sufficient amount of DNA is generated, gives a real-time picture of DNA content. Known standards are run on each plate as well generating a standard curve, which unknown samples are compared against. The number of cycles required for the fluorescence signal of each standard and sample to reach a certain threshold value, normally in early log phase, is the output of the assay. By plotting the threshold cycle number of the unknown samples on the standard curve, the original concentration of DNA present in the samples is obtained. As all viral particles contain either DNA or RNA, QPCR is a reliable assay for viral quantification.

Because QPCR may be performed in 96-well format many samples can be assayed in a short amount of time, generally 3 hours or less. Dilution series, necessary for each sample tested by plaque assay, are generally not needed during QPCR due to the very large linear range (6-7 log copies or more) obtainable (Logan et al., 2009). Cost of assaying viral titer by QPCR is much lower per sample than cell-based plaque assays due to the lack of expensive cell lines, media, and incubation equipment necessary. Though the fluorescent reagents/probes can be quite expensive, hundreds of unknown samples can be assayed per vial of fluorescent reagent. Therefore for the reasons of throughput, large linear range, and cost, QPCR was used as the viral quantification assay for the work completed in this thesis.

1.5 Protein A

Protein A affinity chromatography, and specifically the protein A ligand itself, was the focus of additional research in this thesis. Protein A is a very effective capture step for mAb purification due to its high selectivity, enabling high purity and relatively high concentration in a single affinity chromatographic step. However, protein A does have a few characteristics that limits its utility during mAb purification. Native and recombinant protein A is not stable under alkaline conditions, leaving the ideal cleaning/sanitization solution, 1M NaOH, off the table for protein A cleaning (Jones and Smith, 2004). Binding capacity over protein A columns or protein A membrane adsorbers is also limited by the kinetics of mAb-protein A binding as well as the density of protein A ligand obtainable (Saha et al., 2003; Sheth, 2009).

The production bottleneck with protein A chromatography using packed bead columns is similar to that with the polishing step. Increasing mAb titers create the need for ever larger protein A columns and eventually expensive new hardware such as pumps and columns.

Columns can only be built so large in diameter before their footprint within existing plants becomes prohibitive (Palma, 2005). Increasing the column height is impractical since pressure increases with bed height and higher pressure would either compress the resin or damage the pumps (Thillaivinayagalingam and Keshavarz-Moore, 2007). Therefore as bioreactor titers increase the only method to process the additional material is to increase the number of chromatography cycles which increases both total processing time and resources thereby increasing the total cost.

In the work presented in this thesis small peptides (7 amino acids) were explored as an alternative to protein A (42 kDa) for several reasons. As mentioned above protein A stability is one of the major causes of the protein A chromatography bottleneck and high resin cost. Because of this instability, particularly during resin cleaning and sanitization, the binding capacity tends to decrease over a number of cycles further lowering the product throughput. Small peptides may have greater stability under sanitization conditions, particularly alkaline conditions, because of their lack of easily disrupted secondary and tertiary structures.

Small peptides may also have an advantage over larger ligands such as protein A due to the much higher ligand density attainable on the pore surface. On similar polymer porous beads as the protein A resin MabSelect®, mAb binding capacities on the cation-exchange resin SPXL have reached over 100 mg/mL (Liu et al., 2011); though MabSelect binding capacity is in the 30 – 50 mg/mL range with typical 2 – 3 min column residence times (Ljunglöf et al., 2011). Therefore it is possible to bind mAb to a higher capacity than currently realized with protein A resins. Small peptides may be "grown" from the pore surface via surface-initiated polymerization. Much higher peptide densities compared to protein A may be realized via this surface polymerization method, similar to other chemical ligands (Bhut et al., 2008).

1.6 Phage Display

The method used in this research to identify heptapeptides with binding affinity for the Fc region of antibodies was M13 phage display. Phage display is a powerful method of exploring a large library of peptides/proteins and finding the needle in the haystack, those few proteins with affinity for a given target (Carmen and Jermutus, 2002). This method provides a physical link between the phenotype (the displayed protein on the viral surface) and the genotype within the virus. Viral-based display also provides a method for easily amplifying those proteins with affinity for re-panning during the next round of binding. Therefore successive rounds of binding (panning) result in more enriched populations of virus with binding proteins on their surface. Because there is a link between phenotype and genotype the peptides/proteins can be easily identified by DNA sequencing. Additional background information regarding phage display and its uses may be found in Chapter 6 of this thesis.

1.7 Research Objectives

The overall goal of this thesis was to explore new technologies for protein purification, specifically monoclonal antibody purification, to alleviate known production bottlenecks within the biotechnology industry. Alleviating these bottlenecks will lower the costs of development and production of mAbs translating to lower prices for patients. Specifically two research areas were chosen to explore: anion-exchange membrane adsorbers for polishing applications and identification of small peptides with function similar to Protein A as possible affinity ligands.

Anion-exchange media (resins and membranes) have been shown to successfully bind trace impurities, but are utilized only under very advantageous conditions such as low conductivity and high pH; conditions under which many protein drug products may be unstable

or bind to the anion-exchange media. Little is present in current literature regarding the mechanisms of trace impurity binding, nor how membrane, ligand, or solution properties influence impurity binding.

Therefore a general hypothesis explored in this thesis was how trace impurity removal from protein drug solutions using anion-exchange membrane adsorbers is influenced by both membrane properties and solution properties. Specifically, it was hypothesized that the solution space under which significant binding of impurities occurs is strongly influenced by the characteristics of the anion-exchange ligand; properties such as pore size, ligand type, and ligand density may affect binding along with solution properties such as pH, conductivity, flow rate, and competitive anion concentration.

A separate hypothesis related to monoclonal antibody purification was also explored in this thesis. The hypothesis was that short peptides could be identified via phage display with comparable antibody-binding properties to the protein A ligand used in most industrial mAb purification processes. The advantages of small peptides over protein A as an affinity ligand for large-scale monoclonal antibody purification are discussed in sections 1.5 and 6.2 of this thesis.

To evaluate the above hypotheses, several specific research aims were explored during the work completed for this thesis. Those research aims are presented below.

1) Evaluate Minute Virus of Mice removal for three different anion-exchange membrane adsorbers; variables evaluated were pH, ionic strength, flow rate, and competing anionic buffer species. Understand the dominant binding mechanisms of virus to the different ligands and the contribution of ligand densities present on the three anion-exchange membrane adsorbers.

2) Understand the binding of Minute Virus of Mice, CHO Host Cell Proteins, and DNA in the presence and absence of monoclonal antibody.
3) Investigate how polymer ligand density and length affect protein, DNA, and virus binding on novel strong anion-exchange membrane adsorbers.
4) Investigate the adsorption and desorption properties of membranes modified with N-vinylcaprolactam with a goal of high binding capacity and high recoveries.
5) Identify small peptides using Phage Display that have similar binding specificity and affinity for the constant region of various Immunoglobulins.

1.8 Thesis Organization

Chapter 2: "Anion Exchange Membrane Adsorbers for Flow-through Polishing Steps: Part I. Clearance of Minute Virus of Mice"

In this chapter Minute Virus of Mice binding and removal by anion-exchange membrane adsorbers is investigated. Three commercially available membranes with different membrane and ligand properties were evaluated for virus removal: Sartobind Q®, Mustang Q®, and ChromaSorb®. Solution conditions including pH, NaCl concentration, and competitive anionic species as well as flow rate were investigated. These variables, as well as ligand density and composition, were systematically evaluated for minute virus of mice binding. A quantitative polymerase chain reaction (QPCR) method was developed for quantification of MVM. The results show under which conditions virus will bind to the three different membranes.

Chapter 3: "Anion Exchange Membrane Adsorbers for Flow-through Polishing Steps: Part II. Virus, Host Cell Protein, DNA Clearance, and Antibody Recovery"

Chapter 3 builds on the work from chapter 2 in further investigating trace impurity removal via anion-exchange membrane adsorbers. In addition to removal of virus, host cell protein and DNA removal was also investigated, thus presenting a much more complex mixture of impurities. Host cell proteins presented an especially challenging case for binding as the protein population was diverse, both in terms of size and charge. This work showed that viral binding is affected by the competitive binding of host cell proteins and DNA, and is affected by the presence of monoclonal antibody. The advantage of using a ligand capable of binding via multiple mechanisms was clearly demonstrated. Membrane performance when relying purely on electrostatic ligands is shown to be compromised at both high NaCl concentration and low pH.

Chapter 4: "The Role of Polymer Nanolayer Architecture on the Separation Performance of Anion-Exchange Membrane Adsorbers: I. Protein Separations"

The work in this chapter involves construction of novel strong anion-exchange ligands with higher binding capacity than currently reported in literature. Regenerated cellulose membranes with Q ligands of differing lengths and surface density were constructed by our colleagues at Clemson University. BSA and IgG were used to evaluate the binding capacity as a function of ligand chain length and density. Binding capacities greater than 130 mg protein / mL membrane were achieved. This work suggests tailoring the 3-D architecture of the ligands covering the internal and external pore surfaces significantly increases the binding capacity of proteins; binding capacity was found to be independent of flow rate.

Chapter 5: "The Role of Polymer Nanolayer Architecture on the Separation Performance of Anion-Exchange Membrane Adsorbers: Part II. DNA and Virus Separations"

Chapter 5 presents work furthering the investigation from chapter 4 in which additional impurity binding was evaluated on the novel strong anion-exchange membranes. Ligand chain length and ligand spacing were again investigated this time for DNA and minute virus of mice removal. The goal was different than chapters 2 and 3 in that instead of evaluating impurity binding over a large range of buffer conditions, ligand length and density was optimized for maximum impurity binding capacity. Increasing binding capacity for DNA was observed up to a degree of ligand polymer grafting of 20 wt% indicating steric or electrostatic hindrance between binding ligands was not encountered. Similar results were obtained for minute virus of mice, which has a larger (~20nm) diameter than either mAbs or DNA again suggesting crowding was not an issue during binding. Binding capacities obtained for DNA were greater than current commercial anion-exchange membrane adsorbers, additionally virus removal was equivalent to current technology.

Chapter 6: "Responsive Membranes for Hydrophobic Interaction Chromatography"

Improved hydrophobic interaction membrane adsorbers are evaluated in chapter 6. An environmentally responsive polymer, N-vinylcaprolactam (N-VCL), was grafted from the pore surface of regenerated cellulose membranes using ATRP. In the presence of high ionic strength solution N-VCL dehydrates and adopts a more hydrophobic conformation while low ionic strength causes N-VCL to hydrate and adopt a more hydrophilic confirmation at room temperature. As shown in this chapter, this improves the recovery efficiency of BSA and

monoclonal antibodies. IgG binding capacities of 21 g/L were demonstrated which is significantly higher than current commercially-available hydrophobic membrane adsorbers.

Chapter 7: "Identification and Characterization of Novel Fc-binding Heptapeptides via Phage Display and ELISA"

In chapter 7 small heptapeptides were investigated for specific binding to the Fc region of different immunoglobulins; an interaction very similar to that of protein A. A large library consisting of billions of heptapeptides was searched for those exhibiting antibody binding behavior using M13 phage display. Those peptides showing antibody binding behavior were further screened for specific binding under cell culture conditions and with potentially competitive proteins present using an ELISA developed for this purpose. Seven heptapeptides showing specific binding and affinity at least with micromolar binding affinity or below were identified and characterized.

Chapter 8: "Conclusions and Future Work"

This short chapter presents the conclusions of this thesis and suggested future work.

References

Aitken, M., Berndt, ER., Cutler, DM. 2009. Prescription Drug Spending Trends In The United States: Looking Beyond The Turning Point. *Health Affairs.* 28(1): 151 - 160.

Al-Rubeai, M., editor. 2011. Antibody Expression and Production: Springer.

Allen, L. 2008. Use of Membrane Adsorbers for Impurity Reduction. Second EUFEPS and EAPB Workshop on Monoclonal Antibodies. Heidelberg, Germany.

Antoniou, C., Cox, M., Ostendorp, R., Ottens, M., Shane, E., Zydney, A. 2011. Overcoming Downstream Bottlenecks. *Genet. Eng. Biotechn. N.* 31(18)

Ball-Goodrich, LJ., Moir, RD., Tattersall P. 1991. Parvoviral target cell specificity: acquisition of fibrotropism by a mutant of the lymphotropic strain of minute virus of mice involves multiple amino acid substitutions within the capsid. *Virology.* 184(1): 175 - 186.

Berthold, W., Walter, J., Werz, W. 1992. Experimental approaches to guarantee minimal risk of potential virus in purified monoclonal antibodies. *Cytotechnology.* 9(1 - 3): 189 - 201.

Bhut, BV., Wickramasinghe, SR., Husson, SM. 2008. Preparation of high-capacity, weak anion-exchange membranes for protein separations using surface-initiated atom transfer radical polymerization. *J. Membr. Sci.* 325(1): 176 - 183.

Carmen, S., Jermutus, L. 2002. Concepts in antibody phage display. *Brief Funct. Genomic Proteomic.* 1(2): 189 - 203.

Chartrain, M., Chu, L. 2008. Development and production of commercial therapeutic monoclonal antibodies in Mammalian cell expression systems: an overview of the current upstream technologies. *Curr Pharm Biotechnol.* 9(6): 447 - 467.

Chen, J., Tetrault, J., Ley, A. 2008. Comparison of standard and new generation hydrophobic interaction chromatography resins in the monoclonal antibody purification process. *J. Chromatogr A.* 1177(2): 272 - 281.

Cromwell, MEM., Hilario, E., Jacobson F. 2006. Protein Aggregation and Bioprocessing. *AAPS Journal.* 8(3): 572 - 579.

Curling, J., Gottschalk, U. 2007. Process Chromatography: Five Decades of Innovation. *Biopharm Int.* 20(10).

Davies, J. 2009. A Purification Platform for the Production of MAbs from Fermenters with Titers of 5 g/L and Beyond. *Biopharm Int. Supp.*

DePalma, A. 2012. Downstream Bottlenecks More than Just Perception. *Genet. Eng. Biotechn. N.* 32(11).

Dinnis, D., James, D. 2005. Engineering Mammalian Cell Factories for Improved Recombinant Monoclonal Antibody Production: Lessons from Nature? *Biotechnol Bioeng.* 91: 180 - 189.

Ebert, S., Fischer-Frühholz, S. 2011. Efficient Aggregate Removal from Impure Pharmaceutical Active Antibodies *Bioprocess Int.* 9(2): 36 - 42.

Edelman, DC., Barletta, J. 2003. Real-time PCR provides improved detection and titer determination of bacteriophage. *BioTechniques.* 35: 368 - 375.

Frau, N., Kuczewski, M., Zarbis-Papastoitsis, G., Hirai, M. 2009. Hydrophobic Membrane Adsorbers for Large-Scale Downstream Processing. *Biopharm Int.* Supplements

Fraud, N., Faber, R., Kiss, C., Demmer, W., Hoerl, H-H., Fischer-Fruehholz, S. 2009. Hydrophobic-Interaction Membrane Chromatography for Large-Scale Purification of Biopharmaceuticals. *Bioprocess Int.* June Supplement: 30 - 35.

Fraud, N., Lim, J., Sinclair, A., Gottschalk, U. 2010. Technical and Economic Benefits of Membrane Chromatography During Polishing Steps. *Biopharm Int.* 23(8).

Gagnon, P., Mayes, T., Danielsson, A. 1997. An adaptation of hydrophobic interaction chromatography for estimation of protein solubility optima. *J. Pharm. Biomed Anal.* 16(4): 587 - 592.

Ghosh, R., Wang, L. 2006. Purification of humanized monoclonal antibody by hydrophobic interaction membrane chromatography. *J. Chromatogr A.* 1107(1 - 2): 104 - 109.

Giovannoni, L., Ventani, M., Gottschalk, U. 2009. Antibody Purification using Membrane Adsorbers. *BioPharm Int. Supp.*

Gottschalk, U. editor. 2011. Process Scale Purification of Antibodies: Wiley.

Holzer, M. 2011. Technologies for Downstream Processing. *Biopharm Int.* 24(9):48 - 53.

Itah, R., Tal, J., Davis, C. 2004. Host cell specificity of minute virus of mice in the developing mouse embryo. *J Virol.* 78(17): 9474 - 9486.

Jones, SCB., Smith, MP. 2004. Evaluation of an alkali stable Protein A matrix versus Protein A Sepharose Fast Flow and considerations on process scale-up to 20,000L. 3rd International Symposium on Downstream Processing of Genetically Engineered Antibodies and Related Molecules. Nice, France.

Kelley, BD., Jakubik, J., Vicik, S. 2008. Viral clearance studies on new and used chromatography resins: critical review of a large dataset. *Biologicals.* 36(2): 88 - 98.

Kuczewski, M., Fraud, N., Faber, R., Zarbis-Papastoitsis, G. 2010. Development of a polishing step using a hydrophobic interaction membrane adsorber with a PER.C6-derived recombinant antibody. *Biotechnol. Bioeng.* 105(2): 296 - 305.

Langer, ES. 2011. Alleviating Downstream Process Bottlenecks. *Genet. Eng. Biotechn. N.* 31 (13).

Li, F., Zhou, JX., Yang, X., Tressel, T., Lee, B. 2005. Current Therapeutic Antibody Production and Process Optimization. *J. Bioprocess.* 4(5): 1 - 8.

Liu, H., McCooey, B., Duarte, T., Myers, D., Hudson, T., Amanullah, A., van Reis, R., Kelley, B. 2011. Exploration of overloaded cation exchange chromatography for monoclonal antibody purification. *J. Chromatogr A.* 1218(39): 6943 - 6952.

Liu, HF., Ma, J., Winter, C., Bayer, R. 2010. Recovery and purification process development for monoclonal antibody production. *MAbs.* 2(5): 480 - 499.

Ljunglöf, A., Johansson, HJ., Joseph, J. 2011. Improved Capture with Better Productivity in MAb Bioprocessing. *Bioprocess Int.* 9(7): 66 - 67.

Logan, JMJ., Edwards, KJ., Saunders, NA., editors. 2009. Real-Time PCR: Current Technology and Applications: Caister Academic Press.

Lu, Y., Williamson, B., Gillespie, R. 2009. Recent advancement in application of hydrophobic interaction chromatography for aggregate removal in industrial purification process. *Curr. Pharm. Biotechnol.* 10(4): 427 - 433.

McNeil, C. 2007. Sticker Shock Sharpens Focus on Biologics. *J. Natl. Cancer Inst.* 99(12): 910 - 914.

Müller, E., Schröder, T., Sprauer, A. 2011. Modulation of binding capacity and selectivity in hydrophobic interaction chromatography using various electrolytes and electrolyte mixtures. 7th HIC/RPC Bioseparation Conference. Estoril, PT.

Necina, R., Amatschek, K., Jungbauer, A. 1998. Capture of human monoclonal antibodies from cell culture supernatant by ion exchange media exhibiting high charge density. *Biotechnol. Bioeng.* 60(6): 689 - 698.

Pakiman, N., Isa, NH., Hassan, MAA., Walter, JK., Abdullah, N. 2012. Comparison of Binding Capacity and Affinity of Monoclonal Antibody towards Different Affinity Resins using High-throughput Chromatography Method. *J. Appl. Sci.* 12: 1136 - 1141.

Palma, AD. 2005 Cost-Driven Chromatography. Pharmaceutical Manufacturing Magazine.

Petigara, T., Anderson, G. 2008. Strategies to Reduce the High Cost of Biologics. *Health Policy Monitor*. 12.

Phillips, M., Cormier, J., Ferrence, J., Dowd, C., Kiss, R., Lutz, H., Carter, J. 2005. Performance of a membrane adsorber for trace impurity removal in biotechnology manufacturing. *J. Chromatogr A.* 1078(1-2): 74-82.

Porter, PS. 1980. A review of virus and protein sorption by ion exchange resins. *Environ. Int.* 3 (4): 311 - 319.

Rader, RA. 2011. FDA Biopharmaceutical Product Approvals and Trends: 2011 http://www.biopharma.com/approvals_2011.html

Roper, DK., Lightfoot, EN. 1995. Separation of biomolecules using adsorptivemembranes. *J. Chromatogr A.* 702(1 - 2): 3 - 26.

Saha, K., Bender, F., Gizeli, E. 2003. Comparative Study of IgG Binding to Proteins G and A: Nonequilibrium Kinetic and Binding Constant Determination with the Acoustic Waveguide Device. *J. Anal. Chem.* 75(4): 835 - 842.

Sheth, B. 2009. Characterisation of chromatography adsorbents for antibody bioprocessing: University College of London.

Shire, SJ., Gombotz, W., Bechtold-Peters, K., Andya, J. editors. 2010. Current Trends in Monoclonal Antibody Development and Manufacturing Springer.

Shukla, A., Gupta, P., Han, X. 2007a. Protein aggregation kinetics during Protein A chromatography. Case study for an Fc fusion protein. *J. Chromatogr A.* 1171(1 - 2): 22 - 28.

Shukla, A., Hubbard, B., Tressel, T., Guhan, S., Low, D. 2007b. Downstream processing of monoclonal antibodies--application of platform approaches. *J. Chromatogr B Analyt. Technol. Biomed. Life Sci.* 848(1): 28 - 39.

Strauss, D., Cano, T., Cai, N., Delucchi, H., Plancarte, M., Coleman, D., Blank, G., Chen, Q., Yang, B. 2010. Strategies for developing design spaces for viral clearance by anion exchange chromatography during monoclonal antibody production. *Biotechnol. Prog.* 26(3): 750 - 755.

Teeters, MA., Root, TW., Lightfoot, EN. 2002. Performance and scale-up of adsorptive membrane chromatography. *J. Chromatogr A.* 944(1-2): 129-139.

Thillaivinayagalingam, P., Keshavarz-Moore, E. 2007. Biopharmaceutical Purification Strategies. *Genet. Eng. Biotechn. N.* 27(11).

Tsumoto, K., Ejima, D., Nagase, K., Arakawa, T. 2007. Arginine improves protein elution in hydrophobic interaction chromatography. The cases of human interleukin-6 and activin-A. *J. Chromatogr A.* 1154(1 - 2): 81 - 86.

Varadaraju, H., Schneiderman, S., Zhang, L., Fong, H., Menkhaus, T. 2011. Process and economic evaluation for monoclonal antibody purification using a membrane-only process. *Biotechnol. Prog.* 27(5): 1297 - 1305.

Vázquez-Rey, M., Lang, D. 2011. Aggregates in Monoclonal Antibody Manufacturing Processes. *Biotechnol. Bioeng.* 108(7): 1494 - 1508.

Warner, TN., Nochumson, S. 2003. Rethinking the Economics of Chromatography New Technologies and Hidden Costs. *Biopharm Int.* January New Technology. 58 - 60.

Weaver, J., Husson, SM., Murphy, L., Wickramasinghe, SR. 2013. Anion exchange membrane adsorbers for flow-through polishing steps: Part I. clearance of minute virus of mice. *Biotechnol. Bioeng.* 110(2): 491 - 499.

Yoo, SM., Ghosh, R. 2012. Simultaneous removal of leached protein-A and aggregates from monoclonal antibody using hydrophobic interaction membrane chromatography. *J. Membr. Sci.* 390 - 391: (263 - 269).

Zhou, JX., Tressel, T. 2006. Basic concepts in Q membrane chromatography for large-scale antibody production. *Biotechnol. Prog.* 22(2): 341-349.

Zhou, JX., Tressel, T., Gottschalk, U., Solamo, F., Pastor, A., Dermawan, S., Hong, T., Reif, O., Mora, J., Hutchison, F., and others. 2006. New Q membrane scale-down model for process-scale antibody purification. *J. Chromatogr A* 1134 (1-2):66-73.

Chapter 2

Anion Exchange Membrane Adsorbers for Flow-through Polishing Steps: Part I. Clearance of Minute Virus of Mice[1]

2.1 Summary

Membrane adsorbers may be a viable alternative to the packed-bed chromatography for clearance of virus, host cell proteins, DNA, and other trace impurities. However, incorporation of membrane adsorbers into manufacturing processes has been slow due to the significant cost associated with obtaining regulatory approval for changes to a manufacturing process. This study has investigated clearance of Minute Virus of Mice (MVM), an 18 – 22 nm parvovirus recognized by the FDA as a model viral impurity. Virus clearance was obtained using three commercially available anion exchange membrane adsorbers: Sartobind Q®, Mustang Q®, and ChromaSorb®. Unlike earlier studies that have focused on a single or few operating conditions, the aim here was to determine the level of virus clearance under a range of operating conditions that could be encountered in industry. The effects of varying pH, NaCl concentration, flow rate, and other competing anionic species present in the feed were determined. The removal capacity of the Sartobind Q and Mustang Q products, which contain quaternary ammonium based ligands, is sensitive to feed conductivity and pH. At conductivities above about 20 mS/cm, a significant decrease in capacity is observed. The capacity of the ChromaSorb product, which contains

[1]Weaver, J., Husson, SM., Murphy, L., Wickramasinghe, SR., 2013. Anion Exchange Membrane Adsorbers for Flow-through Polishing Steps: Part I. Clearance of Minute Virus of Mice, *Biotechnol Bioeng.* 110(2): 491 – 499

primary amine based ligands, is much less affected by ionic strength. However the capacity for binding MVM is significantly reduced in the presence of phosphate ions. These differences may be explained in terms of secondary hydrogen bonding interactions that could occur with primary amine based ligands.

2.2 Introduction

Biopharmaceuticals, and in particular monoclonal antibodies (mAbs), represent an increasingly large fraction of the overall pharmaceutical market. Since downstream purification costs can account for up to 80% of the manufacturing cost (Gottschalk, 2005), there is a strong demand for new technologies that reduce the overall manufacturing cost. Here we focus on the chromatographic polishing steps in the production of mAbs as these steps have become a major production bottleneck (Langer, 2009). The impurities and contaminants to be removed during these processing steps are orders of magnitude lower in concentration than the mAb.

Anion-exchange chromatography generally uses packed columns with porous chromatographic beads (Riordan et al., 2009a). However, packed-bed chromatography suffers from a number of disadvantages: the pressure drop across the bed is usually high and may increase during operation due to media deformation or blockage; pore diffusion is slow and often leads to degradation of the protein product, and scale up of packed beds is difficult. In addition, packed beds have been shown to display a very low dynamic capacity for virus particles at common process flow rates of 150 – 450 cm/hr, where binding is restricted to the surface of resin particles, as slow pore diffusion prevents the virus particles from entering the resin pores (Ghosh, 2002; Yao and Lenhoff, 2006; Wickramasinghe et al. 2006). Thus, most of the binding sites in the resin pores are not used, leading to underutilized beds (Han et al. 2005).

Membrane chromatography or membrane adsorption, where a macroporous membrane is used as a support material and the ligands are bound to the pore surface, was first described by Brandt et al. (1988). Membrane adsorbers can be run at much lower pressure drops and are easy to scale up. Importantly, since the feed is pumped through the membrane pores, transport of the solute to the binding sites occurs mainly by fast convective flow. Consequently, the dynamic capacity is independent of flow rate over a much larger range of flow rates compared to packed beds (Curling and Gottschalk, 2007, Specht et al., 2004).

Nevertheless one of the major perceived disadvantages of membrane adsorbers is that the ligand density is generally higher for porous resin particles compared to macroporous membranes. Consequently for smaller protein species that are not excluded from the internal resin pores, the dynamic capacity is higher for packed beds than for membranes (Curling and Gottschalk, 2007). Membrane adsorbers are therefore ideally suited for removal of large molecules and virus particles present at low concentrations (Zhou and Tressel, 2006).

Presently, membrane adsorbers are used in the biopharmaceutical industry almost exclusively in 'flow-through' polishing steps (Boi, 2007, Zhou et al. 2008a). Anion-exchange membranes are used to bind impurities such as viruses, host cell proteins, and DNA while allowing the mAb to flow through. The feed pH is usually greater than 7.0 where the impurities to be removed are negatively charged but the generally higher pI mAb is positively charged. Riordan et al. (2009a, 2009b) indicate that the ionic strength of the feed stream is usually low, as high ionic strength can disrupt electrostatic interactions and reduce the removal of contaminants.

Here we focus on clearance of Minute Virus of Mice (MVM) an 18-22 nm parvovirus by three commercially available anion-exchange membranes: Sartobind Q® (Sartorius AG, Göttingen, Germany), Mustang Q® (Pall Corporation, Port Washington, NY, USA) and

ChromaSorb® (Millipore Corporation, Billerica, MA, USA). Commercial membrane adsorbers have pore sizes ranging from 0.5 – 3 um. Since the feed is pumped through the membrane pores, the kinetics of binding is the rate-limiting step (Teeters et al., 2002). Thus, compared to resin particles, much higher flow rates may be used. This results in the ability to process a much larger load volume or to decrease the process time required for a standard load volume; both cases realize an economic benefit. Current commercially available anion exchange membrane adsorbers are sold as pre-sterilized, disposable devices, negating the need for costly cleaning validation. Zhou et al. (2008a) have demonstrated that an economic benefit can be realized at a product load of 2 kg/m^2 membrane surface area, with cost savings coming predominantly from decreased buffer/WFI usage.

A few investigators have reported the use of membrane adsorbers for removal of low concentration high molecular weight impurities and virus particles during the polishing steps in the manufacture of mAbs (Knudsen et al. 2001; Zhou et al. 2006; Zhou et al. 2008b; van Reis and Zydney, 2001). Brown et al. (2010) have investigated the use of membrane absorbers as a prefiltration step prior to virus filtration. Zhou and Tressel (2006) used a Sartobind Q scale-down model (Sartobind Q 125) to obtain greater than 6.03 LRV at pH 7.2, conductivity, 4.0 mS/cm, at a monoclonal antibody capacity of 3000 g/m^2. However, for many industrial manufacturing processes the feed stream requires a large WFI dilution and/or pH adjustment to reach these conditions, which can be both costly and time consuming. Furthermore, operating at low salt concentration may increase the likelihood of aggregation of the mAb (Ahrer et al. 2006).

Frequently, ligands containing quaternary ammonium ions are grafted onto the surface of a macroporous membrane to produce a strong anion exchange membrane adsorber, e.g., Sartobind Q and Mustang Q. The salt concentration is kept low to prevent screening of the

electrostatic interactions between the ammonium ion and negatively charged impurities. High salt concentrations can severely limit capture of negatively charged impurities by quaternary ammonium based ligands (Curtis et al. 2003; Phillips et al. 2005).

The low binding capacities of quaternary ammonium based ligands at high salt concentration has led to the development of alternative anion-exchange ligands that exhibit high capacities at high salt concentrations (Burton and Harding, 1998, Riordan, 2009a). Recent studies indicate that increased capacity at high salt concentrations is due to secondary hydrophobic and hydrogen bonding interactions between the target species and the ligand (Yang et al. 2007). Johansson et al. (2003) indicate that non-aromatic anion-exchange ligands based on primary and secondary amines display high capacities at high salt concentrations. The presence of hydroxyl groups near the ionic group (primary amine) leads to secondary hydrogen bonding interactions. Unlike the Sartobind Q and Mustang Q, the ChromaSorb membrane adsorber contains primary amine based ion-exchange ligands.

The purpose of this study was to determine the level of virus clearance over a range of operating conditions for three commercial anion exchange membrane adsorbers: Sartobind Q, Mustang Q, and ChromaSorb. This is the first of a two part study. Here we focus exclusively on clearance of MVM. In part 2 we investigate the effects of host cell proteins and DNA as well as a 'model' antibody on MVM clearance. Since the anion exchange polishing step can follow anion or cation exchange packed bed chromatography two different sets of experiments were conducted using an anionic buffer set and a cationic buffer set to represent the feed stream after anion- and cation-exchange chromatography respectively. The results of this study will help determine the effect of changes in operating conditions on the level of MVM clearance.

2.3 Experimental

2.3.1 Experimental Design

The anionic buffer set of experiments was a full-factorial design containing three variables: NaCl concentration (50, 200 mM), pH (7.5, 9.0), and flow rate (4, 20 membrane volume/min (MV/min)). One centerpoint run was also included at 125 mM NaCl, pH 8.25, and 12 MV/min flow rate. The cationic buffer set of experiments was a half-factorial design containing four variables: NaCl concentration (0, 200 mM), pH (6.0, 9.0), phosphate concentration (0, 50 mM), and flow rate (4, 20 MV/min). The effect of phosphate in the feed for the cationic buffer set of experiments was investigated as negatively-charged buffer species are commonly present in the eluate from a cation exchange chromatography step. A centerpoint run was also conducted at 100 mM NaCl, pH 7.5, 12 MV/min flow rate, and 25 mM phosphate. One additional run was conducted using solution conditions that resulted in poor binding for the ChromaSorb (200 mM NaCl, pH 9.0, 50 mM phosphate) where phosphate was replaced by 50 mM acetate. All runs were conducted in duplicate. Table 2.1 gives the feed buffers tested.

2.3.2 Materials

Sartobind Q Nano 1 mL devices, Mustang Q coins with stainless steel housing, and ChromaSorb 0.08 mL devices were obtained through gracious donations from Sartorius AG (Göttingen, Germany), Pall Corporation (Port Washington, NY, USA), and Millipore Corporation (Billerica, MA, USA), respectively. All buffer chemicals (tris-base, tris-HCl, NaCl, NaH_2PO4 (monohydrate), Na_2HPO4 (anhydrous), glacial acetic acid, and sodium acetate trihydrate) were purchased from JT Baker (Phillipsburg, NJ, USA). Table 1 gives the various feed buffers used in order of increasing conductivity. The column labeled ‘design of experiments’ indicates whether the buffer was used for the anionic or cationic buffer set of

Table 2.1: Details of buffers. All buffers contained 20 mM tris.

Conductivity (mS/cm)	NaCl (mM)	pH	Phosphate (mM)	Design of Experiments
0.5	0	9.0	0	CEX
2.3	0	6.0	0	CEX
6.0	50	9.0	0	AEX
6.0	0	6.0	50	CEX
7.2	50	7.5	0	AEX
7.6	0	9.0	50	CEX
14.4	125	8.25	0	AEX
14.6	100	7.5	25	CEX
21.4	200	9.0	0	AEX/CEX
22.0	200	7.5	0	AEX
22.6	200	6.0	0	CEX
23.7	200	9.0	50 (Acetate)	CEX
25.4	200	6.0	50	CEX
26.5	200	9.0	50	CEX

experiments. Three pairs of stock buffers were prepared: (1) 20 mM tris-HCl, 20 mM tris-base; (2) 20 mM tris-HCl and 50 mM monobasic phosphate, 20 mM tris base and 50 mM dibasic phosphate; (3) 20 mM tris HCl and 50 mM acetic acid, 20 mM tris base and 50 mM sodium acetate. The buffers given in Table 1 were prepared by titrating the required volume of each pair of buffers to obtain the desired pH and adding the appropriate mass of NaCl.

pMVM (Minute Virus of Mice prototype strain) and mouse A9 fibroblasts were purchased from ATCC (Manassas, VA, USA). High glucose DMEM media, DMEM containing trypsin/EDTA and fetal bovine serum were obtained from HyClone, a division of Thermo Fisher Scientific (Waltham, MA, USA). A9 cells were thawed and expanded into multiple T-150 culture flasks using high glucose DMEM media with 10% FBS and 100 μg/mL penicillin. Cell culture was performed in jacketed incubators (non-infected and infected cultures in separate incubators) at 37°C with 10% CO2. Cultures were expanded and grown to ~ 80% confluence at

which point infection with MVM was performed. Infection was accomplished by discarding old growth media from culture (cells were adherent) and incubating cells at 37 C for 10 minutes in 1 mL DMEM containing $1\times10^{10} - 1\times10^{11}$ virus particles/mL for an MOI (multiplicity of infection) of greater than 1000 assuring efficient infection. An additional 34 mL of DMEM media (as described above) were added to the cultures after the 10 min incubation for a total 35 mL culture volume. A 6 day infection propagation period was found to be suitable for complete infection/propagation, which consistently yielded MVM titers of $1\times10^{10} - 1\times10^{11}$ particles/mL.

2.3.3 Assays

Quantification of MVM was accomplished through a quantitative PCR (QPCR) assay (Ros et al., 2002, Klee et al., 2006; Wickramasinghe et al. 2010). iQ SYBR green w/ fluorescein master mix was purchased from BioRad (Hercules, CA, USA). Forward (5' GACGCACAGAAAGAGAGTAACCAA 3') and Reverse (5' CCAACCATCTGCTCCAGTAAACAT 3') primers were purchased with standard desalting purification from IDT (Coralville, IA, USA). RQ1 DNase enzyme and buffer was purchased from Promega (Madison, WI, USA). QPCR was performed on a BioRad iQ5 real-time PCR system with iQ5 optical system software v2.0.

QPCR runs were performed in unskirted, low-profile 96-well PCR plates (BioRad) with polypropylene microseal 'B' adhesive sealers with 20 μL per reaction. The reaction recipe was taken directly from the iQ SYBR Green master mix instructions (given per reaction): 10 μL SYBR Green master mix, 8.2 μL distilled water, 0.4 μL forward primer (final 100 nM), 0.4 μL reverse primer (final 100 nM), and 1 μL sample. MVM standards were created by PCR amplification of a highly conserved 501bp portion of the MVM genome using the above mentioned primers and capturing the PCR product in the pCR2.1-TOPO plasmid using a

Invitrogen TOPO TA Cloning kit (Life Technologies, Carlsbad CA). Standards ranging from 1×10^9 copies/μL to 1×10^2 copies/μL were created by serial dilution of the Maxi-prepped (Qiagen, Valencia, CA, USA) cloned PCR product. Annealing temperature was determined through temperature gradient runs and melt curve analysis; 57°C resulted in a single dominant melt curve. The initial PCR cycle was 95°C for 10 min, which functioned to open virus particles, denature DNA, and inactivate RQ1 DNase. Then 45 cycles of the following were repeated: denaturing at 95°C for 15 s, primer annealing at 57°C for 10 s, elongation at 72°C for 45 s, and an additional 10 s at 72°C to collect the real-time fluorescence data.

The QPCR assay limit of detection was determined by serially diluting the 1×10^2 copies/μL standard 2X until a sample with 1 copy/μL was reached. Samples were run in triplicate on a single plate following the above protocol. This plate was repeated 2 additional times for 3 total replicate plates and a total of 9 replicates per sample. Limit of detection was determined at 95% confidence by Probit analysis using Minitab statistical software. The limit of detection was determined to be 14 copies/μL.

Prior to transferring to the QPCR plate, virus-containing samples (1 μL) were pipetted into 96-well plates containing 9 μL of DNase solution (1 μL RQ1 DNase, 1 μL 10X DNase buffer, and 7 μL of dH_2O). The DNase step provided assurance that the QPCR assay would only quantify complete viral particles and not naked viral DNA that would not be infective. These plates were sealed and incubated at 37°C for 40 min. 1 μL each of the DNase treated samples were pipetted into a BioRad PCR plate with 19 μL of iQ SYBR Green master mix with primers (described above). Eight standards were run with every plate (1×10^2 – 1×10^9 copies/μL) from which a linear standard curve was constructed to quantify unknown samples. All samples were run in duplicate.

2.3.4 Virus Clearance

All membrane adsorber evaluation runs were performed on an AKTA FPLC (GE Healthcare Bio-Sciences Corp, Piscataway, NJ, USA) with FRAC-950 fraction collector using the associated Unicorn software v. 5.1. Conductivity, absorbance at 280 nm, backpressure, and temperature were recorded. Prior to testing, all membrane modules were wet with running buffer according to the manufacturers' instructions. The FPLC system was flushed with water followed by running buffer prior to attachment of the membrane module. Membranes were installed with a slow flow rate (~1 MV/min) in the bottom-to-top or reverse direction to minimize the possibility of air entering the membrane devices. Equilibration of the devices was accomplished at flow rates (4 – 20 MV/min) in top-to-bottom or forward direction for 20 membrane volumes or until the conductivity and UV absorbance at 280 nm were stable. After the membranes were equilibrated, the buffer was spiked with a 1:100 dilution of MVM virus stock. Spiking was performed immediately prior to loading to minimize any buffer effects on the virus. MVM challenge titers for all runs were between 10^8 and 10^9 virus particles/mL.

Virus-spiked load volumes were normalized to 500 mL per mL of membrane with the Sartobind Q, Mustang Q, and ChromaSorb having volumes of 1 mL, 0.35 mL, and 0.08 mL, respectively. During the load step, effluent was collected in 10 equal volume fractions. Virus concentration was determined for all fractions. After virus loading, the membranes were washed with at least 20 membrane volumes of running buffer.

2.3.5 Membrane Characterization

Membranes were imaged using field-emission scanning electron microscopy (FESEM) (Model JSM-6500F, Waltham MA, USA) and analyzed using X-ray photoelectron spectroscopy (XPS) (2000 Physical Electronics 5800 ultrahigh vacuum XPS-Auger spectrometer, Chanhassen,

MN, USA). The equilibrium ion-exchange capacities of the membrane adsorbers were determined by titration. Membrane samples were prepared by soaking them overnight in excess 0.5 N NaOH, washing with distilled water until the pH was that of the distilled water, and soaking overnight in 2 M NaCl. Next the solution was titrated with 0.01 N HCl. The ion-exchange capacity is defined as the number of OH- ions per surface area. Membrane geometries as specified by the manufactures were: Sartobind Q; cylindrically wound 15-layer membrane about 36 cm^2 surface area; Mustang Q; 1.8 cm diameter stack of 10 membranes surface area about 24 cm^2; ChromaSorb; 1.5 cm diameter stack of 8 membranes, surface area about 14 cm^2.

2.4 Results and Discussion

Figure 2.1 gives the equilibrium ion-exchange binding capacities for the membrane adsorbers. All measurements were conducted in triplicate using membranes from different lots. Average results are given. ChromaSorb showed a 4-fold higher static binding capacity than Sartobind Q and a 12-fold higher capacity than Mustang Q. While Sartobind Q and Mustang Q contain quaternary amine based anion-exchange ligands, ChromaSorb contains polyallylamine (primary amine based ligands) (Woo et al. 2011).

Figure 2.2 gives FESEM images for the three membrane adsorbers. All three membrane adsorbers possess a very open structure that gives rise to high permeability and rapid convective flow through the membrane pores, which appear to range from 0.5 to 3 μm. According to the manufacturers, Sartobind Q consists of a base regenerated cellulose membrane, nominal pore size 3 μm; Mustang Q consists of a polyethersulfone membrane, nominal pore size 0.8 μm; ChromaSorb consists of a polyethylene base membrane, nominal pore size 0.65 μm.

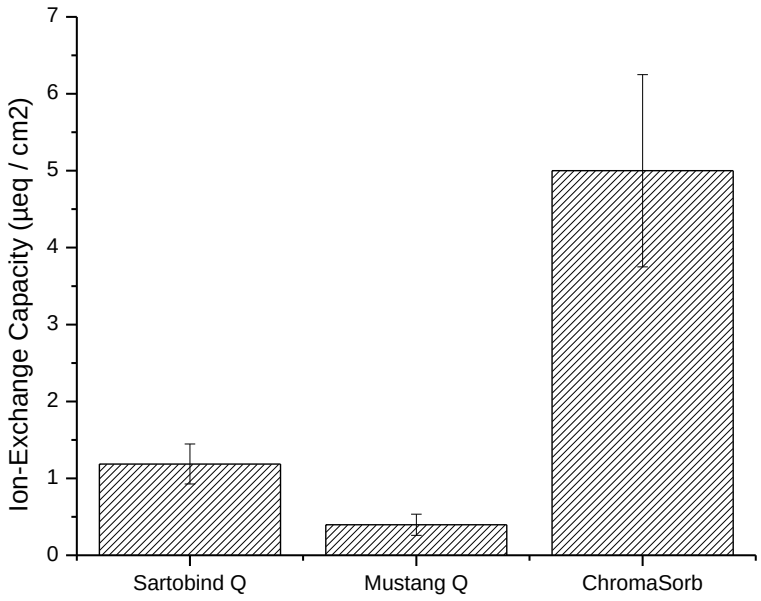

Figure 2.1: Static binding capacity Sartobind Q, Mustang Q and ChromaSorb

High resolution XPS spectra for nitrogen for all three membranes indicate the presence of primary amine (400 eV) and quaternary amine (402 eV) peaks (Liu et al. 2006). For Sartobind Q (Figure 2.3A) only a quaternary amine peak is detected; while for ChromaSorb (Figure 2.3C), only a primary amine peak is present. Though the manufacturer describes Mustang Q as containing quaternary amine based ligands, Figure 2.3B suggests some primary amines are also present at the membrane surface. This is probably a result of the monomer species and the linker/coupling chemistry used (Johansson et al., 2003).

Table 2.2 gives log virus reduction (LRV) for the anionic buffer set of experiments. The results are given in order of increasing conductivity. LRV is defined as log(total virus loaded) - log (virus in all 10 fractions plus in the wash). Limit of detection based on 1 µL samples, and accounting for dilution in DNase solution, was 1.4×10^5 virus particles/mL. Thus, LRV values

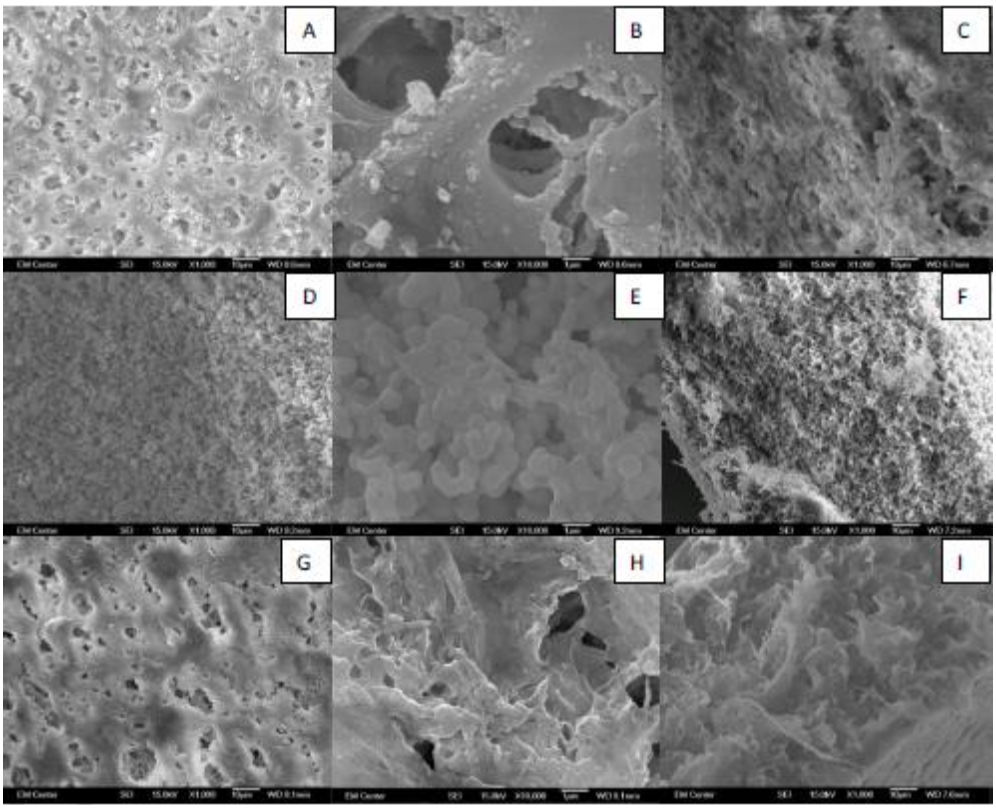

Figure 2.2: FE-SEM images of membranes. Figures A,D,G (1000 X) and B,E,H (10,000X) give images of the Sartobind Q, Mustang Q and ChromaSorb membranes. Figures C,F,I (1000X) give cross sectional images of the Sartobind Q, Mustang Q and ChromaSorb membranes, respectively.

where the virus titer was below limit of detection are given as greater than (>) limit of detection. Uncertainty values for LRV above the level of detection represent 1 standard deviation.

As pore diffusional resistance is minimized in membrane adsorbers, a constant dynamic capacity over a large range of flow rates is frequently observed (Specht et al., 2005; Han et al., 2005). Though experiments were conducted at flow rates between 4 and 20 MV/min, Table 2.2 indicates that for conductivities up to 14.4 mS/cm, all three adsorbers displayed virus clearance greater than limit of detection. Since the pI of MVM is 5-6 (Anouja, F. et al. 1997), MVM is negatively charged at the pH values tested here. Consequently, given the limited data below the limit of detection, it was not possible to determine the effect of flow rate on MVM clearance.

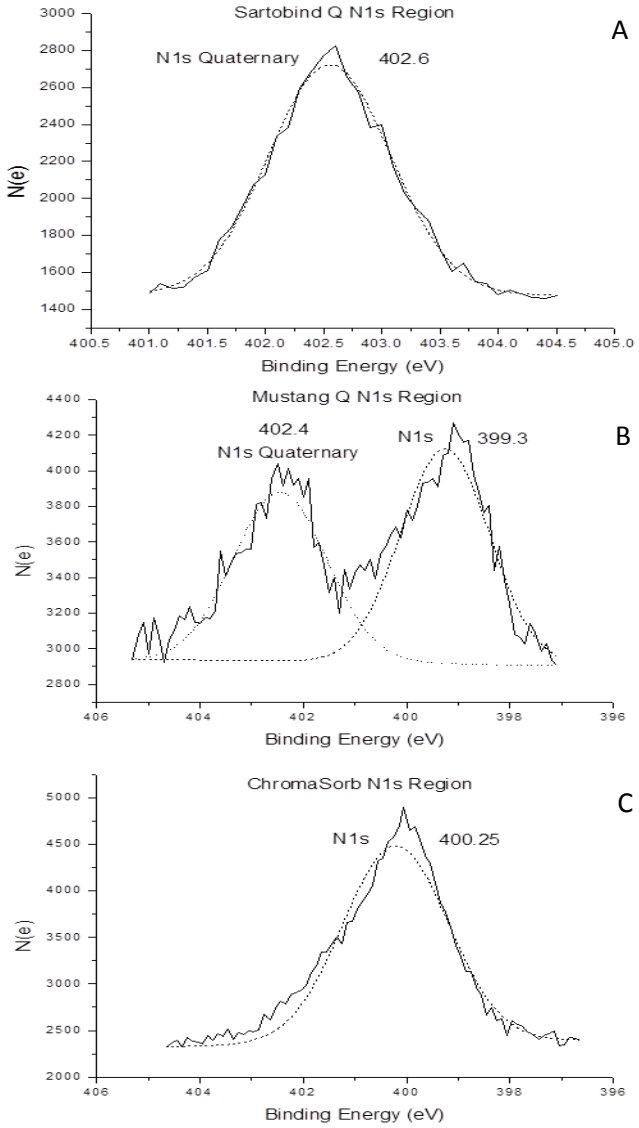

Figure 2.3: XPS N1s high-resolution region scans from top-to-bottom: Sartobind Q, Mustang Q, and ChromaSorb. Counts are plotted against binding energy.

At conductivities above 14.4 mS/cm, Mustang Q gives very low LRV. Sartobind Q displays LRV above the limit of detection for conductivities up to 21.4 mS/cm and pH above 7.5. Salts in solution shield charges between the virus particles and quaternary amine ligands, leading to the lower observed capacities at higher conductivities. Figure 2.1 indicates that Mustang Q has

Table 2.2: MVM removal results from the anionic buffer set of experiments. > indicates virus titers were below level of detection. LRV-S, LRV-M and LRV-C refer to LRV for Sartobind Q, Mustang Q and ChromaSorb, respectively. Errors represent one standard deviation with n = 2.

Conductivity (mS/cm)	NaCl (mM)	pH	Flow Rate (MV/min)	LRV-S	LRV-M	LRV-C
6.0	50	9.0	4	> 3.58	> 3.25	> 3.70
6.0	50	9.0	20	> 3.47	> 3.25	> 4.01
7.2	50	7.5	4	> 3.57	> 3.25	> 4.06
7.2	50	7.5	20	> 3.54	> 3.25	> 4.04
14.4	125	8.25	12	> 3.55	> 3.25	> 4.12
21.4	200	9.0	4	> 3.52	1.17 ± 0.00	> 3.70
21.4	200	9.0	20	> 3.47	1.00 ± 0.07	> 3.95
22.0	200	7.5	4	0.98 ± 0.05	1.62 ± 0.01	> 3.71
22.0	200	7.5	20	1.65 ± 0.04	1.28 ± 0.02	> 4.03

a lower static capacity compared to Sartobind Q, which could explain the compromised virus clearance at 200 mM NaCl, regardless of pH.

ChromaSorb displays virus clearance in excess of the limit of detection at all conductivities tested. As indicated in Figure 2.1, the static binding capacity of ChromaSorb is much higher, which could partially explain the higher capacity at higher salt concentrations. Since quaternary amines are much stronger anion exchangers than primary amines, they are more effective at low ionic strength. The presence of alkyl groups attached directly to the nitrogen atom prevents any secondary hydrogen bonding interactions in these systems. In contrast, the hydrogen atoms of primary amines can lead to secondary, hydrogen bonding interactions that result in higher capacities for primary amine based ligands at high salt concentrations where Coulombic interactions are diminished (Johansson et al. 2003). Consequently, the capacity of the ChromaSorb remains high at all conductivities tested. Figure 2.3B indicates that the Mustang Q

also displays a primary amine peak. However, the much lower static capacity of the Mustang Q may explain the low capacity at higher conductivities.

Table 2.3 gives virus clearance data for the cationic buffer set of experiments arranged in order of increasing conductivity. As was the case for the anionic buffer set of experiments, the effect of flow rate on virus clearance cannot be determined. The difference between the anionic and cationic buffer set of experiments is the presence of phosphate and acetate ions, as well as an expanded pH range. The binding capacities of Sartobind Q and Mustang Q are affected strongly by conductivity, in agreement with the results in Table 2.2. Mustang Q, unlike Sartobind Q, shows a large decrease in capacity at pH 6.0 and conductivities of 6.0 or 22.6 mS/cm. This result is most likely due to the lower static binding capacity for Mustang Q. As was the case in Table 2.2, uncertainty values for LRV above the level of detection represent 1 standard deviation. While the accuracy of the standard deviation is limited given that only two runs were conducted for each condition, the uncertainties do indicate if differences in LRV are likely to be significant.

Table 2.3 indicates that the presence of phosphate ions has a detrimental effect on the ChromaSorb binding capacity. Phosphoric acid has three pKa values: 2.3, 7.2, and 12.1. Consequently, at pH 6.0 most of the phosphate will be present as H_2PO4^-, while at pH 7.5 and 9.0 most will be present as $HPO4^{2-}$. When the phosphate is present as $HPO4^{2-}$ it has the greatest reduction on the static binding capacity of the ChromaSorb. Since phosphate is doubly charged and can form strong hydrogen bonding interactions with the H atoms attached to the primary amine it will preferentially bind to the primary amine. Further the presence of a double negatively charged phosphate will tend to repel negatively charged MVM particles. Consequently a significant decrease in MVM binding capacity is observed. At pH 6.0, the singly charged dihydrogen phosphate ion has a much lower effect on capacity. In fact, at a conductivity

Table 2.3: MVM removal results from the cationic buffer set of experiments. > indicates virus titers were below level of detection. LRV-S, LRV-M and LRV-C refer to LRV for Sartobind Q, Mustang Q and ChromaSorb, respectively. Errors represent one standard deviation with n = 2.

Conductivity (mS/cm)	NaCl (mM)	pH	Flow Rate (MV/min)	Phosphate (mM)	LRV-S	LRV-M	LRV-C
0.5	0	9.0	4	0	> 3.37	> 3.36	> 3.21
2.3	0	6.0	20	0	> 3.23	> 3.37	> 3.21
6.0	0	6.0	4	50	> 3.26	2.81 ± 0.01	> 3.21
7.6	0	9.0	20	50	> 3.16	> 3.34	1.12 ± 0.02
14.6	100	7.5	12	25	2.76 ± 0.05	2.02 ± 0.07	1.95 ± 0.13
21.4	200	9.0	20	0	> 3.26	1.35 ± 0.03	> 3.16
22.6	200	6.0	4	0	2.53 ± 0.05	1.34 ± 0.04	> 3.21
23.7	200	9.0	20	50 (Acetate)	0.64 ± 0.07	0.21 ± 0.04	> 3.11
25.4	200	6.0	20	50	1.23 ± 0.03	1.57 ± 0.01	2.49 ± 0.26
26.5	200	9.0	4	50	0.92 ± 0.02	1.24 ± 0.06	1.34 ± 0.01

of 6.0 mS/cm, the LRV for the ChromaSorb is above the limit of detection. At a conductivity of 25.4 mS/cm, pH 6.0 and 50 mM phosphate, ChromaSorb shows a slight decrease in MVM binding capacity, probably due to combination of charge screening and competitive binding with dihydrogen phosphate ion.

The strong base quaternary amine ligands of Sartobind Q and Mustang Q are much less affected by the presence of the doubly charged hydrogen phosphate ion at pH 9.0. The major contributor to the decrease in MVM binding is due to charge shielding at higher conductivities. The presence of acetate ions has no effect on the binding capacity of the ChromaSorb device. In the case of Sartobind Q and Mustang Q it is again the conductivity of the solution that affects

MVM capacity. Like dihydrogen phosphate, acetate is singly charged. Consequently the capacity of the ChromaSorb is unaffected by the presence of 50 mM acetate.

Interestingly for Sartobind Q and Mustang Q, at pH 9.0 in the presence of 200 mM NaCl the addition of acetate instead of phosphate leads to a greater decrease in LRV. These differences between the behavior of the primary amine and quaternary amine are most likely due to the fact that the quaternary amine acts as a pure ion exchange ligand. The primary amine on the other hand, is affected by acid base interactions. In particular, here the interactions will be affected by the acidity of the conjugate base of the primary amine and the basicity of the acetate and phosphate species present. Improved membrane adsorber performance may be achieved by diafiltering the feed in order to exchange the feed buffer and optimize the ionic strength however this will add to the purification cost and reduce product recovery.

Breakthrough curves for all three membrane adsorbers are given in Figure 2.4. For Sartobind Q and Mustang Q the feed consisted of 200 mM NaCl, pH 7.5 and a flow rate of 4 MV/min. Since the ChromaSorb did not show virus breakthrough at this condition, breakthrough behavior at 100 mM NaCl, 25 mM phosphate, pH 7.5, and flow rate 12 MV/min are presented. Breakthrough occurs for all three membrane adsorbers after 50 MV of feed have passed through the membrane. However, the concentration in the flow through is low and even after 500 MV is still less than 15% of the feed concentration. Similar behavior has been observed by others for adsorption of virus (Wickramasinghe et al. 2006), proteins (Yang and Etzel, 2003) and plasmid DNA (Endres et al. 2003). The slow approach to the feed concentration in the flow through has been explained using the ‘car parking’ model (Talbot et al. 2000). Since MVM particles are large and attach randomly to ligands, geometric blockage, steric hindrance and charge repulsion will slow the rate of binding as surface coverage increases. This effect is greatest when the solute

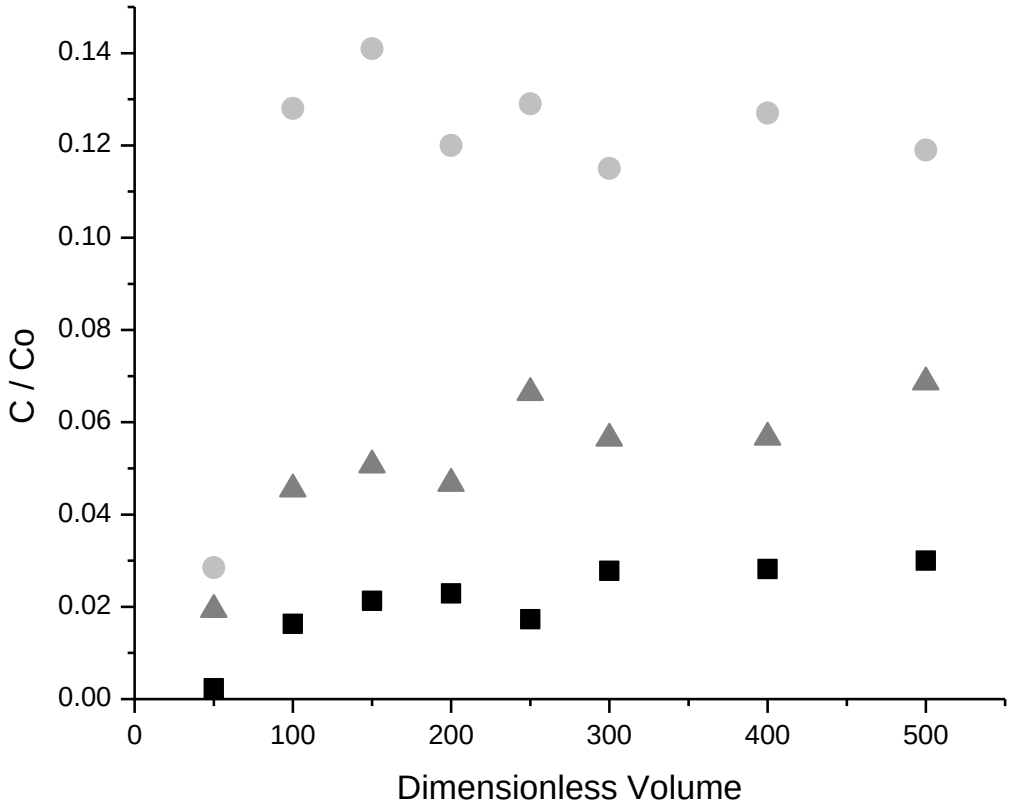

Figure 2.4: Normalized effluent virus concentration (C divided by feed concentration C0) versus dimensionless volume (effluent volume / membrane volume). For Sartobind Q and Mustang Q, the feed buffer consisted of 20 mM Tris, 200 mM NaCl, pH 7.5, 4 MV/min. For ChromaSorb, the feed buffer consisted of 20 mM Tris, 100 mM NaCl, 25mM phosphate, pH 7.5, 12 MV/min run. Symbols are as follows: Mustang Q (■), Sartobind Q (●), ChromaSorb (▲).

species is large relative to the spacing between the binding sites. After breakthrough occurs, the flow through concentration remains low relative to the feed concentration.

Comparing Figure 2.4 and Figure 2.1 indicates that the flow through concentration for the Mustang Q is the lowest though it has the lowest ion-exchange binding capacity. Since MVM particles are much larger than OH^- ions, the capacity of the three membrane adsorbers for MVM could be very different if a large number of ligands are unavailable for MVM binding due to steric hindrance and steric exclusion.

The three membrane adsorbers tested here contain different base membranes with different nominal pore sizes. Thus, in addition to ligand chemistry, optimization of the membrane pore structure and three dimensional arrangement of the ion-exchange ligands are important factors to consider for maximizing virus capture. Stacking multiple membranes (in a radial flow configuration) will modify the 'effective' pore size through the membrane. Further, the membrane pore surface should be covered with an open, three-dimensional layer of ion-exchange ligands. Models that describe attachment of virus particles to the membrane surface indicate that the spacing of the ion-exchange groups relative to the size of the adsorbed species is important. Finally, development of primary amine based ion-exchange ligands that are effective at high conductivities will require appropriate substitution of groups capable of forming secondary interactions with MVM particles near the cationic sites.

2.5 Conclusions

A comprehensive evaluation of virus removal capability of leading commercial anion-exchange membrane adsorbers has been conducted. The capacity for binding MVM is severely compromised at higher conductivities for quaternary amine based membrane adsorbers such as Sartobind Q and Mustang Q. The binding capacity of the primary amine based ChromaSorb is far less sensitive to conductivity of the feed solution. However, it is severely compromised by the presence of competing hydrogen phosphate ions. Membrane adsorbers like ChromaSorb that contain primary amine based ligands make use of secondary interactions to maintain a high capacity at high feed conductivities. Consequently, the presence of ions that also are capable of forming hydrogen bonds with the primary amine groups will have a detrimental effect on the capacity.

Maximizing the capacity of anion exchange membrane adsorbers for capture of large contaminants such as virus particles will require optimization of the membrane pore structure and the three dimensional arrangement of the ion-exchange groups. Maximizing the density of ion-exchange groups alone will not necessarily maximize capacity, as capture of large virus particles can lead to steric hindrance and steric exclusion effects that render a number of the ion exchange groups inaccessible.

References

Ahrer, K., Buchbacher, A., Iberer, G., Jungbauer, A. 2006. Thermodynamic stability and formation of aggregates of human immunoglobulin G characterised by differential scanning calorimetry and dynamic light scattering. *J Biochem Biophys Methods*. 66(1-3): 73-86.

Anouja, F., Wattiez, R., Mousset, S., Caillet-Fauquet. P. 1997. The cytotoxicity of the parvovirus minute virus of mice nonstructural protein NS1 is related to changes in the synthesis and phosphorylation cell proteins. *J Virol*. 71(6): 4671-4678.

Boi, C., 2007. Review: membrane adsorbers as purification tools for monoclonal antibody purification. *J Chromatogr B*. 848(1): 19-27.

Brandt, S. Goffe, R. A., Kessler, S. B., O'Connor, J. L., Zale, S. E. 1988. Membrane-based affinity technology for commercial scale purifications. *BioTechnology*. 6(7): 779-782.

Brown, A., Bechtel, C., Bill, J., Liu, H., Liu, J., McDonald, D., Pai, S., Radhamohan, A., Renslow, R., Thayer, B., Yohe, S., Dowd, C. 2010. Increasing parvovirus filter throughput of monoclonal antibodies using ion exchange membrane adsorptive pre-filtration. *Biotechnol Bioeng.* 106(4): 627-637.

Burton, S. C., Harding, D. R. K. 1998. Hydrophobic charge induction chromatography: salt independent protein adsorption and facile elution with aqueous buffers. *J Chromatogr A*. 814(1-2): 71-81.

Curling, J., Gottschalk, U. 2007, Process Chromatography: Five decades of innovation. *BioPharm International*. 20(10): 70-94.
Curtis, S., Lee, K., Blank, G. S., Brorson, K., Xu, Y. 2003, Generic/Matrix evaluation of SV40 clearance by anion exchange chromatography in flow-through mode. *Biotechnol Bioeng*. 84(2): 179-186.

Endres, H. H., Johnson, J. A. C., Ross, C. A., Welp, J. K., Etzel, M. R. 2003. Evaluation of ion-exchange membrane and purification of plasmid DNA. *Biotchnol Appl Biochem*. 37: 259-266.

Ghosh, R, 2002. Protein separation using membrane chromatography: opportunities and challenges, *J Chromatogr A*. 952(1-2): 13-27.

Gottschalk, U. 2005. Downstream processing of monoclonal antibodies: from high dilution to high purity. *Biopharm Intern*. 18(6): 42-58.

Han, B., Specht, R., Wickramasinghe, S. R., Carlson, J. O., 2005. Binding *Aedes aegypti* densonucleosis virus to ion exchange membranes. *J Chromatogr A.* 1092(1): 114-124.

Johansson, B.-L., Belew, M., Eriksson, S., Glad, G., Lind, O., Maloisel, J.-L., Norrman, N. 2003. Preparation and characterization of prototypes for multi-modal separation media aimed for capture of negatively charged biomolecules at high salt conditions. *J Chromatogr A*, 1016(1): 21-33.

Klee, S.R., Tyczka, J., Ellerbrok, H., Franz, T., Linke, S., Baljer, G., Appel, B. 2006. Highly sensitive real-time PCR for specific detection and quantification of *Coxiella burnetii*. *BMC Microbiology*. 6:2.

Knudsen, H. L., Fahrner, R. L., Xu, Y., Norling, L. A., Blank, G. S. 2001. Membrane ion-exchange chromatography for process-scale antibody purification. *J Chromatogr A*. 907(1-2): 145-154.

Langer, E. S., 2009. Downstream factors that will continue to constrain manufacturing through 2013. *BioProcess J*. 8(4): 24-28.

Liu, X., Wu, N., Wunsch, B. H., Barsotti Jr, R. J., Stellacci, F. 2006. Shape-controlled growth of micrometer sized gold crystals by a slow reduction method. *Small*. 2(8-9): 1046-1050.

Phillips, M., Cormier, J., Ferrence, J., Dowd, C., Kiss, R., Lutz, H., Carter, J. 2005. Performance of a membrane adsorber for trace impurity removal in biotechnology manufacturing. *J Chromatogr A*. 1078(1-2): 74-82.

Riordan, W., Heilmann, S., Brorson, K., Seshadri, K., He, Y., Etzel, M. 2009a. Design of salttolerant membrane adsorbers for viral clearance. *Biotechnol Bioeng*. 103(5): 920-929.

Riordan, W. T., Heilmann, S. M., Brorson, K., Seshadri, K., Etzel, M. R. 2009b. Salt tolerant membrane adsorbers for robust impurity clearance. *Biotechnol Prog*. 25(6): 1695-1702.

Ros, C., Burckhardt, C. J., Kempf, C. 2002. Cytoplasmic trafficking of minute virus of mice: low-pH requirement, routing to late endosomes, and proteasome interaction. *J Virol*. 76(24): 12634-12645.

Specht, R., Han, B., Wickramasinghe, S. R., Carlson, J. O., Czermak, P., Wolf, A., Reif, O.-W. 2004. Densonucleosis virus purification by ion exchange membranes. *Biotechnol Bioeng*. 88(4): 465-473.

Talbot, J., Tarjus, G., van Tassel, P. R., Viot, P. 2000. From car parking to protein adsorption: an overview of sequential adsorption processes. *Colloid Surf A*. 165(1-3): 287-324.

Teeters, M. A., Root, T. W., Lightfoot, E. N. 2002. Performance and scale-up of adsorptive membrane chromatography. *J Chromatogr A*. 944(1-2): 129-139.

van Reis, R., Zydney, A. L. 2001. Membrane separations in biotechnology. *Curr Opin Biotech*. 12(2): 208-211.

Wickramasinghe, S. R., Stump, E. D., Grzenia, D. L. Husson, S. M., Pellegrino, J. 2010. Understanding virus filtration membrane performance. *J Membr Sci*. 365(1-2): 160-169.

Wickramasinghe, S. R., Carlson, J. O., Teske, C., Hubbuch, J., Ulbricht, M. 2006. Characterizing solute binding to macroporous ion exchange membrane adsorbers using confocal laser scanning microscopy. *J Membr Sci*. 281(1-2): 609-618.

Woo, M., Khan, N. Z., Royce, J., Mehta, U., Gagnon, B., Ramaswamy, S., Soice, N., Morelli, M., Cheng, K.-S. 2011. A novel primary amine-based anion exchange membrane adsorber. *J Chromatogr A*. 1218(32): 5386-5392.

Yao, Y., Lenhoff, A. M. 2006. Pore size distributions of ion exchangers and relation to protein binding capacity. *J Chromatogr A*. 1126(1-2): 107-119.

Yang, T., Malmquist, G., Johansson, B.-L., Maloisel, J.-L., Cramer, S. 2007. Evaluation of multimodal high salt binding ion exchange materials. *J Chromatogr A*. 1157(1-2): 171-177.

Yang, H., Etzel, M. R. 2003. Evaluation of three kinetic equations in models of protein purification using ion-exchange membranes. *Ind Eng Chem Res*. 42(4): 890-896.

Zhou, J. X., Tressel, T. 2006. Basic concepts in Q membrane chromatography for large scale antibody production. *Biotechnol Prog.* 22(2): 341-349.

Zhou, J. X., Tressel, Gottschalk, U., Solamo, F., Pastor, A., Dermawan, S., Hong, T., Reif, O. Mora, J., Hutchinson, F., Murphy, M. 2006. New Q membrane scale-down model for process – scale antibody purification. *J Chromatogr A* 1134(1-2): 66-73.

Zhou, J. X., Tressel, Yang, X., Seewoester, T. 2008a. Review: implementation of advanced technologies in commercial monoclonal antibody production. *Biotechnol J*. 3(9-10): 1185-1200.

Zhou, J. X., Solamo, F., Hong, T., Shearer, M., Tressel, T. 2008b. Viral clearance using disposable systems in monoclonal antibody commercial downstream processing. *Biotechnol Bioeng*. 100(3): 488-496.

Chapter 3

Anion Exchange Membrane Adsorbers for Flow-through Polishing Steps: Part II. Virus, Host Cell Protein, DNA Clearance, and Antibody Recovery[1]

3.1 Summary

Anion exchange membrane adsorbers are used for contaminant removal in flow-through polishing steps in the manufacture of biopharmaceuticals. This contribution describes the clearance of Minute Virus of Mice, DNA and host cell proteins by three commercially available anion exchange membranes: Sartobind Q, Mustang Q, and ChromaSorb. The Sartobind Q and Mustang Q products contain quaternary amine ligands; whereas, ChromaSorb contains primary amine based ligands. Performance was evaluated over a range of solution conditions: 0-200 mM NaCl, pH 6.0-9.0, and flow rates of 4-20 membrane volumes/min in the presence and absence of up to 50 mM phosphate and acetate. In addition contaminant clearance was determined in the presence and absence of 5 g/L monoclonal antibody.

The quaternary amine based ligands depend mainly on Coulombic interactions for removal of negatively charged contaminants. Consequently, performance of Sartobind Q and Mustang Q was compromised at high ionic strength. Primary amine based ligands in ChromaSorb enable high capacities at high ionic strength due to the presence of secondary, hydrogen bonding interactions. However, the presence of hydrogen phosphate ions leads to

[1]Weaver, J., Husson, SM., Murphy, L., Wickramasinghe, SR. 2013. Anion Exchange Membrane Adsorbers for Flow-through Polishing Steps: Part II. Virus, Host Cell Protein, DNA Clearance and Antibody Recovery, *Biotechnol Bioeng.* 110(2): 500 – 510

reduced capacity. Monoclonal antibody recovery using primary amine based anion-exchange ligands may be lower if significant binding occurs due to secondary interactions. The removal of a specific contaminant is affected by the level of removal of the other contaminants. The results of this study may be used to help guide selection of commercially available membrane absorbers for flow-through polishing steps.

3.2 Introduction

Membrane adsorbers or membrane chromatography has been proposed as an alternative to packed bed chromatography for many years (Klein, 2000). Today membrane adsorbers are used in the biopharmaceutical industry in 'flow-through' polishing steps (Knudsen et al. 2001, Zhou et al. 2006, Boi, 2007, Zhou and Tressel 2006, Zhou et al 2008a, Zhou et al. 2008b, Shirataki et al. 2011). Anion exchange membranes are used to bind large contaminant species: virus particles, host cell proteins and DNA during the manufacture of monoclonal antibodies (mAbs). The feed pH is typically greater than 7.0. Under these conditions the contaminant species are negatively charged but the mAb is positively charged.

Frequently ligands containing quaternary amine groups are used to produce strong anion exchange membrane adsorbers e.g. Sartobind Q® (Sartorius AG, Göttingen, Germany), Mustang Q® (Pall Corporation, Port Washington, NY, USA). The conductivity of the feed stream is kept low to prevent a reduction in capacity due to interference in the electrostatic interactions between the ammonium ions and the negatively charged impurities. Alternative ligands that make use of secondary hydrophobic and hydrogen bonding interactions between the target species and the ligand can maintain high capacity at high salt concentrations (Yang et al. 2007). Johansson et al. (2003) indicate that primary and secondary amine based ligands display high capacities at high

salt concentrations. The presence of hydrogen atoms attached directly to the amine group as well as hydroxyl groups near the amine group lead to secondary hydrogen bonding interactions. Recently primary amine based anion-exchange membranes have been commercialized. ChromaSorb (Millipore Corporation, Billerica, MA, USA) uses a polyallylamine ligand (Woo et al. 2011). Sartobind STIC also uses a primary amine ligand.

Here the performance of three anion exchange membrane adsorbers: Sartobind Q and Mustang Q which contain quaternary amine ligands and the ChromaSorb which contains primary amine ligands has been compared. In Chapter 2 of this thesis (Weaver et al. 2012), we examined the performance of Sartobind Q, Mustang Q, and ChromaSorb membrane adsorbers for clearance of Minute Virus of Mice (MVM), an 18-22 nm parvovirus recognized by the FDA as a model viral impurity. The capacities of the Sartobind Q and Mustang Q were very sensitive to conductivity. At feed conductivities above 20 mS/cm, a significant decrease in capacity was observed. ChromaSorb was much less sensitive to conductivity; however, the presence of hydrogen phosphate ions led to a significant decrease in capacity.

Here in Chapter 3, we report the capacities of Sartobind Q, Mustang Q and ChromaSorb for simultaneous removal of MVM, host cell proteins and DNA, as well as recovery of a mAb over a range of operating conditions. Since the anion exchange polishing step can follow anion or cation exchange packed bed chromatography, two different sets of experiments, were conducted using an anionic buffer set and a cationic buffer set to represent the feed stream after anion- and cation-exchange chromatography, respectively.

The pI of MVM and DNA is 5-6 (Anouja, 1997) and 5.0 (Cai et al. 2006) respectively. Host cell proteins exhibit a range of isoelectric points. Removal of these proteins based purely on electrostatic interactions will only occur if they are negatively charged. Removal of MVM, host

cell proteins and DNA will depend on competitive binding among the different contaminant species present. In this study, capacities have been determined over a range of feed conductivities, pH and flow rates. The effects of phosphate and acetate ions in the feed stream also have been studied.

Removal of MVM, host cell proteins and DNA in the presence of a mAb with a pI of 7.1 also has been investigated. Since the mAb has a low pI when the feed pH is close to or above the pI of the mAb, significant binding of the mAb was expected. The results obtained here indicate the effect of changes in operating conditions on competitive binding among different contaminant species and the mAb.

3.3 Experimental

3.3.1 Experimental Design

The anionic and cationic buffer sets represent the feed stream after anion- and cation-exchange chromatography, respectively. The anionic buffer set of experiments was a full-factorial design containing three variables: NaCl concentration (0, 200 mM), pH (7.5, 9.0), and flow rate (4, 20 membrane volume/min (MV/min)). Two centerpoint runs were included: 125 mM NaCl, pH 8.25, 12 MV/min flow rate. All runs were conducted in duplicate.

The cationic buffer set of experiments was a half-factorial design containing four variables: NaCl concentration (0, 200 mM), pH (6.0, 9.0), phosphate concentration (0, 50 mM) and flow rate (4, 20 MV/min). Since negatively charged buffer species are commonly present in the eluate from cation-exchange chromatography, the effect of phosphate (50 mM) was investigated. Two centerpoint runs (100 mM NaCl, pH 7.5, 12 MV/min flow rate, 25 mM phosphate) and a run using conditions that resulted in poor binding for the ChromaSorb (200

mM NaCl, pH 9.0, 50 mM phosphate) where phosphate was replaced by 50 mM acetate also were conducted.

3.3.2 Materials

Sartobind Q Nano 1 mL devices (Sartorius-Stedim Biotech), Mustang Q 0.35 mL coins (Pall Corporation) with stainless steel housing, and ChromaSorb 0.08 mL devices (Millipore) were obtained via gracious donations from each company. All buffer chemicals (tris-base, tris-HCl, NaCl, NaH_2PO4 (monohydrate), Na_2HPO4 (anhydrous), glacial acetic acid, and sodium acetate trihydrate) were purchased from JT Baker (Phillipsburg, NJ, USA). Three pairs of stock buffers were prepared: (1) 20 mM tris-HCl, 20 mM tris-base; (2) 20 mM tris-HCl and 50 mM monobasic phosphate, 20 mM tris base and 50 mM dibasic phosphate; (3) 20 mM tris HCl and 50 mM acetic acid, 20 mM tris base and 50 mM sodium acetate. Feed buffers were prepared by titrating the required volume of each pair of buffers to obtain the desired pH. Thus all buffers contained 20 mM tris. Further details are given in Chapter 2 of this thesis (Weaver et al., 2012).

MVM prototype strain (pMVM) and mouse A9 fibroblast cells were purchased from ATCC (Manassas, VA, USA). pMVM stocks were expanded in house by growing A9 cells to ~80% confluence in T-150 flasks and infection at an MOI of greater than 1000 as described earlier (Weaver et al., 2012). Briefly, A9 cells were expanded in high-glucose DMEM media with L-glutamine (Hyclone, Waltham, MA, USA) supplemented with 10% fetal bovine serum (FBS) and 100 μg/mL penicillin. MVM propagation and purification conditions have been described earlier (Weaver et al., 2012). Briefly, infected cultures (> 80% confluent) were maintained at 37ºC and 10% CO_2 for 6 days at which point virus was crudely purified from supernatant by three freeze/thaw cycles and centrifugation followed by 0.22 μm filtration.

Chinese Hamster Ovary Host Cell Protein (CHOP), DNA and purified human IgG4 monoclonal antibody (mAb), pI 7.1, were provided by Eli Lilly (Indianapolis, Indiana, USA). CHOP and DNA stock was prepared by growing a null CHO culture (CHO cells not expressing a recombinant protein). The cells were lysed via freeze/thaw and filtered through a 0.22 μm filter. The resulting supernatant contained a concentrated stock of both CHOP and DNA closely resembling impurities encountered in typical process conditions. The mAb was provided at a concentration of 71 g/L in a buffer containing low concentrations of citrate, surfactant, and NaCl at a pH of 6.7.

3.3.3 Assays

Quantitative PCR was used to quantify the number of copies of viral genomes present in each effluent fraction, and, therefore, the number of virus particles using a BioRad (Hercules, CA, USA) iQ5 real-time PCR system with iQ5 optical system software v2.0. Free viral DNA was digested with DNAse prior to QPCR, while encapsulated viral DNA was protected from digestion allowing QPCR to give a highly accurate virus particle count. iQ SYBR Green master mix (BioRad) provided the reaction buffer, free nucleotide triphosphates, DNA polymerase, and fluorescent SYBR Green intercalating dye. 1 μL of sample was assayed in each well of a 96-well plate; samples were run in duplicate. Samples were diluted 1:10 in wells containing DNAse. 1 μL of this solution was then transferred to wells containing water, iQ SYBR Green master mix, and primers. Primers and PCR conditions have been reported (Weaver et al. 2012). Briefly a forward primer 5’ GACGCACAGAAAGAGAGTAACCAA 3’ and reverse primer 5’ CCAACCATCTGCTCCAGTAAACAT 3’ were used. PCR conditions were as follows: 1) Initial step of 95 ºC for 10 min to inactivate DNAse and open viral capsids. 2) 95 ºC for 15 s. 3) 57 ºC for 10 s. 4) 72ºC for 45 s, followed by another 10 seconds for fluorescence data collection. Steps

2–4 were repeated 44 times for 45 total cycles. DNA concentration and therefore MVM concentration was determined by plotting on a standard curve based on $10^2 – 10^9$ copies/μL.

CHOP was quantified using a commercial CHO HCP ELISA kit (Cat No. F015) purchased from Cygnus Technologies (Southport, NC, USA). The "High-Sensitivity Protocol" was performed as described in the product insert. Limit of detection was determined to be 1 ng/mL. CHOP ELISA 96-well plates were analyzed on a BioRad Benchmark Plus spectrophotometric microplate reader with Microplate Manager 5.2 software.

DNA was quantified using a PicoGreen fluorescence assay kit (Cat No. P11496) purchased from Life Technologies (Carlsbad, CA). PicoGreen is an intercalating dye, which, like SYBR Green, only binds to double-stranded DNA. The PicoGreen assay was performed using 96-well flat-bottom plates (USA Scientific, Ocala, FL, USA) using a BioTek (Winooski, VT, USA) FLx800TBIE fluorescence microplate reader with Gen5 software. The limit of detection of the picogreen assay was 250 pg/mL. DNA removal for runs with mAb present was not determined, as the mAb interfered with the picogreen assay.

The mAb concentration was measured using standard absorbance at 280 nm on a Genesys 10 UV-Vis Spectrophotometer (Thermo Scientific, Waltham, MA, USA). Beer's law was used to derive concentrations using an extinction coefficient of 1.4 $ml*(mg*cm)^{-1}$.

3.3.4 Contaminant Clearance

All ion-exchange membranes were tested using an AKTA FPLC (GE Healthcare, Piscataway, NJ, USA) with a FRAC-950 fraction collector controlled by Unicorn software v. 5.1. Membranes were installed on the FPLC system, wetted, and equilibrated as described earlier (Weaver et al. 2012). Load material was prepared by spiking equilibration buffer 1:100 with MVM stock and 1:1000 or 1:2000 with CHOP/DNA stock producing load conditions with

approximately 1×109 MVM particles/mL, 100-200 ng/mL CHOP, and 40-80 ng/mL DNA. Runs with mAb involved spiking mAb to give a concentration of 5 g/L. These runs contained less than 1 mM citrate and less than 0.001% Tween 80, as they were present in the mAb stock solution.

Contaminant spiked load volumes were normalized to 500 mL per mL of membrane with the Sartobind Q, Mustang Q and ChromaSorb having volumes of 1 mL, 0.35 mL and 0.08 mL respectively. Each run effluent was collected in 10 fractions of identical volume. MVM, CHOP and DNA were determined in each fraction. For runs conducted with mAb, the mAb concentration also was determined in each fraction. After loading, the membranes were washed with at least 20 membrane volumes of running buffer. Impurity and mAb spikes were performed immediately prior to loading to minimize solution effects on impurities/mAb. Each set of experiments, anionic and cationic buffer sets were conducted twice, in the presence and absence of the mAb.

3.4 Results and Discussion

Table 1 gives log virus reduction (LRV) for the anionic buffer set of experiments. The results are presented in order of increasing buffer conductivity. LRV is defined as log(total virus loaded) - log(virus in all 10 fractions plus in the wash). The limit of detection based on 1 µL samples and accounting for dilution in DNase solution was 1.4×10^5 virus particles/mL. Consequently, LRV values where the virus titer was below the limit of detection are given as greater than (>) the limit of detection. Results are given in the presence and absence of the mAb. The two centerpoint runs have a conductivity of 14.4 mS/cm. The difference in LRV for the two centerpoint runs in the presence of the mAb gives an indication of the variability of the LRV results. In addition for each run, uncertainty values which represent ± 1 standard deviation are included. However given

that only two repeat runs were conducted, the accuracy of the standard deviation is limited. The largest value of the standard deviation is 0.41 log units (e.g. Table 3.2, conductivity 14.6 mS/cm). Thus differences in LRV of less than 0.4 log may not be significant. In the absence of the mAb, all three membrane adsorbers gave LRV greater than the limit of detection for buffer conductivities up to 14.4 mS/cm. Table 3.1 indicates that at higher conductivities the capacity of the Mustang Q decreases severely. The capacity of the Sartobind Q is less affected by conductivity at 21.4 mS/cm, but decreases severely at higher conductivity. The capacity of the ChromaSorb is unaffected by feed conductivity.

As indicated in Chapter 2 (Weaver et al., 2012), Sartobind Q has a higher static ion-exchange capacity than Mustang Q, which could explain the higher capacity of Sartobind Q at 21.4 mS/cm. In addition, comparing the LRV in Table 3.1 with our earlier work in the absence of CHOP and DNA, the presence of CHOP and DNA leads to a slight reduction in LRV for Sartobind Q and Mustang Q at higher conductivities. This reduction is due to competitive binding between MVM and the other contaminant species. This reduction is not observed for ChromaSorb as it has a much higher static ion-exchange capacity and displays LRV in excess of the level of detection for the anionic buffer set of experiments. Our results can be explained by the nature of functional groups on each membrane adsorber. Quaternary amines are stronger anion exchangers than primary amines and, at low ionic strength, will be very effective at removing negatively charged contaminant species. In addition, quaternary amines function well at higher pH values where primary amines become neutral. However, at high conductivities, charge shielding between the negatively charged contaminants and quaternary amine ligands can occur, leading to the lower observed capacity for Sartobind Q and Mustang Q, which rely largely on ionic interactions. Primary and secondary amine based anion-exchange ligands on the other

Table 3.1: MVM clearance for anionic buffer set of experiments in the absence and presence of mAb. All buffers contained 20 mM Tris. LRV-C, LRV-M, and LRV-S represent log removal of virus for ChromaSorb, Mustang Q, and Sartobind Q, respectively. All runs were conducted in duplicate. Uncertainty values represent 1 standard deviation.

				No mAb			5 g/L mAb		
Conductivity (mS/cm)	NaCl (mM)	pH	Flow Rate (MV/min)	LRV-S	LRV-M	LRV-C	LRV-S	LRV-M	LRV-C
6.0	50	9.0	4	> 3.75	> 4.15	> 3.94	0.44 ± 0.09	1.44 ± 0.25	1.17 ± 0.19
6.0	50	9.0	20	> 3.73	> 3.95	> 3.94	0.27 ± 0.11	2.56 ± 0.07	1.31 ± 0.54
7.2	50	7.5	4	> 3.60	> 4.15	> 3.61	0.56 ± 0.08	2.46 ± 0.90	1.37 ± 0.17
7.2	50	7.5	20	> 3.67	> 3.95	> 3.61	0.42 ± 0.06	2.88 ± 0.12	1.50 ± 0.07
14.4	125	8.25	12	> 3.71	> 3.95	> 3.61	0.61 ± 0.10	2.73 ± 0.15	1.43 ± 0.04
14.4	125	8.25	12	> 3.71	> 3.71	> 3.61	1.04 ± 0.02	2.01 ± 0.19	1.26 ± 0.48
21.4	200	9.0	4	2.98 ± 0.06	0.64 ± 0.39	> 3.61	0.50 ± 0.00	0.90 ± 0.15	1.53 ± 0.07
21.4	200	9.0	20	3.24 ± 0.28	0.25 ± 0.05	> 3.61	0.46 ± 0.05	0.09 ± 0.17	1.47 ± 0.23
22.0	200	7.5	4	0.62 ± 0.16	0.18 ± 0.01	> 3.61	0.37 ± 0.07	0.43 ± 0.40	1.20 ± 0.29
22.0	200	7.5	20	0.52 ± 0.11	0.41 ± 0.00	> 3.61	0.39 ± 0.42	0.34 ± 0.18	1.87 ± 0.02

hand can display higher capacities at high conductivities due to secondary hydrogen bonding interactions. The capacity results for ChromaSorb show this behavior.

Table 3.1 shows that the presence of 5 g/L mAb results in a significant decrease in LRV for all three membranes. Given the low pI of the mAb used here and its much higher

concentration than the contaminant species, it is expected that at all the pH values investigated in the anionic buffer set of experiments significant binding of the mAb occurs. This competitive binding lowers the capacity for all contaminant species.

Table 3.2 gives virus clearance data for the cationic buffer set of experiments. Again results are presented in order of increasing feed conductivity. The two centerpoint runs have a conductivity of 14.6 mS/cm and the LRV values give an indication of the variability in the data. As was the case for Table 1, uncertainty values which represent ± 1 standard deviation are included. Comparing the result in Tables 3.1 and 3.2, Sartobind Q and Mustang Q give similar results. LRV values are high (often above the level of detection) for conductivities up to 14.4 mS/cm. While the capacity of both Sartobind Q and Mustang Q decrease at conductivities above 14.4 mS/cm, the Sartobind Q displays a higher capacity for feed conductivities between 14.4 and 21.6 mS/cm, due to its higher static ion-exchange capacity. Again the presence of the mAb leads to a decrease in LRV.

The ChromaSorb however behaves very differently. The presence of phosphate appears to have a detrimental effect on LRV which is more clearly seen in the absence of the mAb. A similar result was observed and discussed in Chapter 2 of this thesis. Hydrogen phosphate ($HPO4^{2-}$) appears to have the greatest effect on the LRV of the ChromaSorb. When subjected to dihydrogen phosphate (H_2PO4^-) at pH 6.0, at low feed conductivities, the ChromaSorb displays high LRV. At high conductivities however the LRV is significantly reduced. The same trends were observed in the absence of CHOP and DNA (Weaver et al. 2012). The lower LRV at high conductivity is probably due to the large number of competing species present.

Replacing hydrogen phosphate ions by acetate ions at high conductivity, a LRV above level of detection is again obtained for the ChromaSorb in the absence of the mAb. However for

the two quaternary amine based membrane adsorbers, the LRV is similar in the presence of phosphate or acetate. A similar trend was obtained for clearance of MVM in the absence of CHOP and DNA (Weaver et al. 2012). These differences are most likely due to the fact that the quaternary amine acts as a pure ion exchange ligand. The primary amine on the other hand, is affected by acid base interactions. Here the interactions will be affected by the acidity of the conjugate base of the primary amine and the basicity of the acetate and phosphate species present. The results indicate that the capacity of membrane adsorbers that contain primary amine ligands that display significant secondary bonding interactions can be more difficult to predict.

The aim of this study was to explore the effect of changes in operating condition on the performance of the three membrane adsorbers investigated here. Thus unlike many previous studies a rather large range of conditions has been tested. However as only two repeat runs were conducted per condition the calculated standard deviations are of limited accuracy. Thus for a specific set of operating conditions it will be necessary to conduct sufficient repeat runs for greater statistical accuracy.

Figures 3.1-3.6 give CHOP and DNA removal data. In these figures, the abscissa gives buffer conditions in order of increasing conductivity. Tables 3.1 and 3.2 give the actual conductivities of the various buffers. Log clearance for the two centerpoint runs give an indication of the variability in the results. In addition the average standard deviation for all runs in each figure is given in the figure caption. All buffers contain 20 mM tris.

CHOP removal is given in Figure 3.1 and 3.2 in the absence and presence of the mAb for the anionic buffer set of experiments. Log clearance of CHOP is defined as log(total CHOP loaded) - log(CHOP in all 10 fractions plus the wash). The results in Figure 3.1 indicate that about 2 log CHOP are removed by the ChromaSorb at all conductivities.

Table 3.2: MVM clearance for cationic buffer set of experiments in the absence and presence of mAb. All buffers contained 20 mM tris. LRV-C, LRV-M, and LRV-S represent log removal of virus for ChromaSorb, Mustang Q, and Sartobind Q, respectively. All runs were conducted in duplicate. Uncertainty values represent 1 standard deviation.

					No mAb			5 g/L mAb		
Cond. (mS/cm)	NaCl (mM)	pH	Flow Rate (MV/min)	PO_4 (mM)	LRV-S	LRV-M	LRV-C	LRV-S	LRV-M	LRV-C
0.5	0	9.0	4	0	3.67 ± 1.22	> 4.39	> 3.71	3.13 ± 0.02	0.54 ± 0.13	0.34 ± 0.36
2.3	0	6.0	20	0	3.25 ± 0.18	> 4.39	> 3.71	0.39 ± 0.10	2.93 ± 0.00	1.51 ± 0.19
6.0	0	6.0	4	50	3.61 ± 0.18	3.29 ± 0.02	3.21 ± 0.29	2.89 ± 0.01	2.33 ± 0.05	1.84 ± 0.22
7.6	0	9.0	20	50	> 3.93	> 4.39	0.49 ± 0.24	0.42 ± 0.42	0.33 ± 0.10	0.58 ± 0.05
14.6	100	7.5	12	25	3.74 ± 1.22	1.79 ± 0.19	0.58 ± 0.08	1.77 ± 0.25	0.75 ± 0.09	0.08 ± 0.46
14.6	100	7.5	12	25	3.76 ± 1.22	2.08 ± 0.11	0.49 ± 0.18	2.04 ± 0.15	0.85 ± 0.21	0.49 ± 0.03
21.4	200	9.0	20	0	3.41 ± 1.22	1.07 ± 0.05	3.64 ± 0.26	1.08 ± 0.07	0.53 ± 0.11	0.48 ± 0.10
22.6	200	6.0	4	0	0.64 ± 0.32	0.50 ± 0.07	> 3.71	1.56 ± 0.06	0.56 ± 0.21	1.46 ± 0.33
23.7	200	9.0	20	50 (Ac)	0.73 ± 0.09	0.31 ± 0.01	> 3.74	0.34 ± 0.07	0.49 ± 0.04	0.02 ± 0.45
25.4	200	6.0	20	50	0.20 ± 0.23	0.93 ± 0.11	0.69 ± 0.04	1.25 ± 0.04	1.69 ± 0.21	0.96 ± 0.24
26.5	200	9.0	4	50	0.81 ± 0.40	0.41 ± 0.21	0.13 ± 0.01	0.57 ± 0.05	0.73 ± 0.01	0.63 ± 0.36

The CHOP spiked into the buffers was not conditioned or purified over any binding media that might have changed the distribution of charged CHOP species. Unconditioned CHOP encompasses a large range of isoelectric points and negatively and positively charged proteins will exist at the various buffer pH values tested (Jin et al., 2009). However, ChromaSorb showed

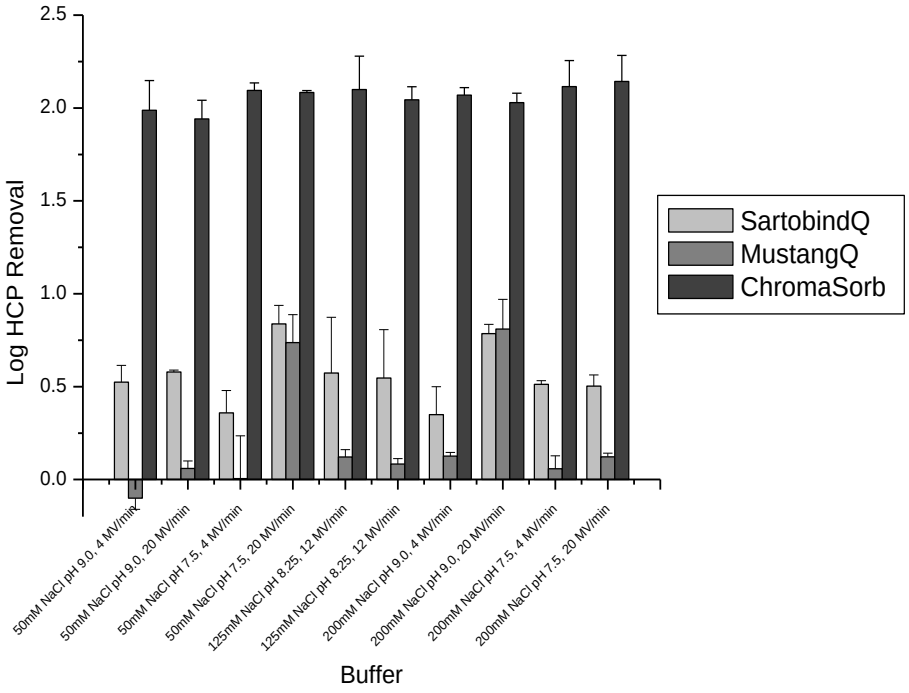

Figure 3.1: CHOP removal for anionic buffer set of experiments in the absence of mAb. The abscissa gives buffer conditions in order of increasing conductivity (see Table 1 for values). All buffers contain 20 mM tris. Uncertainties defined by Log Removal ± 1 standard deviation were determined where the standard deviation is an average for all runs shown in the figure. The uncertainties were ± 0.03 for Sartobind Q, ± 0.07 for Mustang Q, and ± 0.10 for ChromaSorb. Negative value due to inherent assay variability.

at or near limit of detection (1 ng/mL) removal of CHOP. This indicates that even proteins that have an overall positive charge were removed. It appears that besides increasing the binding capacity at high conductivities, primary amine based ligands that promote secondary hydrogen bonding interactions can promote binding of proteins that are neutral overall or even positively charged. It is likely these latter proteins contain patches of negative charge. Figure 3.2 indicates that in the presence of the mAb, CHOP removal is significantly less than in the absence of the mAb. Given the pI of the mAb is 7.1, it will have a net negative charge at all the buffer conditions tested and will compete with the CHOP for binding sites, resulting in lower CHOP

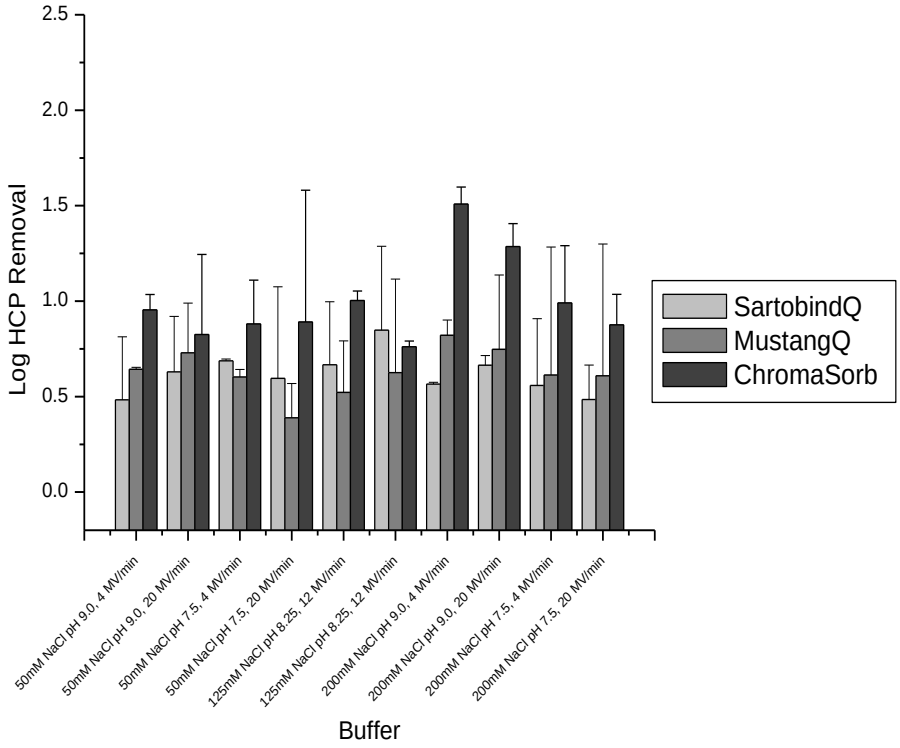

Figure 3.2: Figure 2: CHOP removal for anionic buffer set of experiments in the presence of mAb. The abscissa gives buffer conditions in order of increasing conductivity (see Table 1 for values). All buffers contain 20 mM tris. Uncertainties defined by Log Removal ± 1 standard deviation were determined where the standard deviation is an average for all runs shown in the figure. The uncertainties were ± 0.12 for Sartobind Q, ± 0.15 for Mustang Q and ± 0.18 for ChromaSorb.

clearance. Though there is considerable variability, in general higher pH and low conductivity lead to greater CHOP clearance due to a larger fraction of CHOP being negatively charged and less interference in the Coulombic interaction between the CHOP and ligands.

Figures 3.1 and 3.2 indicate that CHOP removal by Sartobind Q and Mustang Q is significantly less than for ChromaSorb. In the case of quaternary amine based ligands used in these membrane adsorbers, binding depends largely on Coulombic interactions. Consequently, proteins that are neutral or positively charged will have low binding capacity. Figure 3.1 indicates that in the absence of the mAb, the binding capacity decreases as the conductivity of

the feed increases, again highlighting the dominance of Coulombic interactions. Figure 3.2 indicates that for the ChromaSorb, the low pI of the mAb results in competitive binding between contaminant species and the mAb further reducing CHOP clearance. The presence of mAb appears to have less of an effect on CHOP removal by the Sartobind Q and Mustang Q. Figure 3.7 which gives mAb recoveries, indicates, that lower mAb recoveries correspond to lower CHOP clearance by the ChromaSorb.

Results for the cationic buffer set of experiments are given in Figures 3.3 and 3.4 in the absence and presence of the mAb, respectively. The ChromaSorb shows the highest capacity under all feed conditions. This result further suggests that neutral or even positively charged

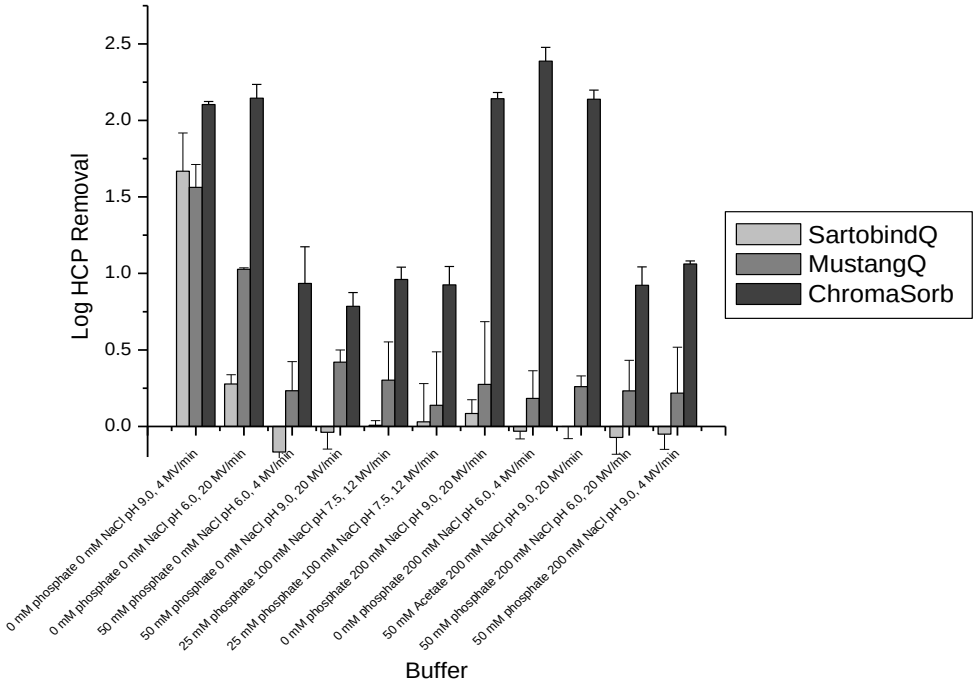

Figure 3.3: CHOP removal for cationic buffer set of experiments in the absence of mAb. The abscissa gives buffer conditions in order of increasing conductivity (see Table 2 for values). All buffers contain 20 mM tris. Uncertainties defined by Log Removal ± 1 standard deviation were determined where the standard deviation is an average for all runs shown in the figure. The uncertainties were ± 0.04 for Sartobind Q, ± 0.12 for Mustang Q, and ± 0.03 for ChromaSorb. Negative value due to inherent assay variability.

proteins may be bound due to secondary hydrogen bonding interactions. Figure 3.3 indicates that unlike MVM removal, almost 1.6 log CHOP removal is observed in the presence of 50 mM phosphate in the absence of NaCl at pH 9.0. In fact, the presence of hydrogen phosphate at low conductivity has little effect on CHOP clearance. It is possible that secondary hydrogen bonding interactions are more effective than for the case of MVM leading to higher CHOP clearance. The presence of NaCl would appear to disrupt hydrogen bonding interactions.

Figure 3.3 indicates that for 50 mM phosphate, 200 mM NaCl at pH 9.0, ChromaSorb

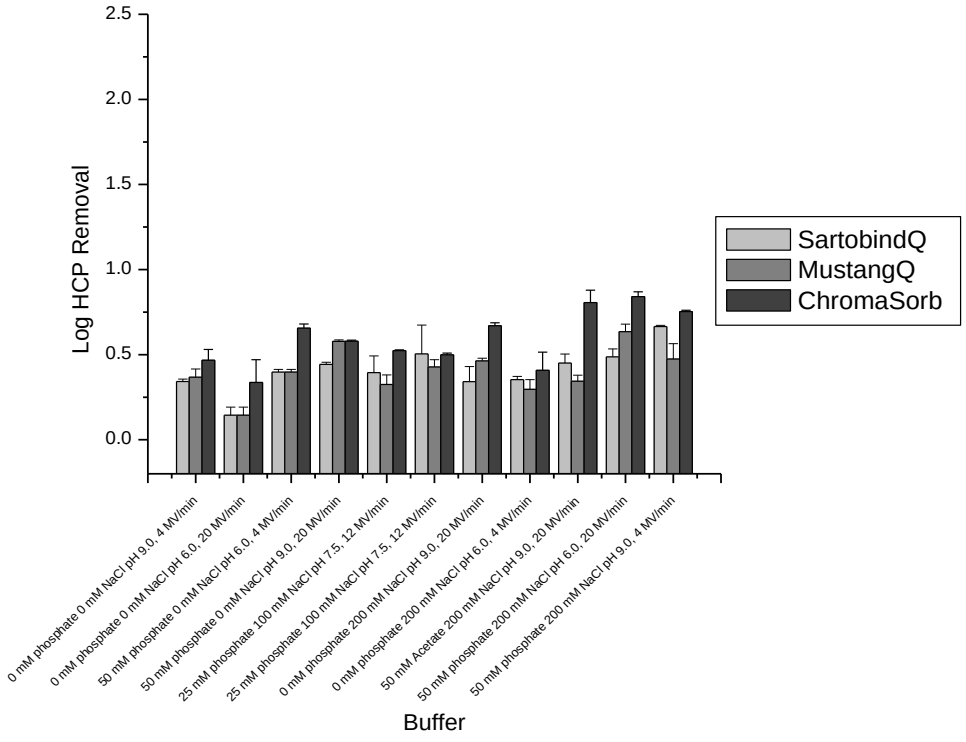

Figure 3.4: CHOP removal for cationic buffer set of experiments in the presence of mAb. The abscissa gives buffer conditions in order of increasing conductivity (see Table 2 for values). Uncertainties defined by ± 1 standard deviation were determined where the standard deviation is an average for all runs shown in the figure. The uncertainties were Log Removal ± 1 standard deviation. The uncertainties were ± 0.02 for Sartobind Q, ± 0.06 for Mustang Q, and ± 0.05 for ChromaSorb.

shows very poor CHOP removal. However, replacing phosphate by acetate almost doubles CHOP clearance. This result highlights the importance of secondary interactions. Since hydrogen phosphate has a double negative charge it will probably interact with two amine groups making the complex neutral. This could explain why CHOP clearance in the presence of acetate at pH 9.0 rather than phosphate leads to much higher CHOP removal. In addition for the primary amine based ligands, acid base interactions between the acetate and phosphate species present will also affect the level of CHOP removal.

The level of CHOP clearance by the primary amine in the presence of phosphate and

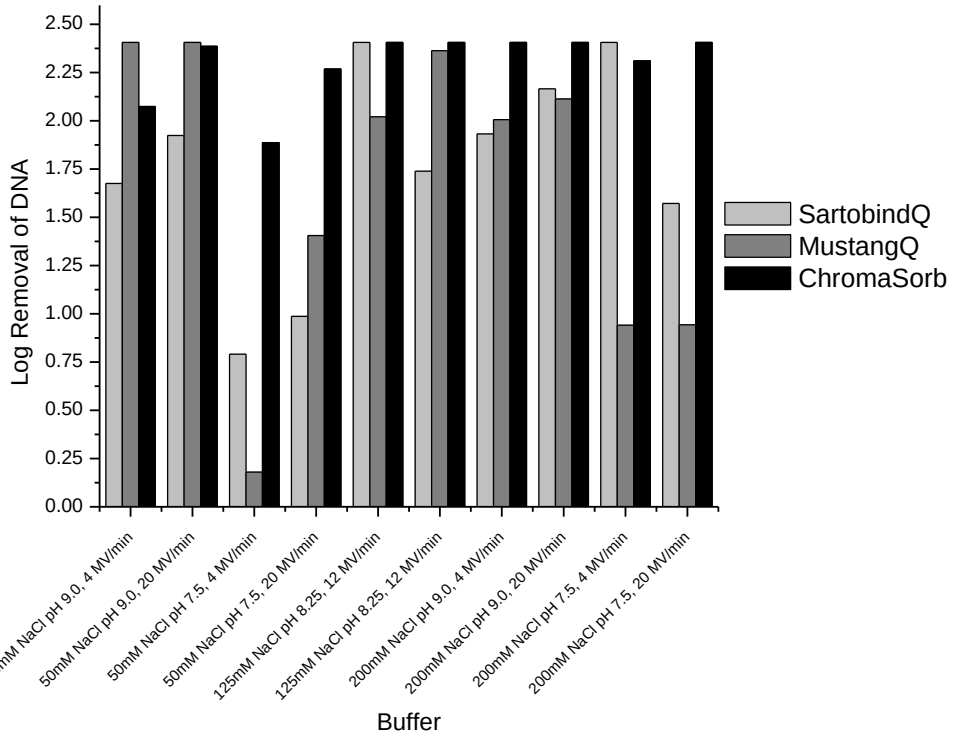

Figure 3.5: DNA removal for anionic buffer set of experiments in the absence of mAb. The abscissa gives buffer conditions in order of increasing conductivity (see Table 1 for values). All buffers contain 20 mM tris. Uncertainties defined by Log Removal ± 1 standard deviation were determined where the standard deviation is an average for all runs in the figure. Uncertainties were ± 0.48 for Sartobind Q, ± 0.24 for Mustang Q and ± 0.02 ChromaSorb for. All values above 2.3 are at limit of detection.

acetate ions is complicated by the fact that the acidity of the conjugate acid of the primary amine and basicity of the acetate and phosphate species present will also affect the extent to which these species will compete for binding sites. In general, the presence of the mAb (Figure 3.4)

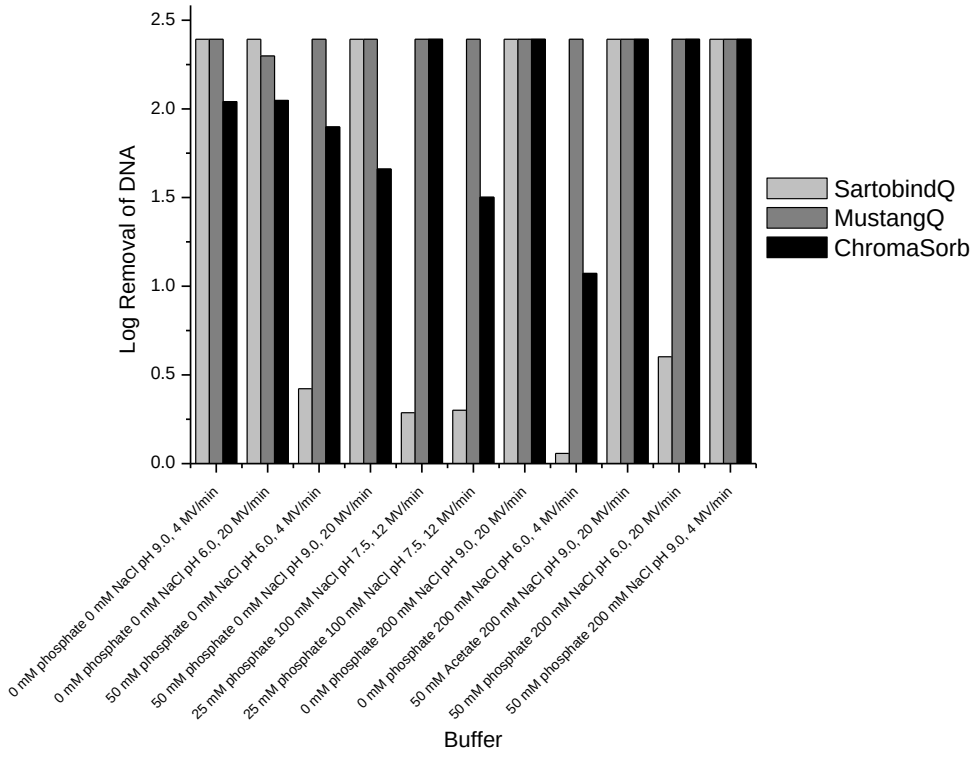

Figure 3.6: DNA removal for cationic buffer set of experiments in the absence of mAb. The abscissa gives buffer conditions in order of increasing conductivity (see Table 2 for values). All buffers contain 20 mM tris. Two centerpoint runs were done (25 mM phosphate, 100 mM NaCl, pH 7.5, 12 MV/min). Uncertainties defined by Log Removal ± 1 standard deviation were determined where the standard deviation is an average for all runs shown in the figure. Uncertainties were ± 0.02 for Sartobind Q, ± 0.02 for Mustang Q and ± 0.62 for ChromaSorb. All values above 2.25 are at limitation of detection.

leads to a significant decrease in CHOP clearance due to competitive binding in agreement with the results in Figure 3.2.

Analogous to the anionic buffer set of experiments Figures 3.3 and 3.4 indicate that CHOP clearance by the Sartobind Q and Mustang Q is generally much lower. One notable

exception is CHOP clearance in Figure 3.3 at pH 9.0 and very low conductivity. In the absence of charge screening and at a high pH above the pI of many of the CHOP proteins, the quaternary amine based ion exchangers display high CHOP clearance. However, in the presence of the mAb, Figure 3.4 indicates that the Sartobind Q and Mustang Q are unsuccessful in clearing CHOP under the same conditions. At pH 9.0, the mAb is charged negatively. As it is present at a much higher concentration, it competes effectively with CHOP for binding sites as evidenced by the low mAb recovery (see Figure 3.8).

Figures 3.5 and 3.6 give DNA removal for the anionic and cationic buffer set of experiments, respectively, in the absence of the mAb. Since the mAb interfered with the assay, no clearance data were obtained in the presence of the mAb. Figure 3.5 indicates that for all conditions investigated, ChromaSorb gave better than or similar clearance to Sartobind Q and Mustang Q. Figure 3.6 indicates that there is significant variability in the results, as seen from the difference in the two centerpoint runs.

Finally, Figures 3.7 and 3.8 give mAb recovery. In general, mAb recovery is better for Sartobind Q and Mustang Q. The results highlight the fact that, while secondary interactions can lead to ion exchange membrane adsorbers that show high contaminant clearance at high ionic strength, these same secondary interactions may lead to high mAb binding and correspondingly lower mAb recovery. Taken together the results indicate that for real systems, clearance of virus, CHOP and DNA occurs competitively. Maximizing removal of all contaminants will require that the total capacity of the membrane adsorber is well in excess of the contaminant species present.

When selecting a membrane adsorber, the expected performance depends on the type of ligand present. Quaternary amine based ligands, which depend largely on Coulombic interactions, show reduced capacities at high ionic strength. Primary amine based ligands can

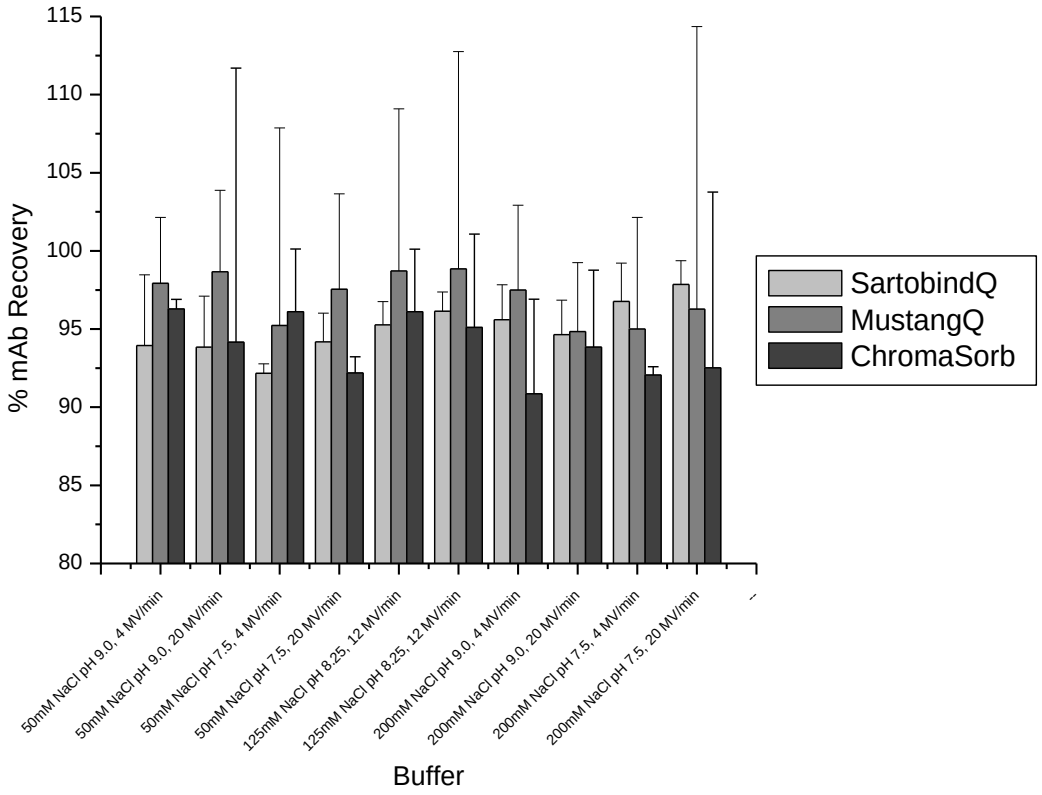

Figure 3.7: Antibody recovery for anionic buffer set of experiments. The abscissa gives buffer conditions in order of increasing conductivity (see Table 1 for values). All buffers contain 20 mM tris. Uncertainties defined by ± 1 standard deviation were determined where the standard deviation is an average for all runs shown in the figure. Uncertainties were Log Removal ± 1% for Sartobind Q, ± 1% for Mustang Q, and ± 1% for ChromaSorb

display high capacities at high ionic strength due to secondary bonding interactions. However, the effect of other ionic species in solution, as well as recovery of the product mAb, can be more difficult to predict as they depend on a balance among Coulombic interactions, hydrogen bonding and other secondary interactions.

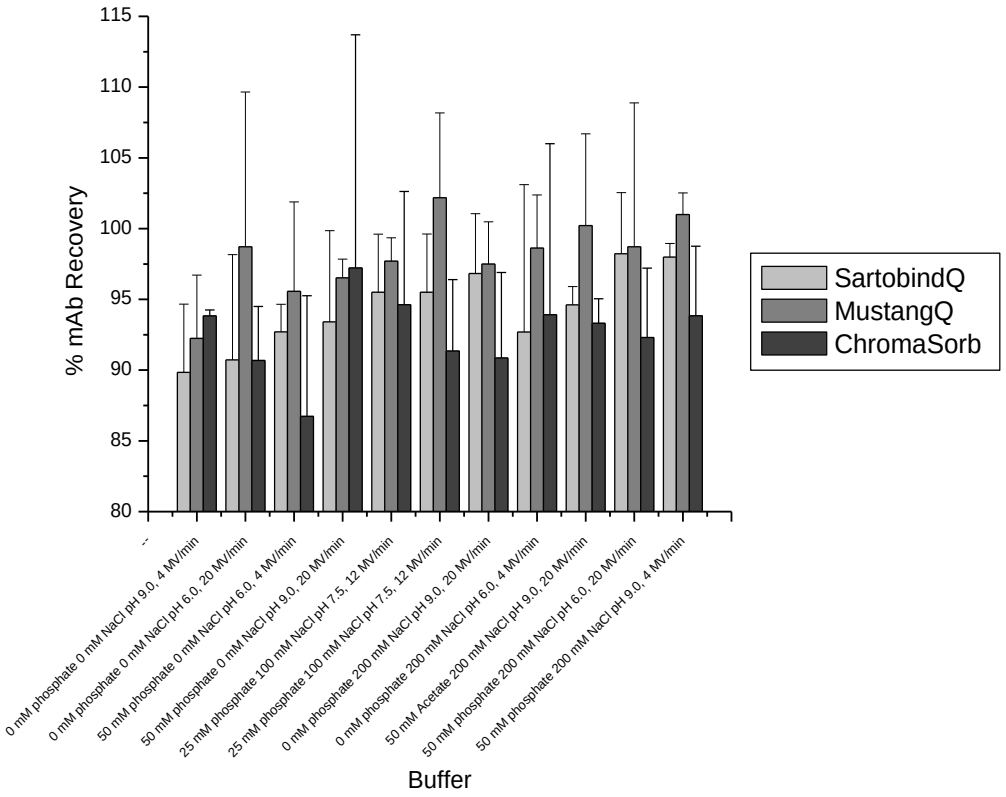

Figure 3.8: Antibody recovery for cationic buffer set of experiments. The abscissa gives buffer conditions in order of increasing conductivity (see Table 1 for values). Uncertainties defined by ± 1 standard deviation were determined where the standard deviation is an average for all runs shown in the figure. Uncertainties were Log Removal ± 1% for Sartobind Q, ± 2% for Mustang Q, and ± 3% for ChromaSorb.

3.5 Conclusions

The Sartobind Q and Mustang Q membranes, both using strong quaternary amine ligands, demonstrated high degrees of removal of MVM and DNA at low NaCl/high pH but showed reduced removal, especially of CHOP, at medium and high NaCl concentration and low pH highlighting the importance of Coulombic interactions. ChromaSorb by contrast showed greater than limit of detection removal of MVM in all buffers not containing phosphate (in the absence of mAb), while reduced binding was observed in the presence of phosphate, especially at higher

pH where hydrogen phosphate was the primary phosphate species. CHOP removal by the ChromaSorb indicates that it is possible to remove neutral as well as positively charged protein species due to secondary binding interactions. DNA clearance was in general high due mainly to Coulombic interactions. Though use of a mAb with a low pI meant that the mAb was negatively charged at the higher pH values investigated and could be bound due to Coulombic interactions, secondary binding effects also were shown to lead to lower recoveries for ChromaSorb.

Predicting the performance of quaternary amine based membrane adsorbers that rely mainly on Coulombic interactions is simpler than for primary amine based adsorbers that display secondary interactions. High conductivity reduces the effect of Coulombic interactions. Furthermore, it is essential that the feed pH be chosen to ensure that the contaminant species are negatively charged. For primary amine based ligands, the existence of secondary bonding interactions means that even neutral or slightly positively charged species could be bound. However, the effect of charged species such as phosphate and acetate in solution is complicated to predict for ligands that show significant secondary bonding effects. The charge and level of hydration of these ionic species will determine their effect on contaminant removal. Lower product recoveries may occur due to higher product binding by secondary interactions.

References

Anouja, F., Wattiez, R., Mousset, S., Caillet-Fauquet. P. 1997. The cytotoxicity of the parvovirus minute virus of mice nonstructural protein NS1 is related to changes in the synthesis and phosphorylation cell proteins. *J Virol*, 71(6): 4671-4678.

Boi, C. 2007. Review; membrane adsorbers as purification tools for monoclonal antibody purification. *J Chromatogr B.* 848(1): 19-27.

Burton, SC., Harding, DRK. 1998. Hydrophobic charge induction chromatography: salt independent protein adsorption and facile elution with aqueous buffers. *J Chromatogr A.* 814(1-2): 71-81.

Cai, P., Huang, Q., Jiang, D., Rong, X., Liang, W. 2006. Microcalorimetric studies on the adsorption of DNA by soil colloidal particles. *Colloids Surface B.* 49(1): 49-54.

Curling, J., Gottschalk, U. 2007, Process Chromatography: Five decades of innovation. *BioPharm Int*. 20(10): 70-94.

Jin, M., Szapiel, N., Zhang, J., Hickey, J., Ghose, S. 2010. Profiling of host cell proteins in two dimensional difference gel electrophoresis (2D-DIGE): Implications for downstream process development. *Biotechnol Bioeng*. 105(2): 306-316.

Johansson, B.-L., Belew, M., Eriksson, S., Glad, G., Lind, O., Maloisel, J.-L., Norrman, N. 2003. Preparation and characterization of prototypes for multi-modal separation media aimed for capture of negatively charged biomolecules at high salt concentrations. *J Chromatogr A.* 1016(1): 21-33.

Klein, E. 2000. Affinity membranes: a 10-year review. *J Membr Sci*. 179(1-2): 1-27.

Knudsen, HL., Fahrner, RL., Xu, Y., Norling, LA., Blank, GS. 2001. Membrane ion-exchange chromatography for process-scale antibody purification. *J Chromatogr A.* 907(1-2): 145-154.

Shirataki, H., Sudoh, C., Eshima, T., Yokoyama, Y., Okuyama, K. 2011. Evaluation of an anion-exchange hollow-fiber membrane adsorber containing x-ray grafted glycidyl methacrylate chains. *J Chromatogr A.* 1218(17): 2381-2388.

Weaver, J., Husson, SM., Murphy, L., Wickramasinghe, SR. 2013. Anion exchange membrane adsorbers for flow-through polishing steps: Part I. Clearance of minute virus of mice, *Biotechnol Bioeng*. 110(2): 491 – 499.

Woo, M., Khan, NZ., Royce, J., Menta, U., Gagnon, B., Ramaswamy, S., Soice, N., Morelli, M., Cheng, K-S. 2011. A novel primary amine-based anion exchange membrane adsorber. *J Chromatogr A.* 1218(32): 5386-5392.

Yang, T., Malmquist, G., Johansson, B-L., Maloisel, J-L., Cramer, S. 2007. Evaluation of multi-modal high salt binding ion exchange materials, *J Chromatogr A.* 1157(1-2): 171-177.

Zhou, JX., Tressel, T. 2006. Basic concepts in Q membrane chromatography for large scale antibody production. *Biotechnol Prog.* 22(2): 341-349.

Zhou, JX., Tressel, T., Gottschalk, U., Solamo, F., Pastor, A., Dermawan, S., Hong, T., Reif, O. Mora, J., Hutchinson, F., Murphy, M. 2006. New Q membrane scale-down model for process-scale antibody purification, *J Chromatogr A.* 1134(1-2): 66-73.

Zhou, JX., Tressel, Yang, X., Seewoester, T. 2008a. Review: implementation of advanced technologies in commercial monoclonal antibody production, *Biotechnol J.* 3(9-10): 1185-1200.

Zhou, JX., Solamo, F., Hong, T., Shearer, M., Tressel, T. 2008b. Viral clearance using disposable systems in monoclonal antibody commercial downstream processing, *Biotechnol Bioeng.* 100(3): 488-496.

Chapter 4

The Role of Polymer Nanolayer Architecture on the Separation Performance of Anion-Exchange Membrane Adsorbers: I. Protein Separations[1]

4.1 Summary

This contribution describes the preparation of strong anion-exchange membranes with higher protein binding capacities than the best commercial resins. Quaternary amine (Q-type) anion-exchange membranes were prepared by grafting polyelectrolyte nanolayers from the surfaces of macroporous membrane supports. A focus of this study was to better understand the role of polymer nanolayer architecture on protein binding. Membranes were prepared with different polymer chain graft densities using a newly developed surface-initiated polymerization protocol designed to provide uniform and variable chain spacing. Bovine serum albumin and immunoglobulin G were used to measure binding capacities of proteins with different size. Dynamic binding capacities of IgG were measured to evaluate the impact of polymer chain density on the accessibility of large size protein to binding sites within the polyelectrolyte nanolayer under flow conditions. The dynamic binding capacity of IgG increased nearly linearly with increasing polymer chain density, which suggests that the spacing between polymer chains

[1]Bhut, BV., Weaver, J., Carter, AR., Wickramasinghe, SR., Husson, SM. 2011, The Role of Polymer Nanolayer Architecture on the Separation Performance of Anion-Exchange Membrane Adsorbers: I. Protein Separations, *Biotechnol Bioeng.* 108(11): 2645 – 2653

*My contributions to the published manuscript presented in this chapter include experimental design of protein dynamic capacity measurements and buffer conditions.

is sufficient for IgG to access binding sites all along the grafted polymer chains. Furthermore, the high dynamic binding capacity of IgG (>130 mg/mL) was independent of linear flow velocity, which suggests that the mass transfer of IgG molecules to the binding sites occurs primarily via convection. Overall, this research provides clear evidence that the dynamic binding capacities of large biologics can be higher for well-designed macroporous membrane adsorbers than commercial membrane or resin ion-exchange products. Specifically, using controlled polymerization leads to anion-exchange membrane adsorbers with high binding capacities that are independent of flow rate, enabling high throughput. Results of this work should help to accelerate the broader implementation of membrane adsorbers in bioprocess purification steps.

4.2 Introduction

Building ‘‘tentacles’’ on a support matrix is an effective method to increase the protein adsorption capacity of chromatography materials (Bowes et al., 2009; Muëller, 1986; Tsuneda et al., 1995). Polymeric tentacles with adsorptive functionality extend into the protein solution that fills the porous volume, providing a scaffold for protein molecules to adsorb. A variety of resin beads for column chromatography (Bowes et al., 2009; Franke et al., 2010; Ghose et al., 2007; Langford et al., 2007; Muëller, 1986; Tao and Carta, 2008; Zhang and Sun, 2002) and macroporous membranes for membrane chromatography (Balachandra et al., 2003; Bhut et al., 2008; Bhut and Husson, 2009; He and Ulbricht, 2008; Singh et al., 2008; Tsuneda et al., 1995) have been modified with adsorptive polymeric tentacles. Incorporating polymeric tentacles into macroporous membranes has even greater importance since the surface area per volume of the membrane is much lower than a bed of resin particles (Bhut et al., 2010; Wang et al., 2009). A

focus of this study was to better understand how membrane performance is affected by the architecture of polyelectrolyte nanolayers grafted from the pores of macroporous membranes.

The separation performance of a membrane adsorber depends on the chemistry and architecture of the adsorptive layer, physical properties of the base membrane and membrane module design (Charcosset, 1998; Ghosh, 2002; Roper and Lightfoot, 1995; Singh et al., 2008; Thömmes and Kula, 1995; Wang et al., 2009; Zeng and Ruckenstein, 1999). Membranes with a high density of adsorptive sites are essential for high-throughput chromatography. However, the accessibility of binding sites and mass transfer characteristics of the adsorptive polymer layer must be good to enable the full utilization of these adsorptive sites. Gebauer et al. (1996) conducted a theoretical analysis of the mass-transfer behavior for ion-exchange membranes with different degrees of grafting. They showed that differences in degree of grafting affect the rate of mass transfer of small size proteins. Camperi et al. (1999) demonstrated that adsorption capacity of lysozyme increases with increasing sulfonate group density for tentacle cation-exchange hollow-fiber membranes. In their study, the sulfonate group density was varied by controlling the extent of reaction during the conversion of epoxy functionality into sulfonate groups; polymer chain graft density was not varied. Ulbricht and coworkers (He and Ulbricht, 2008; Wang et al., 2009) studied the effect of grafting density on the protein adsorption capacities of anion-exchange (He and Ulbricht, 2008) and cation-exchange membrane adsorbers (Wang et al., 2009) prepared by UV grafting. Because conventional photografting methods offer no control mechanism for chain growth, significant irreversible termination may occur, and the grafted polymer chains have relatively higher polydispersity and may have reduced mobility (e.g., radical combination yields chains with both ends tethered to the surface). Thus, the impact of

polymer chain density may be different for this case than for the case when polymer grafting is done using a controlled radical polymerization technique that minimizes chain termination.

Thus, the objectives of this study were to design a surface-initiated, controlled graft polymerization protocol to prepare quaternary amine (i.e., Q-type) anion-exchange membranes with high protein binding capacities and to evaluate the impact of polymer nanolayer architecture on the mass-transfer resistance and accessibility of binding sites for large size biomolecules. Surface-modified adsorptive membranes with different polymer chain graft density, and, thus, different chain spacing, were prepared using surface-initiated atom transfer radical polymerization. Bovine serum albumin (BSA) and immunoglobulin G (IgG) were used for protein binding studies. BSA was selected as a model protein, as is done commonly, to allow comparison with other products reported in the literature. IgG was selected because it is larger in size and has a well-defined structure. We draw attention to the fact that binding studies were done under pH conditions that would not be used in ordinary practice. The reason for selection of these conditions is that our focus was adsorptive membrane development, and we wanted to understand the role of chain density on binding capacity of proteins with different size. Dynamic binding capacities of IgG were measured to evaluate the impact of polymer chain density on the accessibility of these large biomolecules to binding sites within the polyelectrolyte nanolayer under flow conditions. This research provides clear evidence that the dynamic binding capacities of large biomolecules can be much higher for well-designed macroporous membrane adsorbers than commercial ion-exchange adsorbers and resin columns.

4.3 Materials and Methods

4.3.1 Materials

Regenerated cellulose macroporous membranes (RC 60) with 70 mm thickness, 47mm diameter and 1.0 mm average effective pore diameter were purchased from Whatman, Inc. (Piscataway, NJ) These proteins, chemicals and solvents were purchased from Sigma-Aldrich (St. Louis, MO): Albumin from bovine serum (BSA, further purified fraction V, 99%, M_r=66 kDa), 2,2'-bipyridyl (≥99%), 1-bromocarbonyl-1-methylethyl acetate (1-BCMEA, 96%), 2-bromoisobutyryl bromide (2-BIB, 98%), copper(I) chloride (99.995+%), copper(II) chloride (99.99%), ethanol (anhydrous, ≥99.5%), hydrochloric acid (HCl, ACS reagent, 37%), IgG from bovine serum (reagent grade, ≥95% (SDS–PAGE), M_r=150 kDa), [2-(methacryloyloxy) ethyl]trimethylammonium chloride solution (METAC, 80 wt.% in H2O), methanol (≥99.9%), sodium chloride (NaCl, >99.5%), sodium hydroxide (NaOH, ≥98%), tetrahydrofuran (THF, anhydrous, ≥99.9%), tris(hydroxymethyl) aminomethane (Tris–base, ≥99%), and water (ACS reagent, HPLC grade).

4.3.2 Buffers and Chromatography Instrumentation

Loading buffer B1 (20mM Tris–base, adjusted to pH 8 with HCl) was used for BSA static protein binding capacity measurements. Loading buffer B2 (25mM Tris–base, adjusted to pH 9.0 with HCl) and elution buffer E2 (prepared by adding 1M NaCl to loading buffer B2) were used for IgG dynamic binding capacity measurements. Buffers were prepared using distilled water that had been passed through a Milli-Q1 Ultrapure purification system (Millipore Corp., Bedford, MA). All buffers were degassed by ultrasonication immediately prior to use.

Dynamic binding capacities of IgG were measured using an AKTA Purifier 100 chromatography system (GE Healthcare Bio-Sciences, Piscataway, NJ). Membranes were cut

into 16mm diameter discs and equilibrated with loading buffer prior to loading them into a membrane holder. A stack of 6–10 membrane discs was placed between sheets of filter paper (Grade-6, 3mm pore size, Whatman Inc.) and loaded into a Mustang1 Coin Unit (Pall Corporation, Port Washington, NY) to prepare a membrane adsorber. Steel flow distribution discs were present on both sides of the membrane stack. The outer edge of the membrane is covered by an o-ring when it is loaded into the unit. Therefore, the effective filtration diameter of membranes stacked into this module is 14 mm. The actual sample diameter of 16mm was used for calculation of the membrane bed volume because radial distribution of the adsorbing species within the membrane stack is likely to happen during adsorption. Thus, reported capacities are conservative values. The effective filtration diameter (14 mm) was used to calculate the linear flow velocities. Next, the membrane adsorber was attached to the AKTA Purifier. Loading sample was injected using a 50mL capacity SuperloopTM (GE Healthcare Bio-Sciences). The effluent from the membrane adsorber was monitored continuously using UV detection (280nm) and pH and conductivity meters.

4.3.3 Preparation of Strong Anion-Exchange Membranes

4.3.3.1 Membrane Surface Modification

Details of the surface-modification process were given in our previous publications (Bhut et al., 2008; Bhut and Husson, 2009). In the first step, RC60 membranes were activated by covalent anchoring of an ATRP initiator. Membrane activation was carried out in solution at 35 ± 2ºC for 2 h. A typical solution comprised an ATRP initiator precursor, 2-BIB (28–111 mL, 4.5–18.0mM); a non-ATRP-active molecule with similar structure to 2-BIB, 1-BCMEA (0 – 99 mL, 0–13.5 mM); and solvent, THF (50 mL). The solution volume per membrane (50 mL) was kept constant for all experiments. The membrane was placed in a specially designed Teflon cage,

and a magnetic stir bar was placed on the top of the cage to agitate the reaction mixture. Next, the membrane was washed with THF, HPLC water, and ethanol, and dried at 80ºC for 30 min.

Activated membranes were modified further by surface-initiated ATRP. Grafting of polymer with quaternary amine functionality was carried out from the membrane pore surfaces. A typical polymerization solution comprised monomer, METAC (10.4 g, 2.0 M); a catalyst system composed of activator, copper(I) chloride (2.0 mg, 1.0mM), deactivator, copper(II) chloride (0.3 mg, 0.1mM), and ligand, 2,2'-bipyridyl (8.1 mL, 2.2mM); and a mixture of solvents composed of methanol (8.7 mL) and HPLC water (1.8 mL). Here, the values of mass and volume are given per membrane sample, along with the final solution concentrations. To increase measurement accuracy, the batch volumes for the membrane activation and polymerization solutions were scaled-up to allow modification of 5 – 10 membranes at a time, and syringes (Hamilton, Inc., Reno, NV) with range of 0 – 50 or 0 – 100 µL and a precision of ± 1 µL were used for dispensing. Monomer and solvents were mixed in a flask and this mixture was de-oxygenated using a procedure reported earlier (Bhut et al., 2008). The flask was isolated under nitrogen gas and transferred to an oxygen-free glove box, where catalyst components were added. The solution was stirred for 15 min until it became homogeneous. The temperature was raised to 50ºC using a bead bath (ISOTEMP 145D, Fisher, Waltham, MA), and an activated membrane was placed into the reaction mixture.

4.3.3.2 Systematic Control of Polymer Chain Density

The density of polymer chains grafted from the membrane pore surface was controlled by varying the concentration ratio of 2-BIB to 1-BCMEA during the membrane activation. The concentration ratio of 2-BIB to 1-BCMEA was varied from 0.25 to 1.0 by keeping the total

concentration of 2-BIB+1-BCMEA at 18 mM. In a previous study (Bhut and Husson, 2009), we found this concentration to be sufficient to activate the maximum number of –OH groups.

The initiator degree of grafting (DG_{init}) and polymer degree of grafting (DG_{poly}) were determined by weighing the same 5 – 10 membranes before and after each modification step:

$$\mathrm{DGinit} = \frac{w1-w0}{w0} x\ 100\% \qquad (4.1)$$

$$DGpoly = \frac{(w2-w0)}{w0} x\ 100\% \qquad (4.2)$$

w0, w1, and w2 are the masses of unmodified, initiator-activated, and polymer-grafted membranes.

4.3.4 Performance Properties of Surface-Modified Anion-Exchange Membranes

4.3.4.1 Effect of Grafting Density and Polymerization Time on Protein Binding Capacity

BSA was used to measure static protein adsorption capacities of poly(METAC)-modified membranes. BSA concentrations of 1.0 – 3.0 mg/mL were prepared in loading buffer B1. An anion-exchange membrane (47mm dia.) was placed in a glass bottle and incubated in 10mL of BSA solution for 20 h to reach equilibrium in a shaker bath at 22ºC. After 20 h, membranes were removed from the protein solutions and equilibrium protein concentrations were measured as reported earlier (Bhut et al., 2008). Binding capacities were calculated by mass balance using initial and equilibrium concentrations of protein solution determined from a calibration plot.

4.3.4.2 Dynamic Binding Capacity of IgG

IgG was used to measure dynamic binding capacities of poly(METAC)-modified membranes. IgG was dissolved into loading buffer B2 to prepare a 1.0 mg/mL solution. The

protein solution was placed into a shaker bath at 18ºC and agitated overnight. Prior to use, solutions were pre-filtered through disposable cellulose acetate syringe filters with 0.2 mm pore diameter (Puradisc 30, GE Healthcare Bio-Sciences) to remove any protein aggregates. The IgG concentration after pre-filtration was measured using UV absorbance at 280 nm.

The dynamic binding capacities were determined from breakthrough curve analysis. Each run started with passage of 10 column volumes (CVs) of loading buffer to equilibrate the membrane adsorber bed. Next, IgG solution was injected. The bound IgG was eluted with an elution buffer until a stable baseline was observed with UV detection. After every run, the membrane bed was cleaned and regenerated with 5 CVs of 0.5M sodium hydroxide solution, followed by 10 CVs of 1M NaCl solution, and finally rinsed with 20 CVs of loading buffer to prepare the bed for the next run. Three different flow rates (1, 3, and 5mL/min) were used to study the effect of linear flow velocity on the dynamic binding capacities of the anion-exchange membranes. Two measurements were taken at each flow rate, and protein binding capacities are reported as the average of these two measurements. The same membrane bed was used for these measurements. The system dead volume was determined using the retention time of IgG through the bed prepared from a stack of equivalent un-modified membranes (substrate membrane without any treatment). Dynamic binding capacities were calculated at 10% breakthrough and 50% breakthrough using a method described previously (Bhut et al., 2010).

4.4 Results and Discussion

Husson and co-workers (Bhut et al., 2008; Bhut and Husson, 2009) have demonstrated that surface-initiated ATRP can be used to prepare weak anion-exchange adsorptive membranes for bioseparations. For these surface-modified adsorptive membranes, the binding capacity

derives exclusively from the polymer nanolayer (Bhut et al., 2008). The objectives of the current study were to design a surface-initiated graft polymerization protocol to prepare strong anion-exchange membranes with high protein binding capacities and to evaluate the impact of nanolayer architecture on the adsorption and mass transfer properties of large size protein.

4.4.1 Preparation of Strong Anion-Exchange Membranes

Membranes with different polymer chain grafting densities were prepared by activating the surfaces of cellulose macroporous membranes with ATRP initiator groups and using surface-initiated ATRP to graft poly(METAC) chains from the initiator groups, yielding quaternary amine (i.e., Q-type) anion-exchange membranes. In our previous study (Bhut and Husson, 2009), the grafting density was manipulated by using sub-stoichiometric amounts (relative to the number of active –OH groups) of the initiator precursor, 2-BIB, during the membrane-activation step. This method may lead to an uneven distribution of initiator immobilized onto the membrane surface. For example, at low initiator precursor concentration, all of the initiator precursor molecules may react near the external surface of the membrane or at pore entrances as shown in Figure 4.1, resulting in a high density of initiators, and thus polymer chains, at the surface. As we increase concentration, the reactive front may move deeper into the membrane/pores. If high chain density hinders protein binding, then spacing initiator groups, and consequently polymer chains, more uniformly throughout the membrane may lead to higher capacities. In this work, the grafting density of polymer chains, and, thus, the spacing between them, was varied using different concentration ratios of an ATRP initiator precursor (2-BIB) and a non-ATRP-active molecule (1-BCMEA) during the surface-activation step. The hypothesis was that the 1-BCMEA will compete with 2-BIB for –OH groups during surface activation and act as a site blocker to ensure variable spacing between the ATRP initiator groups throughout the

membrane, as shown in Figure 4.1. By keeping a fixed number of reactive molecules (2-BIB+1-BCMEA) well above the stoichiometric amount relative to the membrane –OH groups (Bhut et al., 2008), the distribution of ATRP initiators immobilized onto the membrane surface will be uniform throughout, leading to better uniformity in polymer chain density and possibly higher binding capacities. 1-BCMEA was selected because we wanted the –OH reactivity of the site blocker to be similar to 2-BIB. Bromine and acetate are both electron-withdrawing substituents, with similar impacts on reactivity (McMurray, 1988).

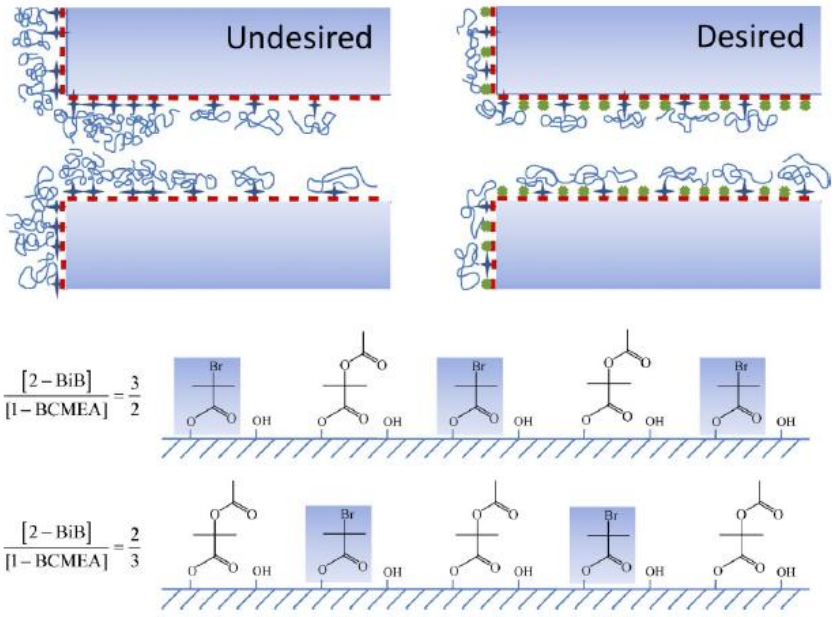

Figure 4.1: Uniform distribution of initiator molecules throughout the membrane pores yields uniformly grafted polymer chains (top right) and avoids locally high densities and potential pore constriction near the membrane external surface (top left). Initiator is spaced apart using a non-ATRP-active molecule. Initiator grafting density was varied by changing the concentration ratio of 2-BIB/1-BCMEA in solution (bottom)

4.4.1.1 Degree of Grafting (DG)

Figure 4.2 shows the dependence of initiator degree of grafting (DG_{init}) and polymer degree of grafting (DG_{poly}) on the concentration ratio of 2-BIB to 1-BCMEA. The percentage of 2-BIB in solution was increased from 40 to 100 mol% during the membrane surface-activation

step. Surface-activated membranes were modified further with poly(METAC) using surface-initiated ATRP for 20 h. The degrees of grafting were calculated from Equations (4.1) and (4.2). Figure 4.2 shows that DG_{init} did not change significantly by increasing the fraction of 2-BIB during the membrane activation step. This observation agreed with our expectation. Since the concentration of 2-BIB+1-BCMEA always exceeded that needed to react fully with all –OH

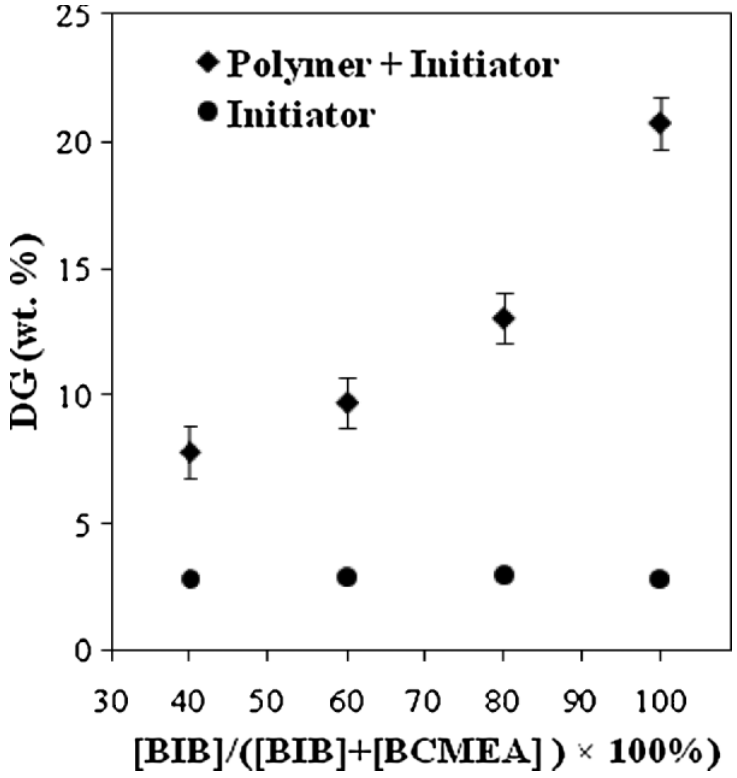

Figure 4.2: Dependence of degree of grafting on the concentration ratio of 2-BIB to 1-BCMEA during membrane activation. Surface-activated membranes were modified further by surface-initiated ATRP (METAC (2M)/Cu(I)/Cu(II)/2,20-bipyridyl: 2000/1/0.1/2.2) for 20 h. Symbols represent degrees of grafting for poly(METAC) (♦) and initiator (2-BIB or 2-BIB+1-BCMEA) (●).

groups in the membrane, and since the two reactive species have similar molecular weight, replacing 2-BIB with 1-BCMEA should not change DG_{init} significantly. However, by increasing the molar fraction of 2-BIB, DG_{poly} increased in a regular fashion. This observation validates our hypothesis that by changing the concentration ratio of ATRP-initiator to non-ATRP-active molecule, the mass of poly(METAC) grafted from the internal pore surface of the membrane can

be varied without changing polymerization time. Increasing initiator density leads to higher chain densities and, thus, increased polymer mass for a given polymerization time. If termination of polymer chains and chain transfer are negligible, as we expect for controlled ATRP and as suggested by the results for protein adsorption (vide infra), then the poly(METAC) chains grafted from the membrane surface should have similar molecular weight. Thus, differences in DG_{poly} result only from differences in the grafting density of poly(METAC) chains. Another observation from Figure 4.2 is that the relationship between the molar fraction of 2-BIB and DG_{poly} is not linear as one would expect if 2-BIB and 1-BCMEA had equal reactivity. Nevertheless, our newly introduced method provides relatively precise control over polymer chain density.

4.4.1.2 Effect of Degree of Grafting and Polymerization Time on Static BSA Binding Capacity

Figure 4.3 shows the dependence of BSA static (equilibrium) binding capacity on the polymerization time and concentration ratio of 2-BIB to 1-BCMEA. As polymerization time increases, the protein binding capacity of poly(METAC)- modified anion-exchange membranes increases relatively linearly at any given concentration ratio of 2-BIB to 1-BCMEA. These results demonstrate clearly that the mass of poly(METAC) grafted from the membrane surface, and, thus, the average molecular weight of polymer chains increases with increasing polymerization time. The nonlinear behavior at higher 2-BIB to 1-BCMEA ratios may indicate deviation from controlled growth. As the grafting density increases, the probability of radical combination increases, and deviations from controlled behavior are seen (Bao et al., 2006). For a constant polymerization time, the BSA static binding capacity increases with increasing molar fraction of ATRP initiator molecule used in the membrane activation step.

Overall, the newly designed two-step graft polymerization protocol offers independent and nearly linear control of grafting density and average molecular weight of poly(METAC) chains grown from cellulose macroporous membranes. The result is anion-exchange membranes with very high per volume BSA binding capacities for membrane chromatographic bioseparations.

4.4.2 Effect of Poly(METAC) Chain Density on the Dynamic Binding Capacity of IgG

The effect of polymer grafting density on the dynamic binding capacity of IgG was evaluated for our newly designed membranes. The isoelectric point (pI) of IgG is about 5.8–7.5 (Baruah et al., 2006; Hahn et al., 1998; Hemmings and Jones, 1974). Working at a pH value 1 unit greater than pI, the IgG carries a net negative surface charge and will bind to an anion-exchange stationary phase (Staby et al., 2000; Staby and Jensen, 2001). Anion-exchange membranes with four different polymer chain densities, and, thus, different spacing between polymer chains, were prepared using surface-initiated ATRP for 20 h. Volumetric flow rate was used as process variable to study the effect of linear flow velocity on the dynamic binding capacities.

4.4.2.1 Dynamic Binding Capacity of IgG

Table 4.1 shows the dependence of dynamic binding capacity on DG_{poly}. Dynamic binding capacity was measured at 10% and 50% breakthrough. The dynamic binding capacity of this large antibody protein increases nearly linearly with increasing DG_{poly}. This observation suggests that the accessibility of IgG to the binding sites along the polymer chains is not impeded by the highest graft densities achieved in this work. If grafting densities were too high, then IgG molecules would be excluded from the polymer layer, and we would expect to see the capacity go through a maximum with respect to polymer chain density (i.e., DG_{poly} since polymerization

time was constant). We do not see such behavior; therefore, it appears that the spacing between polymer chains is enough for IgG to access binding sites all along the poly(METAC) chains grafted from the membrane pore surface. Table 4.1 also compares the utilization of grafted

Table 4.1: Dynamic binding capacity measured at 10% and 50% breakthrough for poly(METAC)-modified membranes (bed height: 420mm; loading buffer B2: 25mM Tris–HCl, pH 9; elution buffer E_2: 1M NaCl in loading buffer B_2; feed solution: 1mg IgG/mL buffer B_2). Surface initiated ATRP (METAC (2M)/Cu(I)/Cu(II)/2,2'-bipyridyl: 2000/1/0.1/2.2) was used for 20 h to produce the anion-exchange membranes.

	Flow rate			IgG dynamic binding capacity (mg/mL)		Polymer utilization (mg IgG/mg poly (METAC)	
DGpoly (% 2-BIB)	mL/min	cm/hr	CV/min	10% breakthrough	50% breakthrough	10 breakthrough	50% breakthrough
9.52 (40)	1	39	12	50	73	0.63	0.92
	3	117	36	52	74		
	5	195	59	49	71		
11.20 (60)	1	39	12	72	96	0.76	1.01
	3	117	36	73	96		
	5	195	59	72	99		
14.01 (80)	1	39	12	87	120	0.69	0.92
	3	117	36	90	118		
	5	195	59	89	116		
21.92 (100)	1	39	12	135	180	0.61	0.81
	3	117	36	138	184		
	5	195	59	134	176		

poly(METAC) at different values of DG_{poly}. The mass of IgG bound per mass of polymer under dynamic process conditions remains nearly constant as grafting density increases. This observation further strengthens our conclusion that the IgG binding is not hindered. This trend contrasts that for resin particles. Franke et al. (2010) discussed the effects of ligand density on the dynamic protein binding capacity for linear polymer chain grafted Fractogel EMD SO_3^- (strong cation-exchange resin, Merck, Darmstadt, Germany). They reported that, at higher grafting densities, the number of overall available sites increases but the number of accessible sites decreases. Thus, the dynamic binding capacity shows a maximum with respect to ligand density. The maximum dynamic binding capacity of Fractogel EMD SO_3^- media with optimized ligand density was reported to be about 60 mg/mL at 181 cm/h for IgG. Our values are

significantly higher. Ghose et al. (2007) studied the effect of ligand density on the dynamic binding capacities of antibodies and Fc-Fusion proteins on various commercial protein A chromatographic media. They demonstrated that ligand utilization decreases with increasing amounts of ligand immobilized on the surface. They attribute this behavior to the spacing limitation and inter-ligand steric hindrance at high ligand density.

Table 4.1 summarizes the effect of linear flow velocity on the dynamic binding capacities of IgG. The flow rate was increased five-fold, and, thus, the residence time for IgG molecules through the membrane bed was decreased by the same factor. The dynamic binding capacities calculated at 10% and 50% breakthrough did not change by increasing linear flow velocity. Protein bound to the membrane bed was recovered during elution with a recovery of 100 ± 2%, suggesting completely reversible protein binding capacities of membrane bed. The shape of the breakthrough curves remained un-changed despite increasing flow rate five-fold. These data demonstrate that the mass transfer of IgG molecules to the binding sites for our newly designed anion-exchange membranes is primarily via convection, not diffusion, which is the rate controlling mechanism for resin beds (Franke et al., 2010; Ghose et al., 2007; Tao and Carta, 2008). If the diffusion of IgG to the binding sites was the rate limiting step, then the dynamic binding capacity of adsorptive material should have varied with residence time inside the adsorptive bed. For example, Franke et al. (2010) demonstrated that the dynamic binding capacity of polymer chain-grafted resin decreases with increasing volumetric flow rate. They concluded that the optimization of ligand density in resins becomes complicated since it is a function of volumetric flow rate. Our membranes do not have such complication.

The contrasting effect of grafting density for resin and membrane substrates may be explained by their structural differences: for membranes, the polymer chains with adsorptive

functionalities (binding sites) are grafted from the surface of macropores; thus, controlled grafting of longer polymer chains (100–200 nm) (Bhut et al., 2008; Singh et al., 2008) in a macroporous membrane substrate does not reduce the pore diameter drastically. As long as the spacing between grafted polymer chains is sufficient, the accessibility of proteins to the binding site is not hindered. While for the resin, the grafting of longer polymer chains in the cylindrical and closed-end, nanometer-sized pores hinders the accessibility to binding sites and slows mass transfer, even for smaller size proteins such as BSA (Zhang and Sun, 2002) and lysozyme (Langford et al., 2007). This effect is exacerbated at high graft densities.

To better understand the limit of grafting density on protein binding capacity, we used Equation (4.3) to estimate the distance between grafted chains (D) as a function of the concentration ratio of 2-BIB to 1-BCMEA used during membrane activation. These values were compared with reported dimensions for the proteins that were tested. Equation (4.3) relates inter-

$$D = \sqrt{\left(\frac{2}{\sqrt{3}\sigma}\right)} \qquad (4.3)$$

chain distance to chain density(s) assuming that each chain occupies a hexagonal volume element. Equation (4.4) was used to determine chain density. M is the average molar mass of the polymer, Na is Avogadro's number, A is surface area per unit mass of the membrane, and s has dimensions of chains/area. The surface area per unit mass of the membrane was found using the BET method to be 1.35m2/g.

$$\sigma = \frac{(DGpoly)Na}{MA} \qquad (4.4)$$

The average molar mass of the grafted polymer chains was determined by first estimating the thickness of the dry polymer nanolayer grafted from the membrane surface. Samadi et al. (2010) provides layer thickness versus time data for ATRP of poly(METAC) using the same

catalyst and solvent system at 25ºC and 0.37M METAC. We have shown for surface-initiated ATRP that the increase in film thickness with time is proportional to the monomer concentration (Sankhe et al., 2006), and that monomer concentration is a constant for controlled polymerization of nanolayer films from low surface area substrates (Gopireddy and Husson, 2002). To account for the difference in polymerization temperature between this study and Samadi et al. (2010), we applied the Arrhenius equation using activation energy of -14 kJ/mol, estimated from Li et al. (2005), who studied the temperature effect on conversion of METAC by ATRP with the same catalyst. With these data, dry layer thickness was estimated from Equation (4.5) to be 250 nm.

$$T(50°C, 2.0M) = T(25°C, 0.37M)x\left(\frac{kp(50°C)}{kp(25°C)}\right)x\left(\frac{[2.0M]}{[0.37M]}\right) \qquad (4.5)$$

This layer thickness was used to determine an approximate molar mass of the polymer, M = 360,000 g/mol, using a linear correlation between molar mass and dry layer thickness found for another methacrylate-based polymer system (Ejaz et al., 1998).

Table 4.2 presents the estimated D values. As expected, this distance decreases (i.e., grafting density increases) with increasing percentage of 2-BIB used during membrane activation. We compared the estimated inter-chain distances with the dimensions for the proteins tested. Serum albumin is reported to be an oblate ellipsoid with dimensions of 14 nm x 4 nm (Bendedouch and Chen, 1983). IgG is reported to have a cross-sectional diameter of 4.8 ± 0.3nm (Mayans et al., 1995). In both cases, one dimension of the protein is similar in size to the estimated inter-chain distances reported in Table 4.2. While more work needs to be done to provide accurate values for the inter-chain distances, our estimates suggest that we should be approaching the chain densities that will result in maximum binding for these two model proteins.

Table 4.2: Estimated inter-chain distances for poly(METAC) grafted from regenerated cellulose macroporous membranes.

[BIB]/([BIB]+[BCMEA]) x 100%	Σ (chains/nm^2)	D_c (nm)	D_h (nm)
40	0.09	3.8	3.6
60	0.12	3.3	3.1
80	0.16	2.8	2.7
100	0.26	2.2	2.1

Overall, results indicate clearly that the spacing between grafted polymer chains is sufficient for IgG to access binding sites all along the polymer chains. Our membranes operate under predominantly convective mass transfer mode and, as a result, the dynamic binding capacity is independent of protein residence time inside the membrane bed. Importantly, the new anion-exchange membranes have high and completely reversible protein dynamic binding capacities, even for a large size protein. Historically, lower dynamic protein binding capacities of membranes have been the bottleneck for implementation of membrane adsorbers in the capture step of protein therapeutics (Charcosset, 1998; Ghosh, 2002; Roper and Lightfoot, 1995; Thömmes and Kula, 1995; Van Reis and Zydney, 2007; Zeng and Ruckenstein, 1999; Zhou and Tressel, 2006). Our current results and those from recent studies (Bhut et al., 2010; Bhut and Husson, 2009; Singh et al., 2008) show sizeable improvements in dynamic capacity that may expand the range of use of membrane adsorbers in bioprocessing. Our design of a strong anion-exchange membrane with unprecedented and flow rate-independent dynamic binding capacity for a model antibody is a highly significant milestone for membrane chromatography.

4.5 Conclusion

Macroporous regenerated cellulose membranes were modified by grafting polyelectrolyte quaternary amine polymers from the pore surface thereby generating strong anion-exchange

membrane adsorbers with three-dimensional binding architecture. It was shown that polymer chain length and density could be independently controlled via polymerization time and initiator concentration. IgG binding capacity was shown to increase with both polymer chain length and density suggesting chain spacing was not a limiting factor. IgG dynamic binding capacities of greater than 130 g/L were realized which is much greater than current commercially available anion-exchange membrane adsorbers. The high capacities shown herein prove the utility of three-dimensional binding layers grafted from pore surfaces.

References

Balachandra, AM., Baker, GL, Bruening, ML. 2003. Preparation of composite membranes by atom transfer radical polymerization initiated from a porous support. *J Membr Sci.* 227: 1–14.

Bao, Z., Bruening, ML., Baker, GL. 2006. Control of the density of polymer brushes prepared by surface-initiated atom transfer radial polymerization. *Macromolecules.* 39: 5251–5258.

Baruah, GL., Nayak, A., Belfort, G. 2006. Scale-up from laboratory microfiltration to a ceramic pilot plant: Design and performance. *J Membr Sci.* 274: 56–63.

Bendedouch, D., Chen, SH. 1983. Structure and interparticle interactions of Bovine Serum Albumin in solution studied by small-angle neutron scattering. *J Phys Chem.* 87: 1473–1477.

Bhut BV., Christensen, KA., Husson, SM. 2010. Membrane chromatography: Protein purification from E. coli lysate using newly designed and commercial anion-exchange stationary phases. *J Chromatogr A.* 1217: 4946–4957.

Bhut, BV., Husson, SM. 2009. Dramatic performance improvement of weak anion-exchange membranes for chromatographic bioseparations. *J Membr Sci.* 337: 215–223.

Bhut, BV., Wickramasinghe, SR., Husson, SM. 2008. Preparation of highcapacity, weak anion-exchange membranes for protein separations using surface-initiated atom transfer radical polymerization. *J Membr Sci.* 325: 176–183.

Bowes, BD., Koku, H., Czymmek, KJ., Lenhoff, AM. 2009. Protein adsorption and transport in dextran-modified ion-exchange media. I: Adsorption. *J Chromatogr A.* 1216: 7774–7784.

Charcosset, C. 1998. Purification of proteins by membrane chromatography. *J Chem Technol Biotechnol.* 71: 95–110.

Camperi, SA., Navarro del Can˜izo AA., Wolman, FJ., Smolko, EE., Cascone, O., Grasselli, M. 1999. Protein adsorption onto tentacle cation-exchange hollow-fiber membranes. *Biotechnol Prog.* 15: 500–505.

Ejaz, M., Yamamoto, S., Ohno, K., Tsujii, Y., Fukuda, T. 1998. Controlled graft polymerization of methyl methacrylate on silicon substrate by the combined use of the Langmuir–Blodgett and atom transfer radical polymerization techniques. *Macromolecules.* 31: 5934–5936.

Franke, A., Forrer, N., Butte, A., Cvijetic, B., Morbidellia, M., Johnck, M., Schulte, M. 2010. Role of the ligand density in cation exchange materials for the purification of proteins. *J Chromatogr A.* 1217: 2216–2225.

Gebauer, KH., Thommes, J., Kula, MR. 1996. Breakthrough performance of high-capacity membrane adsorbers in protein chromatography. *Chem Eng Sci.* 52: 405–419.

Ghosh, R. 2002. Protein separation using membrane chromatography: Opportunities and challenges. *J Chromatogr A.* 952: 13–27.

Ghose, S., Hubbard, B., Cramer, SM. 2007. Binding capacity differences for antibodies and Fc-Fusion proteins on protein A chromatographic materials. *Biotechnol Bioeng.* 96: 768–779

Gopireddy, D., Husson, SM. 2002. Room temperature growth of surface-confined poly(acrylamide) from self-assembled monolayers using atom transfer radical polymerization. *Macromolecules.* 35: 4218–4221.

Hahn, R., Schulz, PM., Schaupp, C., Jungbauer, A. 1998. Bovine whey fractionation based on cation-exchange chromatography. *J Chromatogr A.* 795: 277–287.

He, D., Ulbricht, M. 2008. Preparation and characterization of porous anion-exchange membrane adsorbers with high protein-binding capacity. *J Membr Sci.* 315: 155–163.

Hemmings, WA., Jones, RE. 1974. Isoelectric focusing analysis of transmission of fractions of bovine IgG across the gut of the suckling rat. *Immunology.* 27: 343–350.

Langford, JF Jr., Xu, X., Yao, Y., Maloney, SF., Lenhoff, AM. 2007. Chromatography of proteins on charge-variant ion exchangers and implications for optimizing protein uptake rates. *J Chromatogr A.* 1163: 190–202.

Li, J., Xiao, H., Kim, YS., Lowe, TL. 2005. Synthesis of water-soluble cationic polymers with star-like structure based on cyclodextrin core via ATRP. *J Polym Sci A: Polym Chem.* 43: 6345–6354.

Mayans, MO., Coadwell, WJ., Beale, D., Symons, D., Perkins, SJ. 1995. Demonstration by pulsed neutron scattering that the arrangement of the Fab and Fc fragments in the overall structures of bovine IgG1 and IgG2 in solution is similar. *Biochem J.* 311: 283–291.

McMurray, JE. 1988. Organic chemistry. 2nd edn. Belmont, CA: Thomson Brooks/Cole.

Muller, W. 1986. New phase supports for liquid-liquid partition chromatography of biopolymers in aqueous poly(ethyleneglycol)-dextran systems. Synthesis and application for the fractionation of DNA restriction fragments. *Eur J Biochem.* 155: 213–222.

Roper, KD., Lightfoot, EN. 1995. Separation of biomolecules using adsorptive membranes. *J Chromatogr A.* 702: 3–26.

Samadi, A., Kemmerlin, RK., Husson, SM. 2010. Polymerized ionic liquid sorbents for CO2 separation. *Energy Fuels.* 24: 5979–5804.

Sankhe, AY., Husson, SM., Kilbey, SM II. 2006. Effect of catalyst deactivation on polymerization of electrolytes by surface-confined atom transfer radical polymerization in aqueous solutions. *Macromolecules.* 39: 1376 – 1383.

Singh, N., Wang, J., Ulbricht, M., Wickramasinghe, SR., Husson, SM. 2008. Surface-initiated atom transfer radical polymerization: A new method for the preparation of polymeric membrane adsorbers. *J Membr Sci.* 309: 64–72.

Staby, A., Jensen, IH. 2001. Comparison of chromatographic ion-exchange resins II. More strong anion-exchange resins. *J Chromatogr A.* 908: 149–161.

Staby, A., Jensen, IH., Mollerup, I. 2000. Comparison of chromatographic ion-exchange resins I. Strong anion-exchange resins. *J Chromatogr A.* 897: 99–111.

Tao, Y., Carta, G. 2008. Rapid monoclonal antibody adsorption on dextran-grafted agarose media for ion-exchange chromatography. *J Chromatogr A.* 1211: 70–79.

Thömmes, J., Kula, MR. 1995. Membrane chromatography – An integrative concept in the downstream processing of proteins. *Biotechnol Prog.* 11: 357–367.

Tsuneda, S., Saito, K., Furusaki, S., Sugo, T. 1995. High-throughput processing of proteins using a porous and tentacle anion-exchange membrane. *J Chromatogr A.* 689: 211–218.
Van Reis, R., Zydney, AL. 2007. Bioprocess membrane technology. *J Membr Sci.* 297: 16–50.

Wang, J., Faber, R., Ulbricht, M. 2009. Influence of pore structure and architecture of photo-grafted functional layers on separation performance of cellulose-based macroporous membrane adsorbers. *J Chromatogr A.* 1216: 6490–6501.

Zeng, X., Ruckenstein, E. 1999. Membrane chromatography: Preparation and applications to protein separation. *Biotechnol Prog.* 15: 1003–1019.

Zhang, S., Sun, Y. 2002. Study on protein adsorption kinetics to a dye-ligand adsorbent by the pore diffusion model. *J Chromatogr A.* 964: 35–46.

Zhou, JX., Tressel, T. 2006. Basic concepts in Q membrane chromatography for large-scale antibody production. *Biotechnol Prog.* 22: 341–349.

Chapter 5

The Role of Polymer Nanolayer Architecture on the Separation Performance of Anion-Exchange Membrane Adsorbers: Part II. DNA and Virus Separations[1]

5.1 Summary

The surface-initiated polymerization protocol developed in chapter 4 of this thesis was used to prepare strong anion-exchange membranes with variable polymer chain graft densities and degrees of polymerization for DNA and virus particle separations. A focus of chapter 5 was to evaluate the role of polymer nanolayer architecture on DNA and virus binding. Salmon sperm-DNA (ssDNA) was used as model nucleic acid to measure the dynamic-binding capacities at 10% breakthrough. The dynamic-binding capacity increases linearly with increasing poly ([2-(methacryloyloxy)ethyl]-trimethylammonium chloride) chain density up to the highest chain density used in this study. The new membranes yielded threefold higher ssDNA-binding capacity (30 mg/mL) than a leading commercial membrane with the same functional group chemistry. Elution of bound DNA yielded a sharp peak, and resulted in a 13-fold increase relative to the feed concentration. This concentration effect further demonstrates the highly favorable transport properties of the newly designed Q-type membranes. However, unlike findings in chapter 4 on protein binding, ssDNA binding was not fully reversible. Minute virus of mice (MVM) was used

---

[1]Bhut, BV., Weaver, J., Carter, AR., Wickramasinghe, SR., Husson, SM. 2011, The Role of Polymer Nanolayer Architecture on the Separation Performance of Anion-Exchange Membrane Adsorbers: Part II. DNA and Virus Separations, *Biotechnol Bioeng.* 108 (11): 2654 – 2660

* My contribution to the published manuscript presented in this chapter includes all viral production, viral binding studies and viral quantification assays.

as model virus to evaluate the virus clearance performance of newly designed Q-type membranes. Log reduction of virus (LRV) of MVM increased with increasing polymer chain density. Membranes exhibited > 4.5 LRV for the given MVM impurity load and may be capable of higher LRV values, as the MVM concentration in the flow-through fraction of these samples was below the limit of detection of the assay.

5.2 Introduction

In chapter 4 of this thesis a two-step surface modification protocol was used to prepare strong anion-exchange membranes with high and fully reversible protein-binding capacities for chromatographic bioseparations. Macroporous membranes were modified by grafting polyelectrolyte chains from the pore surfaces using surface-initiated atom transfer radical polymerization (ATRP). Results showed that (1) polyelectrolyte chain density can be varied by changing the concentration ratio of ATRP-initiator to non-ATRP active spacer molecule during membrane activation, and (2) the mass of polyelectrolyte grafted from the membrane surface, and, thus, the average molecular weight of polymer chains increases with increasing polymerization time. Overall, the protocol offers independent and nearly linear control of grafting density and average molecular weight of polyelectrolyte chains grown from cellulose macroporous membranes.

Performance testing was done using two proteins: bovine serum albumin and IgG. The dynamic binding capacity of the larger protein, IgG, was shown to increase nearly linearly with increasing polyelectrolyte chain density, suggesting that the spacing among polymer chains was sufficient for IgG to access-binding sites all along the polymer chains. Furthermore, the dynamic-binding capacity of IgG did not change by increasing linear flow velocity, which

suggests that the mass transfer of IgG molecules to the binding sites is primarily via convection, not diffusion. Overall, the results presented in chapter 4 clearly demonstrated that the accessibility of binding sites and the diffusional mass transfer are not limiting factors for the high dynamic-binding capacities of large size proteins.

Here the newly designed membranes were evaluated for DNA and virus separations. Dynamic-binding capacities of salmon sperm-DNA (ssDNA) were measured to evaluate the impact of polymer chain density on the accessibility of these large biomolecules to binding sites within the polyelectrolyte nanolayer under flow conditions. Volumetric flow rate was used as an independent variable to study the effect of polymer chain density on mass transfer resistance of ssDNA. Membranes also were evaluated for clearance of minute virus of mice (MVM).

5.3 Materials and Methods

5.3.1 Materials

Descriptions of materials used for membrane preparation are provided in chapter 4. UltraPureTM Salmon Sperm DNA Solution in a stock concentration of 10 mg/mL (SS-DNA, 2-kbp size range) was purchased from Life Technologies (Gaithersburg, MD).

Initial pMVM (Minute Virus of Mice prototype strain) and mouse A9 fibroblasts were purchased from ATCC (Manassas, VA). High glucose DMEM media and DMEM containing Trypsin/EDTA and fetal bovine serum (FBS) were obtained from HyClone, a division of Thermo Fisher Scientific (Waltham, MA). Quantification of MVM was accomplished through a quantitative PCR (QPCR) assay developed in our laboratory. iQ SYBR green with fluorescein master mix was purchased from BioRad (Hercules, CA). Forward (5’ GACGCACAGAAAGAGAGTAACCAA 3’) and reverse (5’

CCAACCATCTGCTCCAGTAAACAT 3') primers, originally developed by Ros et al. (2002), were purchased with standard desalting purification from IDT (Coralville, IA). RQ1 DNase enzyme and buffer were purchased from Promega (Madison, WI).

5.3.2 MVM Propagation

Due to the large number of runs conducted during the membrane adsorber performance testing, it was necessary to propagate MVM. A9 cells were thawed and expanded into multiple T-150 culture flasks using high glucose DMEM media with 10% FBS and 100 µg/mL penicillin. Cell culture was performed in jacketed incubators (non-infected and infected cultures in separate incubators) at 37ºC with 10% CO_2. Cultures were expanded and grown to ~ 80% confluence at which point infection with MVM was performed. Infection was accomplished by discarding old growth media from culture (cells were adherent) and incubating cells at 37ºC for 10 min in 1mL DMEM containing $1x10^{10}$ to $1x10^{11}$ virus particles/mL for an multiplicity of infection (MOI) of > 1,000, ensuring efficient infection. An additional 34mL of DMEM media (as described above) was added to the cultures after 10 min incubation to yield a 35mL total culture volume. It was determined that a 6-day infection propagation period was suitable for complete infection/propagation. This time period consistently yielded MVM titers of $1x10^{10}$ to $1x10^{11}$ particles/mL, which was acceptable for use in the membrane adsorber performance tests.

5.3.3 Buffers and Chromatography Instrumentation

5.3.3.1 Buffers

Loading buffer B_1 (25 mM Tris-base with 50 mM NaCl, adjusted to pH 8.0 with HCl) and elution buffer E_1 (prepared by adding 1.15 M NaCl to loading buffer B_2) were used for SS-DNA dynamic-binding capacity measurements. Loading buffer B_2 (20 mM Tris-base at pH 9.0,

with a conductivity of 0.5 mS/cm) and elution buffer E_2 (3 M KCl) were used for virus-binding studies. Buffers were prepared using distilled water that had been passed through a Milli-Q1 Ultrapure purification system (Millipore, Bedford, MA). All buffers were degassed by ultrasonication immediately prior to use.

5.3.3.2 Chromatography Instrumentation

Dynamic-binding capacities of SS-DNA were measured using an AKTA Purifier 100 chromatography system (GE Healthcare Bio-Sciences, Piscataway, NJ). Membranes that had been surface modified with anionic polyelectrolytes were cut into small diameter (16 mm) discs and equilibrated with 20mL of loading buffer in a constant-temperature shaker bath prior to loading them into a membrane holder. A stack of 6–10 membrane discs was placed between sheets of filter paper (Grade-6, 3-mm pore size; Whatman Inc., Piscataway, NJ) and loaded into a Mustang® Coin Unit (Pall Corporation, Port Washington, NY) to prepare a membrane adsorber. Details of membrane adsorber assembly are given in chapter 4. The membrane adsorber was attached to the AKTA Purifier. Loading samples (SS-DNA) were injected using a 50mL capacity SuperloopTM (GE Healthcare Bio-Sciences). The effluent from the membrane adsorber was monitored continuously using UV detection (260nm) and pH and conductivity meters installed in the AKTA Purifier system for online measurements. All data were recorded and viewed in Unicorn 5.1 software (GE Healthcare Bio-Sciences).

All virus-binding studies were performed using an AKTA FPLC (GE Healthcare Bio-Sciences) with FRAC-950 fraction collector. Conditions of the effluent from the membrane adsorber were monitored and recorded continuously during all runs using UV detection (280 nm), a conductivity meter, thermocouple, and pressure transducers installed in the AKTA FPLC. Data were recorded and viewed in Unicorn 5.1. Membrane disks were immersed in 20% (v/v)

ethanol for 5 min to ensure complete wetting and displace trapped air. Membranes were equilibrated with loading buffer prior to loading them into the membrane holder described above. The FPLC system was flushed with water and then running buffer prior to installation of the membrane adsorber. After installation of the membrane adsorber, loading buffer was flowed at a low rate (0.2 mL/min) in the bottom-to-top direction to minimize the possibility of air entering the membrane adsorber. Next, the adsorber was equilibrated by flowing buffer at the test flow rate (2mL/min, 20 column volumes/min, 70 cm/h) in top-to-bottom direction for 10mL or until the effluent conductivity and UV absorbance at 280 nm became stable.

5.3.4 QPCR Development and Protocol

QPCR was performed on a BioRad iQ5 real-time PCR system with iQ5 optical system software v2.0. Runs were performed in unskirted, low-profile 96-well PCR plates (BioRad) with polypropylene microseal ‘‘B’’ adhesive sealers with 20 µL per reaction. The reaction recipe was taken directly from the iQ SYBR Green master mix instructions (given per reaction): 10 µL SYBR Green master mix, 8.2 µL dH2O, 0.4 µL forward primer (final 100 nM), 0.4 µL reverse primer (final 100 nM), and 1 µL sample. MVM standards were created by PCR amplification of a highly conserved 501 bp portion of the MVM genome using the above-mentioned primers and capturing the PCR product in the pCR2.1-TOPO plasmid using a TOPO TA Cloning kit from Invitrogen. Standards ranging from $1x10^9$ copies/mL to $1x10^2$ copies/mL were created by serial dilution of the Maxi-prepped (Qiagen, Valencia, CA) cloned PCR product. Annealing temperature was determined through temperature gradient runs and melt curve analysis; 57ºC resulted in a single dominant melt curve. The initial PCR cycle was 95ºC for 10 min which functioned to open virus particles, denature DNA, and inactivate RQ1 DNase. Then 45 cycles of the following were repeated: denaturing at 95ºC for 15 s, primer annealing at 57ºC for 10 s,

elongation at 72ºC for 45 s, and an additional 10 s at 72ºC to collect the real-time fluorescence data.

The QPCR assay limit of detection was determined by serial dilution of the $1x10^2$ copies/µL standard 2X until a sample with 1 copy/µL was reached. Samples were run in triplicate on a single plate following the above protocol. This plate was repeated two additional times for three total replicate plates and a total of nine replicates per sample. Limit of detection was determined by Probit analysis using Minitab statistical software; the limit of detection was determined to be 14 copies/µL. One microliter of each unknown virus-containing sample was pipetted into 96-well plates containing 9 µL of DNase solution (1 µL RQ1 DNase, 1 µL DNase buffer, and 7 µL of dH2O). The DNase step provided assurance that the QPCR assay would only quantify complete virus particles and not naked DNA, which would not be infective. These plates were sealed and incubated at 37ºC for 40 min. The DNase-treated samples (1 µL each) were pipetted into a BioRad PCR plate with 19 µL of iQ SYBR Green master mix with primers. Eight standards were run with every plate ($1x10^2$ to $1x10^9$ copies/µL) from which a linear standard curve was constructed to quantify unknown samples.

5.3.5 Preparation of Strong Anion-Exchange Membranes

The surface-modification process was carried out in two steps, as detailed in chapter 4. In the first step, regenerated cellulose macroporous membranes (RC 60) were activated by covalent anchoring of an ATRP initiator. Surface-activated membranes were modified further by grafting poly([2-(methacryloyloxy)ethyl]trimethylammonium chloride) (poly(METAC)) chains from the membrane pore surfaces by surface-initiated ATRP.

The density of polymer chains grafted from the membrane pore surface was controlled by varying the molar concentration ratio of an ATRP initiator precursor and a non-ATRP analogue

during the surface-activation step. Chapter 4 details this procedure and the method used for measuring the initiator degree of grafting (DG_{init}) and polymer degree of grafting (DG_{poly}).

5.3.6 Performance Properties of Surface-Modified Anion-Exchange Membranes

5.3.6.1 Effect of Grafting Density on Dynamic-Binding Capacity of SS-DNA

SS-DNA was used to measure dynamic-binding capacities of surface-modified anion-exchange membranes. A 10 mg/mL stock solution of SS-DNA was mixed with loading buffer B_1 to prepare a 60 µg/mL sample solution.

The dynamic-binding capacities were determined from breakthrough curve analysis. For all the measurements, equal experimental conditions were applied starting with passage of 10 column volumes (CVs) of loading buffer to equilibrate the membrane adsorber bed. Next, SS-DNA solution was injected. The bound SS-DNA was eluted with an elution buffer until a stable baseline was observed with UV detection. The mass of SS-DNA in the elution peak was estimated from the area under the elution curve and an independent calibration curve prepared by UV analysis of SS-DNA solutions of known concentration. Three different volumetric flow rates (1, 3, and 5 mL/min; equivalent to 39, 117, and 195 cm/h) were used to study the effect of linear flow velocity on the dynamic-binding capacities of the anion-exchange membranes. A new membrane was used for each run. The system dead volume was determined using the retention time (initial breakthrough) of SS-DNA through the bed prepared from a stack of equivalent un-modified membranes (substrate membrane without any treatment). Dynamic-binding capacities (q, mg SS-DNA/mL column) were calculated at 10% breakthrough, as described in chapter 4.

5.3.6.2 Effect of Grafting Density on Virus Clearance Performance

MVM was used as model virus to evaluate the virus clearance performance of our newly designed Q-type membranes. Virus-loading samples comprised B_2 buffer spiked 1:100 with MVM virus stock solution (MVM Propagation section). Spikes were performed immediately prior to loading to minimize any buffer effects on the virus particles. The load volume was 160 mL for each run. After loading, the membranes were washed with 15mL of B_2 buffer, and virus was eluted with 10mL of E_2 buffer.

5.4 Results and Discussion

In this work, the role of polymer nanolayer architecture on the separation performance of strong anion-exchange membranes was investigated for large biomolecules. The binding capacity of surface-modified membranes is attributed exclusively to the adsorptive polymer nanolayer (Bhut et al., 2008). Chapter 4 was focused on membrane development and the separation of proteins. Here the focus is on the role of polymer chain graft density on the mass transfer resistance and accessibility of DNA and virus molecules to binding sites within the 3-dimensional polymer nanolayer scaffold.

Anion-exchange membranes with different polymer chain grafting densities were prepared using the two-step surface-modification protocol described in chapter 4. In the first step, the surfaces of regenerated cellulose macroporous membranes were activated with ATRP initiator groups using a new formulation that ensures variable spacing between the ATRP initiator groups throughout the membrane. This step was followed by surface-initiated ATRP of poly(METAC), using polymerization time to control the degree of polymerization.

5.4.1 Effect of Poly(METAC) Chain Density on the Dynamic-Binding Capacity of SS-DNA

Strong anion-exchange chromatography is the most widely used unit operation for polishing stage purification to remove trace levels of DNA, virus, host cell protein (HCP) and endotoxins (Ghosh, 2002; Zhou and Tressel, 2006). The efficiency of trace impurity removal is measured using log removal value (LRV). LRV is related directly to the volume of process fluid and, thereby, the adsorption capacity of the membranes. Anion-exchange membranes with high-binding capacity provide higher process capacity. Membrane anion-exchange chromatography in bind-and-elute mode also is under investigation to purify large quantities of plasmid DNA for vaccine and gene therapy applications (Eon-Duval and Burke, 2004; Knudsen et al., 2001; Syre´n et al., 2007). Therefore, a comprehensive set of experiments was conducted to evaluate the effect of polymer chain density on the dynamic-binding capacity of DNA for our newly designed Q-membranes. SS-DNA was used as model nucleic acid to measure the dynamic-binding capacities at 10% breakthrough.

Figure 5.1 shows the bind-and-elute chromatogram for SS-DNA obtained using a newly designed Q-type anion-exchange membrane adsorber prepared using surface activation with [2-BIB]/([2-BIB] + [1-BCMEA] = 0.80. The set of breakthrough curves in Figure 5.1 correspond to multiple runs using the same membrane bed. As quantified and discussed in more detail below, there is significant irreversible adsorption for DNA, which is common for strong anion-exchange media. The breakthrough curves were self-sharpening, indicating highly favorable sorption isotherms under the conditions used for loading. Using an adsorptive material with a self-sharpening breakthrough curve is highly advantageous for large-scale industrial application because it offers maximum utilization of binding capacity before breakthrough (Gebauer et al., 1996; Roper and Lightfoot, 1995). Elution of bound DNA yielded a sharp peak, and more than

95% of the area under the elution curve can be collected in a volume fraction of 2mL (20 CV). The mass of SS-DNA recovered under the elution curve was 1.60 ± 0.05 mg. Taken together, the concentration of the eluted SS-DNA was > 0.8 mg/mL, a 13-fold increase relative to the feed concentration. This concentration effect further demonstrates the highly favorable transport properties of our newly designed Q-membranes.

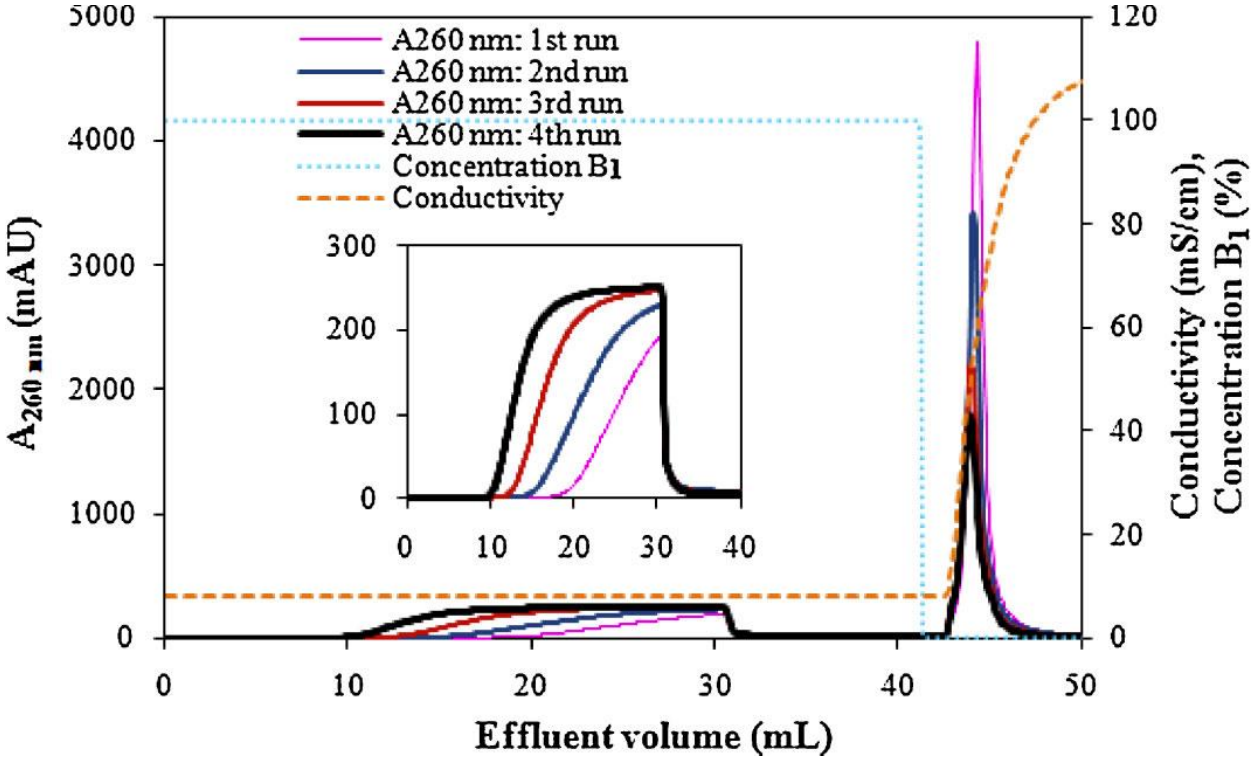

Figure 5.1: Bind-and-elute breakthrough curves of Salmon sperm-DNA obtained using the newly designed strong anion-exchange membrane adsorber (loading buffer B_1: 25mM Tris–HCl + 50mM NaCl, pH 8; elution buffer E_1: 1.15M NaCl in loading buffer B_1; flow rate: 5mL/min; sample load volume: 30 mL). The feed solution was 60 mg SS-DNA/mL buffer B_1. Surface activation ([2-BIB]/([2-BIB] + [1-BCMEA]) = 0.80) and surface-initiated ATRP (METAC (2M)/Cu(I)/Cu(II)/2,20-bipyridyl: 2000/1/0.1/2.2) for 20 h were used to produce the poly(METAC) modified membranes. Solid line (—) breakthrough curves represent the UV absorbance at 260 nm. Dotted line (…) represents the conductivity. Dashed line (---) represents the % of loading buffer B1. The same membrane adsorber bed was used to obtain the four breakthrough curves, labeled as 1st, 2nd, 3rd, and 4th run.

Figure 5.2 shows the effect of DG_{poly} (chain density) on the dynamic-binding capacity of SS-DNA. The dynamic-binding capacity increases linearly with increasing poly(METAC) chain

density up to the highest chain density used in this study. This observation suggests that the accessibility of SS-DNA molecules to the binding sites along the polymer chains is not impeded by the highest graft densities achieved in this work, which were reported in chapter 4. Table 5.1 also compares the utilization of grafted poly(METAC) at different values of DG_{poly}. The mass of SS-DNA bound per mass of polymer under dynamic process conditions remains nearly constant

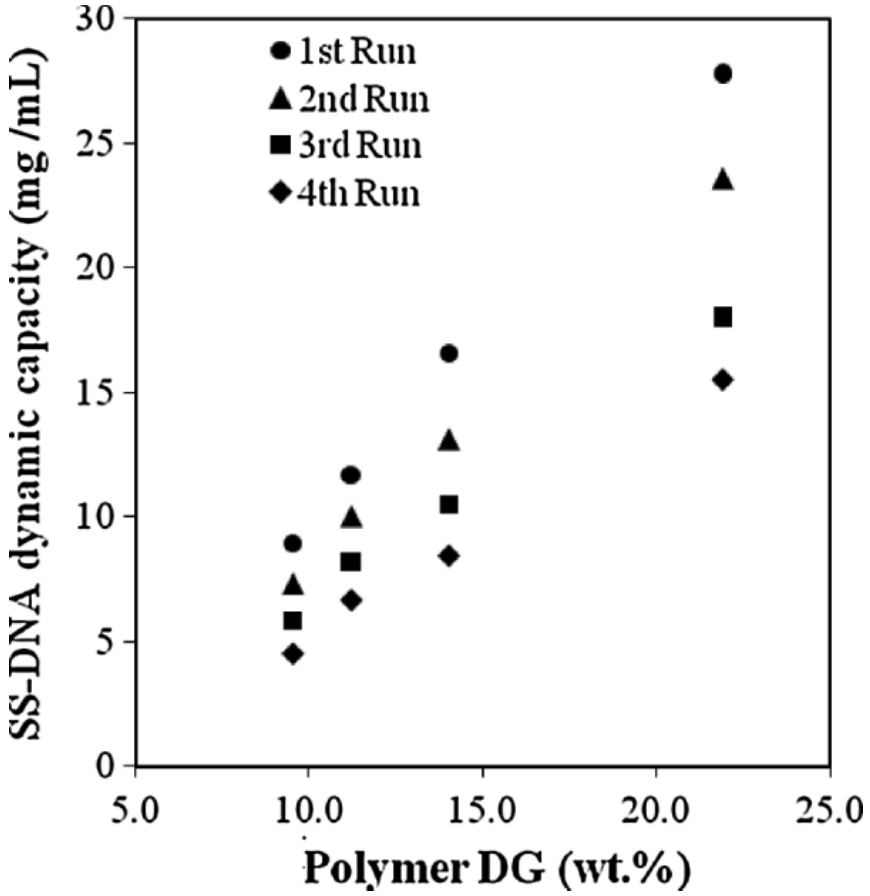

Figure 5.2: Dependence of SS-DNA dynamic-binding capacities on the degree of polymer grafting for poly(METAC)-modified membranes (loading buffer B_1: 25mMTris– HCl + 50mM NaCl, pH 8; elution buffer E_1: 1.15 M NaCl in loading buffer B_1; flow rate: 5mL/min; sample load volume: 20–30 mL). The feed solution was 60 mg SS-DNA/mL buffer B_1. Surface activation ([2-BIB]/([2-BIB] + [1-BCMEA]) = 0.40, 0.60, 0.80, and 1.00) and surface-initiated ATRP (METAC (2M)/Cu(I)/Cu(II)/2,20-bipyridyl: 2000/1/0.1/2.2) for 20 h were used to produce the poly(METAC) modified membranes. Symbols represent the 1st (●), 2nd (▲), 3rd (■), and 4th run (♦) using the same membrane bed.

as grafting density increases. This observation further strengthens our conclusion that the SS-DNA binding is not hindered. Given the large size of the DNA, it appears, perhaps, that insertion of the linear DNA chains in a parallel orientation to the grafted polymer chains allows access to binding sites all along the polymer chains. Considering the large size of DNA [radius of gyration > 50nm for 2.0 kbp size (Latulippe et al., 2007)] and the available adsorptive surface area of membrane [0.53 ± 0.02 m^2/mL (Bhut et al., 2010)], the parallel orientation of DNA is most likely. This orientation is consistent with the findings of Tarmann and Jungbauer (2008), who

Table 5.1: Normalized SS-DNA dynamic-binding capacities at 10% breakthrough for the 1st and 4th runs obtained using poly(METAC)-modified membranes.

	mg ss-DNA/mg PMETAC	
Membrane DG_{poly} (% 2-BIB)	1st run	4th run
9.52 (40)	0.11	0.09
11.20 (60)	0.12	0.10
14.01 (80)	0.13	0.10
21.92 (100)	0.13	0.11

demonstrated using a correlation between theoretical calculations and DNA uptake experiments that the binding of DNA to an ion-exchange resin surface occurred preferential in an upright position. It is clear from the chain densities estimated in chapter 4 that the polymer chains also are oriented (‘‘stretched’’) normal to the surface. To support this claim, the radius of gyration (Rg) for the polymer in a good solvent (water) was calculated using Equation 5.1 for comparison to the estimated inter-chain distances (D) given in chapter 4:

$$R_g = CN^{0.595} \qquad (5.1)$$

C is a constant for a particular polymer, and N is the degree of polymerization of the polymer. For poly(METAC), C value was estimated using data for polymers with similar characteristics, poly[(3-methacryloylamino)propyltrimethylammonium chloride] and poly(2 (dimethylamino)ethyl methacrylate). Based on values for R_g and polymer molar mass reported

by Rivas et al. (2004) and Jiang et al. (2006), we estimated C = 0.38 for poly(METAC). Accordingly, R_g = 30nm for our case. Comparison with the data in chapter 4 shows that D < 2 Rg in all cases, indicating that the grafted chains have adopted the characteristic stretched configuration of a polymer brush (Kilbey et al., 2001).

The dynamic-binding capacity of our newly designed anion-exchange membrane is remarkably high. The literature reports that the DNA dynamic-binding capacity of the commercial Sartobind® Q membrane is much higher than the widely used resins (Eon-Duval and Burke, 2004; Knudsen et al., 2001; Syre´n et al., 2007). Knudsen et al. (2001) reports that the dynamic capacity of Sartobind® Q membrane was about 9 ± 1 mg/mL under the same process conditions used in our study. Therefore, our newly designed membrane has threefold higher SS-DNA-binding capacity than the Sartobind® Q membrane. The same membrane bed was used repeatedly to generate the reversible dynamic capacity data and it was found that the dynamic capacity was not completely reversible. This observation is common for strong anion-exchange media (Eon-Duval and Burke, 2004; Syre´n et al., 2007). The negatively charged DNA strands bind strongly to the strong anion exchangers and are difficult to elute with a salt gradient.

Volumetric flow rate was used as an independent variable to investigate the impact of residence time on the DNA dynamic-binding capacities. The volumetric flow rate was increased fivefold. Table 5.2 shows the results. Surprisingly, the dynamic-binding capacity of DNA increased slightly with increasing volumetric flow rate. We attribute this behavior to the molecular structure of DNA molecules and flow-induced shear forces. Zydney and co-workers (Latulippe et al., 2007; Latulippe and Zydney, 2009) have done extensive studies on the effect of volumetric flow rate on the sieving of DNA through UF membranes. They reported that DNA elongates due to high shear caused by increased flow rate at the pore entrance and that, in turn,

Table 5.2: Dynamic-binding capacity measured at 10% breakthrough for poly(METAC)-modified membranes (bed height: 420mm; loading buffer B_1: 25mM Tris–HCl + 50mM NaCl, pH 8; elution buffer E_1: 1.15 M NaCl in loading buffer B_2; feed solution: 60mg SS-DNA/mL buffer B_2).

Flow rate			Dynamic capacity
mL/min	cm/hr	CV/min	mg ss-DNA/mL
1	39	15	24 ± 0.8
3	117	46	30 ± 1.0
5	195	77	32 ± 0.7

DNA flux increases with increasing flow velocity. As mentioned earlier, insertion of linear DNA chains appears to occur in a parallel orientation to the grafted polymer chains. Thus, at higher volumetric flow rate, the DNA elongates, which may lead to easier insertion and packing into the polymer brush network. In any case, these data demonstrate that the mass transfer of DNA molecules to the binding sites of our macroporous membrane beds is limited primarily by convection; diffusional limitations are minimal.

5.4.2 Effect of Poly(METAC) Chain Density on the Virus Removal Performance

Figure 5.3 shows the effect of DG_{poly} (directly related to chain density) on LRV of MVM. While the LRV initially increases with increasing poly(METAC) chain density, it is not possible to know whether LRV continues to increase for DG_{poly} > 14 wt%. Membranes exhibiting >4.5 LRV for the given MVM impurity load may be capable of higher LRV values; however, the MVM concentration in the flowthrough fraction of these samples was below the limit of detection of the QPCR assay. Increasing the reportable LRV value or viral capacity, without altering the method of detection, is possible by either increasing the concentration of virus in the load solution or increasing the viral load volume. In the case of this study, viral titers of the MVM stock solution were comparable to industrial values, and increasing the concentration by ultrafiltration or other means usually results in altered viral stocks, mainly aggregated virus

particles that display different binding characteristics. Increasing the virus solution load volume is certainly possible; however, because the QPCR assay is not a real-time assay and is labor intensive, a constant load volume was maintained for all evaluation runs to enable more direct comparisons between runs.

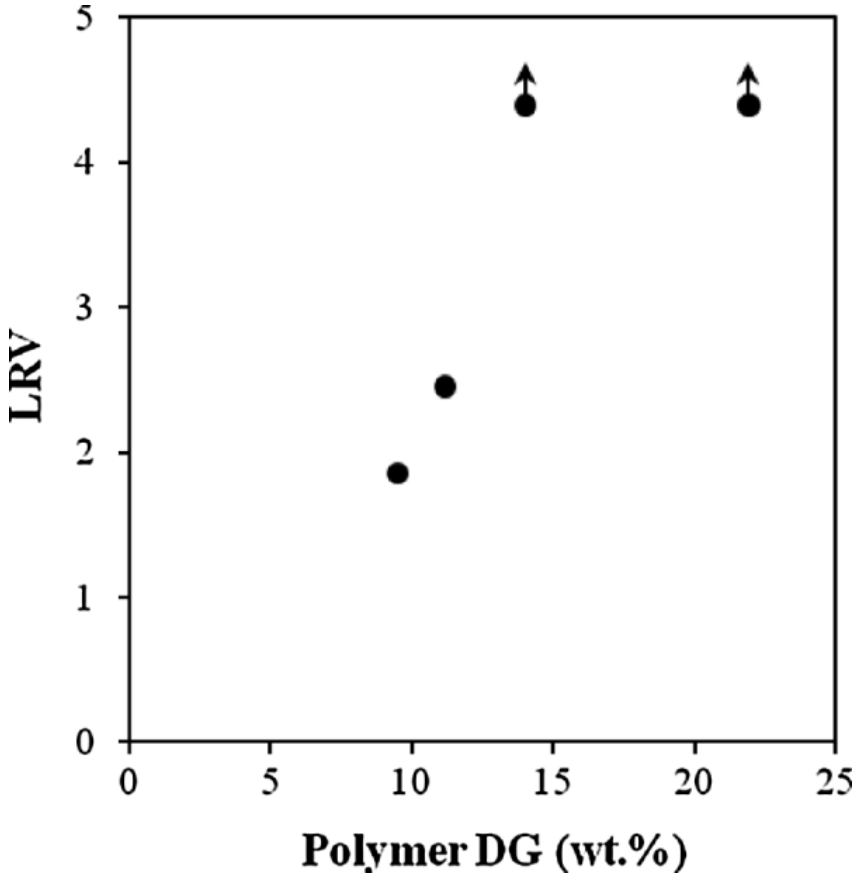

Figure 5.3: Dependence of virus log removal (LRV) performance on the degree of polymer grafting for poly(METAC)-modified membranes (loading buffer B_2: 20mM Trisbase, pH 9.0, conductivity of 0.5 mS/cm; eluent E_2: 10mL 3MKCl; flow rate: 2 mL/min (20 CVs/min, 70 cm/h); sample load volume: 160 mL). The feed solution was loading buffer spiked 1:100 with MVM virus stock solution. Surface activation ([2-BIB]/([2-BIB] + [1-BCMEA]) = 0.40, 0.60, 0.80, and 1.00) and surface-initiated ATRP (METAC (2M)/Cu(I)/ Cu(II)/2,20-bipyridyl: 2000/1/0.1/2.2) for 20 h were used to produce the poly(METAC) modified membranes. Arrows pointing upward indicate that the actual LRV value may be higher for these entries because the concentration of MVM was below the limit of detection.

Despite the inability to determine true LRV values for membranes prepared with the highest poly(METAC) chain densities, it can be said that the achieved value of LRV > 4.5 represents a high level of MVM clearance for a single unit operation (CPMP, 1996). These results are encouraging, but further work with MVM in the presence of protein is needed to truly judge the viral removal capabilities of the membranes.

5.5 Conclusion

The work presented in this chapter continues the research presented in chapter 4. Regenerated cellulose macroporous membranes were prepared with varying strong anionic polymer chain lengths and densities grafted from the pore surface via ATRP. The binding of larger solutes such as DNA and viral particles were explored in this chapter. Single-stranded sperm DNA binding was evaluated as a function of chain length and density. The dynamic binding capacity of DNA increased up to the maximum achievable chain density and with increasing polymer chain length. Minute Virus of Mice binding capacity also increased with both polymer chain length and density; viral clearance is directly applicable to all biologics purification in the pharmaceutical industry.

References

Bhut, BV., Wickramasinghe, SR., Husson, SM. 2008. Preparation of high capacity, weak anion-exchange membranes for protein separations using surface-initiated atom transfer radical polymerization. *J Membr Sci.* 325: 176–183.

Bhut, BV., Christensen, KA., Husson, SM. 2010. Membrane chromatography: Protein purification from E. coli lysate using newly designed and commercial anion-exchange stationary phases. *J Chromatogr A.* 1217: 4946–4957.

Committee for Proprietary Medicinal Products (CPMP). 1996. Note for guidance on virus validation studies: the design, contribution and interpretation of studies validating the inactivation and removal of viruses [monograph on the Internet]. CPMP/BWP/268/95. London: The European Agency for the Evaluation of Medicinal Products. Available from: http://www.emea.eu.int/pdfs/human/bwp/026895en.pdf.

Eon-Duval, A., Burke, G. 2004. Purification of pharmaceutical-grade plasmid DNA by anion-exchange chromatography in an RNase-free process. *J Chromatogr B.* 804: 327–335.

Gebauer, KH., Thömmes, J., Kula, MR. 1996. Breakthrough performance of high-capacity membrane adsorbers in protein chromatography. *Chem Eng Sci.* 52: 405–419.

Ghosh, R. 2002. Protein separation using membrane chromatography: Opportunities and challenges. *J Chromatogr A.* 952: 13–27.

Jiang, XL., van der Horst, A., van Steenbergen, MJ., Akeroyd, N., van Nostrum, CF., Schoenmakers, PJ., Hennink, WE. 2006. Molar-mass characterization of cationic polymers for gene delivery by aqueous size-exclusion chromatography. *Pharmaceut Res.* 23: 595–603.

Kilbey, SM. II, Watanabe, H., Tirrell, M. 2001. Structure and scaling of polymer brushes near the u condition. *Macromolecules.* 34: 5249–5259.

Knudsen, HL., Fahrner, RL., Xu, Y., Norling, LA., Blank, GS. 2001. Membrane ion-exchange chromatography for process-scale antibody purification. *J Chromatorg A.* 907: 145–154.

Latulippe, DR., Zydney, AL. 2009. Elongational flow model for transmission of supercoiled plasmid DNA during membrane ultrafiltration. *J Membr Sci.* 329: 201–208.

Latulippe, DR., Ager, K., Zydney, AL. 2007. Flux-dependent transmission of supercoiled plasmid DNA through ultrafiltration membranes. *J Membr Sci.* 294: 169–177.

Rivas, BL., Pereira, ED., Horta, A., Renamayor, CS. 2004. Macromolecular size of polyelectrolytes containing ammonium and sulfonic acid groups, as determined by light scattering. *Eur Polym J.* 40: 203–209.

Roper, KD., Lightfoot, EN. 1995. Separation of biomolecules using adsorptive membranes. *J Chromatogr A.* 702: 3–26.

Ros, C., Burckhardt, C., Kempt, C. 2002. Cytoplasmic trafficking of minute virus of mice: Low-pH requirement, routing to late endosomes, and proteasome interaction. *J Virol.* 76: 12634–12645.

Syren, P., Rozkov, A., Schmidt, SR., Stromberg, P. 2007. Milligram scale parallel purification of plasmid DNA using anion-exchange membrane capsules and a multi-channel peristaltic pump. *J Chromatogr B.* 856: 68–74.

Tarmann, C., Jungbauer, A. 2008. Adsorption of plasmid DNA on anion exchange chromatography media. *J Sep Sci.* 31: 2605–2618.

Zhou, JX., Tressel, T. 2006. Basic concepts in Q membrane chromatography for large-scale antibody production. *Biotechnol Prog.* 22: 341–349.

Chapter 6

Responsive Membranes for Hydrophobic Interaction Chromatography[1]

6.1 Summary

Poly N-vinylcaprolactam (PVCL) chains were grown from the surface of regenerated cellulose membranes using atom transfer radical polymerization (ATRP). Modified membranes were characterized using scanning electron microscopy, infrared spectroscopy, X-ray photoelectron spectroscopy and by measuring surface contact angles. The grafting degree of PVCL increases with increasing ATRP initiator immobilization time. PVCL is a thermo-responsive polymer with a lower critical solution temperature (LCST) that depends on the concentration of salt ions present in solution. The LCST decreases below room temperature in buffer containing 1.8 M $(NH_3)_2SO_4$ where the polymer adopts a more hydrophobic/collapsed conformation. At low ionic strength, the LCST remains above room temperature. Contact angles for PVCL in 20 mM phosphate buffer with and without 1.8 M $(NH_3)_2SO_4$ were determined. Contact angles in the buffer with high ionic strength were higher than those in low ionic strength.

Adsorption and desorption of bovine serum albumin (BSA) and immunoglobulin G (IgG) have been investigated. Loading was conducted in high ionic strength buffer. Elution was conducted in low ionic strength buffer. By using a responsive ligand that changes its

[1]Himstedt, HH., Qian, X., Weaver, JR., Wickramasinghe, SR. 2013. Responsive membranes for hydrophobic interaction chromatography. *J Membr Sci.* 447: 335-344

*My contribution to the manuscript presented in this chapter includes experimental planning, data analysis, and a portion of the chromatography work.

conformation during loading and elution, high protein recoveries were obtained. Ligands that respond to solution ionic strength show promise for high performance hydrophobic interaction chromatography.

6.2 Introduction

Chromatography is frequently used in the biotechnology industry to isolate and purify protein based therapeutics. Here the term chromatography is used to represent any packed bed process as is a common practice in the biotechnology industry. Membrane adsorbers have been proposed as alternatives to traditional packed columns that contain chromatographic resin particles (Klein, 2000; Ghosh et al, 2002). One of the first descriptions of membrane adsorption or membrane chromatography as a process of commercial relevance was by Brandt et al (Brandt et al, 1988). A macroporous membrane is used as a support material and ligands are attached to the surface of the membrane pores.

Packed bed chromatography suffers from a number of limitations (Specht et al, 2004; Wickramasinghe et al, 2006; Thömmes el al, 1995). The pressure drop across the bed is usually high and may increase during operation due to media deformation. Porous particles are used where the majority of the binding sites are located on the surface of the internal pores. While this leads to increased capacity, pore diffusion is often slow and leads to early breakthrough and incomplete usage of the packed bed. Adsorptive membranes overcome all of these limitations (Specht et al, 2004). The feed is pumped through the macroporous membrane pores, thus eliminating pore diffusion. The pressure drop is much lower compared to packed beds since the flow path is much shorter. In addition scale up of membrane modules is much easier than packed beds.

Membrane adsorbers are a subset of a much larger group of membrane based separation devices known as membrane contactors. Common examples include non-dispersive liquid-gas and liquid-liquid contactors. Membrane adsorbers represent a liquid-solid contactor (Kovvali el al, 2003). Today membrane adsorbers are used routinely in the biopharmaceutical industry in flow through polishing steps. Anion exchange membranes are used to bind large contaminant species such as virus particles, host cell proteins and DNA (Weaver et al, 2013; Weaver et al, 2013). Slow pore diffusion renders packed beds particularly inefficient for removal of these large contaminant species. In this method of operation, since contaminant species are bound to the membrane, there is no need for elution and regeneration of the membrane; however, the adsorber is only suitable for single use.

Membrane adsorbers may also be used in bind and elute applications (Specht et al, 2004; Endres et al, 2003; Teeters et al, 2003). Recent publications indicate growing commercial interest in the use of membrane adsorbers to bind and elute target solutes (Kuczewski et al, 2010; Vogel et al, 2012). Here we focus on membrane adsorbers for use in hydrophobic interaction chromatography (HIC). Traditional HIC depends on reversible interactions between the hydrophobic surface patches on proteins and hydrophobic ligands attached to chromatographic resin particles (Lienqueo et al, 2007). Proteins are typically loaded at high salt concentration and eluted with decreasing salt concentration (Chen et al, 2007). Factors that affect protein adsorption and recovery in HIC include protein hydrophobicity and size, ligand chemistry, type and concentration of salt and buffer pH (Lienqueo et al, 2007). Both salt-induced protein precipitation and HIC depend on surface hydrophobicity of proteins (Nfor et al, 2001; Melander et al, 1977; Porath et al, 1973). Due to differences in the interaction between the ligands and different proteins the concentration of salt needed for adsorption can vary considerably, allowing

different selectivities for different proteins (Machold et al, 2002; Melander et al, 1989; Fausnaugh et al, 1986).

Membrane based HIC affords all of the advantages of membrane adsorbers: dynamic capacities that are independent of flow rate, higher throughput and easy scale up (Hahn et al, 2003; Kubota et al, 1997; Yoo et al, 2012; Yu et al, 2008; Ghosh et al, 2006; Ghosh, 2001). Recent studies indicate a growing industrial interest in membrane based HIC. Here we focus on the use of stimuli-responsive membranes for HIC (Kuczewski et al, 2010; Vogel et al, 2012; Frau et al, 2009). Stimuli-responsive membranes change their physiochemical properties due to change in environmental conditions such as pH, temperature, ionic strength, etc (Wandera et al, 2010). These physiochemical changes can lead to changes in membrane performance.

Here poly N-vinylcaprolactam (PVCL) is grafted from the surface of commercially available microfiltration membranes. PVCL displays a lower critical solution temperature (LCST) at around 32 °C (Maeda et al, 2002). In solution, PVCL phase separates at temperatures above the LCST (Vihola et al, 2002). Crosslinking PVCL results in a thermally responsive hydrogel that dehydrates at temperatures above its LCST but swells below its LCST (Peng et al, 2001; Ling et al, 2009; Ramos et al, 2012). When grafted to a solid surface such as a chromatographic particle or membrane, the PVCL nanostructure will swell and collapse below and above its LCST, respectively (Prabaharan et al, 2008).

Previous investigators have proposed the use of temperature-responsive ligands for hydrophobic interaction chromatography (Kanazawa et al, 1996; Miserez et al, 2010). At temperatures above the LCST the ligands adopt a collapsed conformation that promotes protein adsorption. The temperature is reduced below the LCST during elution where the ligands adopt a

more hydrated conformation promoting protein desorption. However, changing temperature during operation is undesirable for bioseparations where purification is often conducted at 4 °C.

The dependence of LCST on ionic strength, however, may be exploited in HIC (Maeda et al, 2002). As the ionic strength increases, the LCST will decrease. The actual decrease in LCST depends on the ionic species present (Du et al, 2010; Du et al, 2011). For example Maeda et al. (Maeda et al, 2002) indicate that the LCST of PVCL decreases to below 20 °C in the presence of 1.0 M KCl. In addition the LCST depends on the degree of polymerization of N-vinylcaprolactam (Ieong et al, 2012). Consequently, when conducting HIC at room temperature (approximately 25 °C) at high salt concentration above its LCST, PVCL will adopt a collapsed conformation that will promote protein adsorption. At low salt concentration, the LCST remains above room temperature. This will lead to a more swollen conformation which will promote desorption of the adsorbed protein at room temperature.

Huang et al. (Huang et al, 2009) have modified commercially available polyvinylidene fluoride membranes by UV-initiated graft polymerization in order to graft a hydrogel consisting of cross-linked PVCL. They show that at high ionic strength the grafted nanostructure collapses due to exclusion of water. At low salt concentration, hydration leads to swelling of the grafted layer. The use of stimuli-responsive ligands should lead to higher recovery of adsorbed protein. In a more recent study Mah and Ghosh (Mah et al, 2010) used a PVCL based ligand to purify humanized Immunoglobulin (hIgG) using HIC. PVCL is desirable for bioseparations compared to similar temperature-responsive polymers, as it is very stable against hydrolysis and is more biocompatible (Maeda et al, 2002; Vihola et al, 2002; Ramos et al, 2012). The use of a ligand as well as buffer conditions that actively promote adsorption and desorption should lead to high

capacity as well as product recovery. However, recent studies indicate that it is often difficult to obtain both high capacity and high recovery (Huang et al, 2009; Mah et al, 2010).

Here atom transfer radical polymerization (ATRP) is used to grow PVCL chains from the surface of commercially available regenerated cellulose microfiltration membranes. ATRP is a controlled polymerization technique that allows both chain density and molecular weight to be varied independently (Himstedt et al, 2012). Further the polydispersity of the grafted chains is much lower than for less controlled polymerization methods. Since the LCST depends slightly on chain molecular weight (Ieong et al, 2012), obtaining a more uniform molecular weight distribution will lead to a sharper transition between the collapsed and swollen conformation at the LCST. This in turn should lead to higher protein recovery. Protein binding capacity can be maximized by optimizing chain density.

Here binding capacity and recovery for bovine serum albumin (BSA) and a monoclonal antibody have been determined. Unlike earlier studies the grafted PVCL chains are not cross linked. It is likely that cross-linked chains will be more constrained, limiting their response at the LCST. Regenerated cellulose membranes were chosen to minimize non-specific binding of the target solute to the base membrane.

6.3 Materials and Methods

6.3.1 Chemicals

All purified water (0.06 μS/cm) was obtained from a combination Water Pro/RO reverse osmosis and Pro Plus deionization purification system from Labconco Corp. (Kansas City, MO). All chemicals were 97% or higher purity unless otherwise noted. Triethylamine (TEA), and 4-N,N-dimethylaminopyridine (DMAP) were purchased from Fluka (Munich, Germany); ethanol

(pure), methanol, acetonitrile, and hydrochloric acid (6 M) were purchased from VWR (West Chester, PA); α-bromoisobutyrlbromide (BiB), boric anhydride, bovine serum albumin (>99%, product #A7638), immunoglobulin G from human serum (>95%, product #I4506), N-vinylcaprolactam (VCL), CuCl, $CuCl_2$, $CuBr_2$, 2,2'-bipyridine (BPY), and N,N,N′,N′,N″-pentamethyldiethylenetriamine (PMDTA) were purchased from Sigma-Aldrich (St. Louis, MO). Sodium phosphate monobasic, sodium phosphate dibasic, and ammonium sulfate were purchased from JT Baker (Phillipsburg, NJ). Regenerated cellulose membranes (0.45 μm) were purchased from Whatman (Piscataway, NJ) as 47 mm diameter discs. Two 20 mM phosphate buffers containing 0 and 2.4 M ammonium sulfate at pH 7.0 were made in-house and vacuum filtered using Whatman 0.2 μm pore diameter PES sterile membrane filters (Piscataway, NJ). Additional buffers containing 1.5, 1.8, and 2.1 M ammonium sulfate were prepared by dilution of the 2.4 M ammonium sulfate buffer.

6.3.2 Membrane Modification

To prepare the initiator immobilization solution 61 mg DMAP and 1387 μL TEA were dissolved in 100 mL of distilled acetonitrile. Boric anhydride (3 g) were added to 150 mL of acetonitrile, and the mixture was heated in a 125^{o}C oil bath for 30 minutes. A water-filled cooling column was attached during heating to collect the distilled acetonitrile. Individual membrane samples were placed into jars containing 15 mL of this solution. 150 μL of BiB initiator were added to each jar, which was quickly sealed. The membranes were reacted in the immobilization solution for a desired amount of time (1-24 hours), on a shaker table. The membrane discs were then removed from the jar, rinsed twice with DI water and then placed in excess DI water on a shaker table for 4 hours. The membranes were then dried in a 30^{o}C vacuum oven for at least four hours. This reaction is illustrated in Figure 6.1a.

The ATRP reaction solution was prepared by dissolving 525 mg BPY, 27 g VCL monomer, and 30.24 mg $CuCl_2$ in 150 mL equal parts DI water and methanol. This solution was degassed with argon under strong stirring for 15 minutes. 148.5 mg CuCl was then added. The solution was degassed for an additional 15 minutes under strong stirring. Four membrane discs were placed into flasks which were then thrice evacuated and back-filled with argon. 10 mL of ATRP solution was injected into each flask, and the reaction proceeded at room temperature for 12 hours. This reaction is illustrated in Figure 6.1b.

Following the reaction, the membranes were placed in a quenching solution consisting of 500 mg $CuBr_2$ and 1250 μL PMDETA in 100 ml equal parts DI water and methanol to stop the polymerization. After 10 minutes in the quenching solution the membranes were washed with Milli-Q water for 2 minutes, washed with methanol for 1 minute, and placed in excess DI water on a shaker table for 4 hours. The membranes were then dried in a vacuum oven at 30^{o}C for at least four hours. This reaction is illustrated in Figure 6.1c.

6.3.3 Degree of Grafting

The amount of PVCL which was grafted onto the membrane, the degree of grafting (DG), was calculated by dividing the difference in mass of the membrane before and after ATRP grafting by the cross-sectional area of the membrane.

$$DG = \frac{m_{ATRP} - m_{base}}{A_{cross}} \qquad (6.1)$$

Since regenerated cellulose membranes are hygroscopic, it was critical to standardize mass measurements. Before a membrane was weighed, it was first dipped in ethanol and dried in a vacuum oven at 30^{o}C for one hour. The membrane was removed from the oven and allowed to rest at atmospheric conditions for 30 minutes before the mass was recorded.

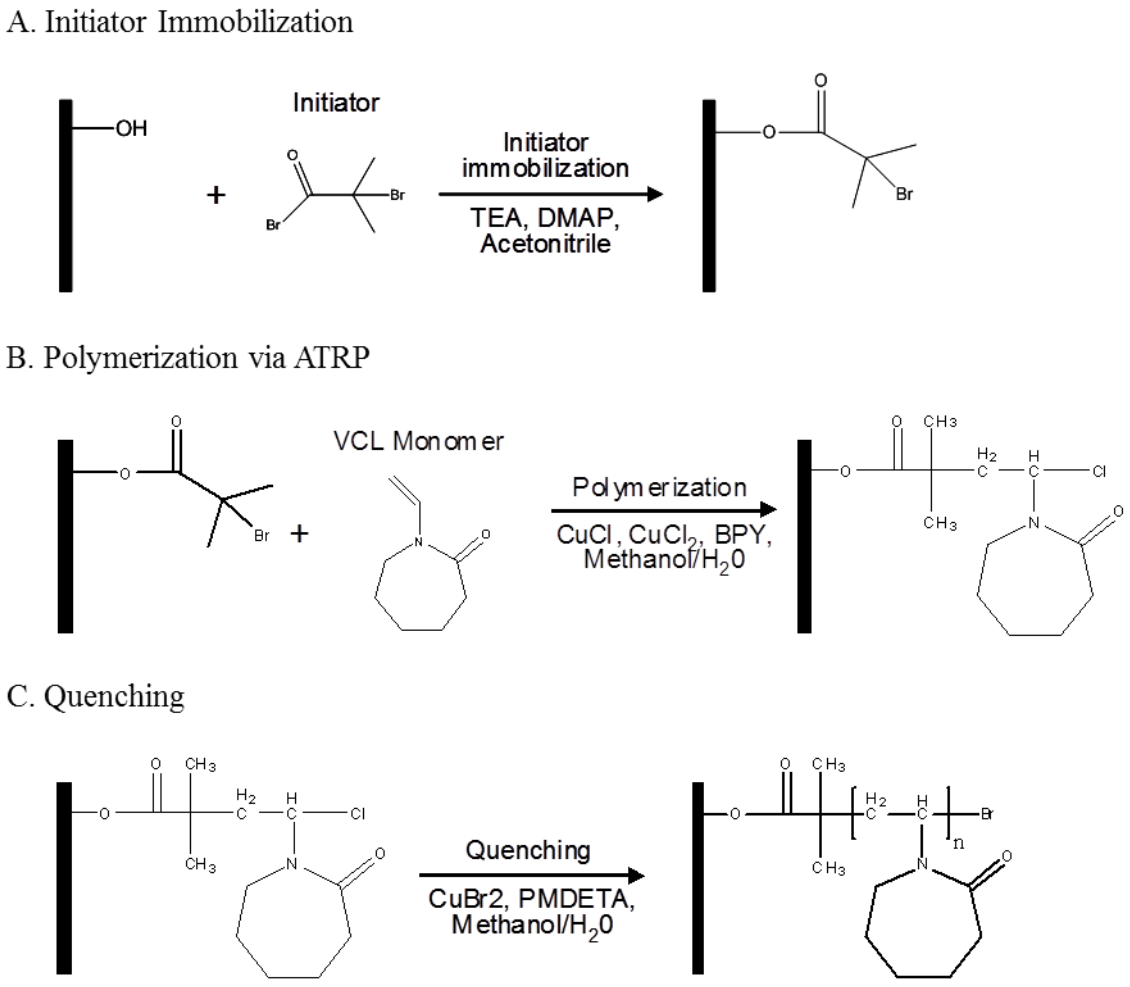

Figure 6.1: Reaction scheme for surface-initiated ATRP of PVCL showing (A) initiator immobilization, (B) polymerization, and (C) quenching steps.

6.3.4 Contact Angle

Static contact angles were determined with a contact angle goniometer (Model 100, Rame-Hart Instrument Company, Netcong, NJ) using the sessile drop method at room temperature and pressure. A 2 μL drop of 20 mM phosphate buffer at pH 7.0 containing no ammonium sulfate was applied to the surface of the membrane with a syringe. Using the circle fitting method, the angle made between the water drop and the membrane surface was measured every 0.1 second. Data were collected for 5 seconds at three locations on each membrane. Average contact angles

calculated from these 50 measurements are reported. The measurements were then performed at three new locations using the same buffer to which 1.8 M ammonium sulfate had been added.

6.3.5 Field Emission Scanning Electron Microscopy (FESEM)

FESEM was used to image the surface and cross section of the membranes in order to study the effect of membrane modification on the structural properties of the membranes. To prevent pore collapse, critical point drying was performed prior to analysing samples with a JEOL field-emission scanning electron microscope (JSM-6500F, JEOL Ltd., Tokyo, Japan). To perform critical point drying membrane samples which had been soaked in ethanol were placed into a steel vessel. The ethanol was exchanged by flushing the samples inside the vessel with supercritical CO_2 (37 ^{o}C, 85 bar) 5-7 times.

6.3.6 Attenuated Total Reflectance Fourier-Transform Infrared Spectroscopy (ATR-FTIR)

ATR-FTIR spectroscopy provides qualitative information on the types of functional groups present at depths between 500 and 2000 nm. A Nicolet Magna 760 FTIR spectrometer, Thermo Electron Corporation (Madison, WI), equipped with a mercury-cadmium-tellurium (MCT) detector with a resolution of 4 cm^{-1} and zinc selenide (ZnSe) crystal plate with an incidence angle of 45^{o} was used. ATR-FTIR spectra were averaged over 512 scans covering a range of 600-4000 cm^{-1}.

6.3.7 X-ray Photoelectron Spectroscopy (XPS)

XPS is particularly useful for studying membrane surface chemistry; i.e. the top 1-10 nm of the sample. For each sample, 5 survey scans over the range 0-1100 eV with a resolution of 1 eV were averaged using a Physical Electron 5800 ultra-high vacuum XPS-Auger spectrometer (Chanhassen, MN). Additionally, 20 scans at high resolution of 0.1 eV focusing on individual

regions of interest were averaged to characterize small changes in the surface chemistry with respect to carbon, nitrogen, and oxygen.

6.3.8 Protein Binding and Elution

All chromatography runs were performed on an ÄKTA FPLC from GE Healthcare Bio-Sciences Corp. (Piscataway, NJ, USA) with FRAC-950 fraction collector using the associated Unicorn software v. 5.31. A stack of four membranes were loaded into a GE Healthcare stainless steel flow cell purchased with the FPLC. Flow distributers were placed at the inlet of the flow cell to ensure the flow was uniform across the entire membrane cross-sectional area.

Bovine serum albumin (BSA) or human serum Immunoglobulin (IgG) solutions were created by dissolving 10 mg of protein into 10 mL of 20 mM phosphate buffer (pH 7), which contained no ammonium sulfate. 90 mL of buffer containing 2 M ammonium sulfate was then added to yield a 100 mL solution of 0.1 mg/mL protein. Solutions containing other concentrations of protein or ammonium sulfate were prepared in an analogous manner.

A method was developed within the Unicorn software to automate the protein (BSA or IgG) binding and elution experiments. The membrane stack was loaded into the flow cell and wet with 20 mM phosphate buffer (pH 7) in the reverse flow configuration over 5 minutes by increasing the flow rate from 0.2 mL/min to 1.0 mL/min in 0.2 mL/min increments. The membranes were then equilibrated in the forward flow configuration in the feed buffer (typically 1.8 M) at 1 mL/min for 10 minutes.

Protein sample solution was loaded onto the membrane stack at a flow rate of 1 mL/min for 10 minutes. The membrane stack was then washed with the feed buffer for 10 minutes at 1 mL/min. Finally, the membranes were eluted with 20 mM phosphate buffer, pH 7, at 1 mL/min until the UV absorbance measured by the Unicorn software was constant. The washing fraction

and elution fraction were collected and the volume determined. Protein concentrations in the sample solution, washing fraction, and elution fraction were calculated via UV absorbance at a wavelength of 280 nm.

6.4 Results and Discussion

6.4.1 Degree of Grafting (DG) and Contact Angle

Figure 6.2 shows the effect of varying initiator immobilization time on DG. Only a very small amount of PVCL is grafted for one hour initiator immobilization; however, the amount of PVCL grafted to the membrane increases quickly with increasing initiator immobilization time. It can further be seen that for initiator immobilization times above 5 hours the increase in DG decreases rapidly. The variation of chain density with initiator immobilization time will depend on the kinetics of immobilization. Further, higher chain densities will increase the probability of chain termination due to reaction between two adjacent chains. The observed variation of DG with initiator immobilization time for 12 hour ATRP reaction as shown in Figure 6.2 is a result of these effects.

The effect of increasing PVCL DG and buffer ionic strength on the membrane contact angle is shown in Figure 6.3. Regenerated cellulose is quite hydrophilic due to the abundance of hydroxyl and ether groups capable of forming hydrogen bonds with water. This corresponds to the very low contact angle for the unmodified regenerated cellulose membranes. The contact angle increases with increased grafting of the more hydrophobic PVCL. The contact angle in low ionic strength buffer (0 M ammonium sulfate) increases with increasing grafting degree, as the degree of coverage of the base membrane increases. The same trend exists for the much higher ionic strength buffer (1.8 M ammonium sulfate).

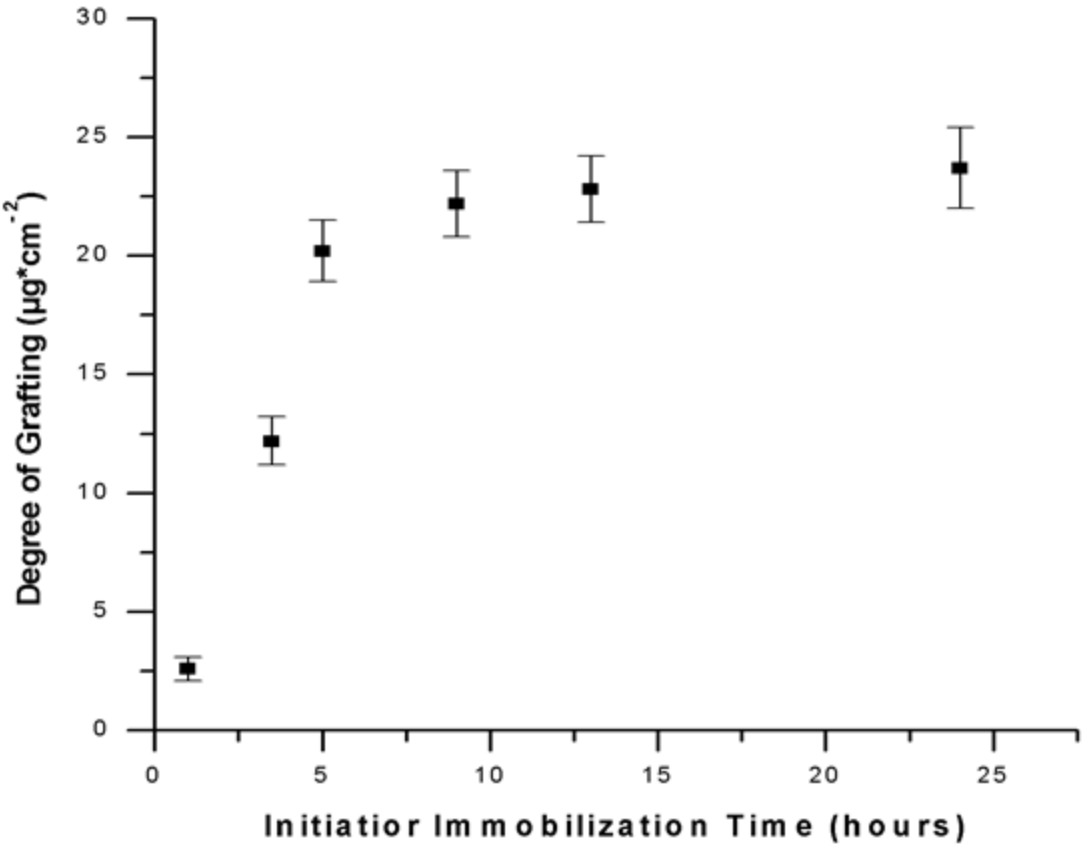

Figure 6.2: Average degree of grafting of PVCL as a function of initiator immobilization time.

Figure 6.3 further indicates that the contact angle for the higher ionic strength buffer is much higher than for the low ionic strength buffer for the same initiator immobilization time. The LCST for PVCL in water is reported to be about 32 °C (Peng et al, 2001) while in 1.0 M KCl it is below 20 °C (Maeda et al, 2002). The actual LCST of tethered PVCL will depend not only on the molecular weight of the grafted chains but also on the grafting density (Maeda et al, 2002). The contact angle data given in Figure 6.3 provide strong evidence that for the low ionic strength buffer at room temperature (around 25 °C), the grafted PVCL chains are below their LCST and adopt a more hydrated conformation leading to a low contact angle. However, in the high ionic strength buffer the grafted PVCL chains are above their LCST and adopt a more

dehydrated and collapsed conformation leading to the observed higher contact angles. The contact angle data are in agreement with the measured degree of grafting shown in Figure 6.2; for initiator immobilization times above 5 hours little change in contact angle is observed with increasing initiator immobilization time.

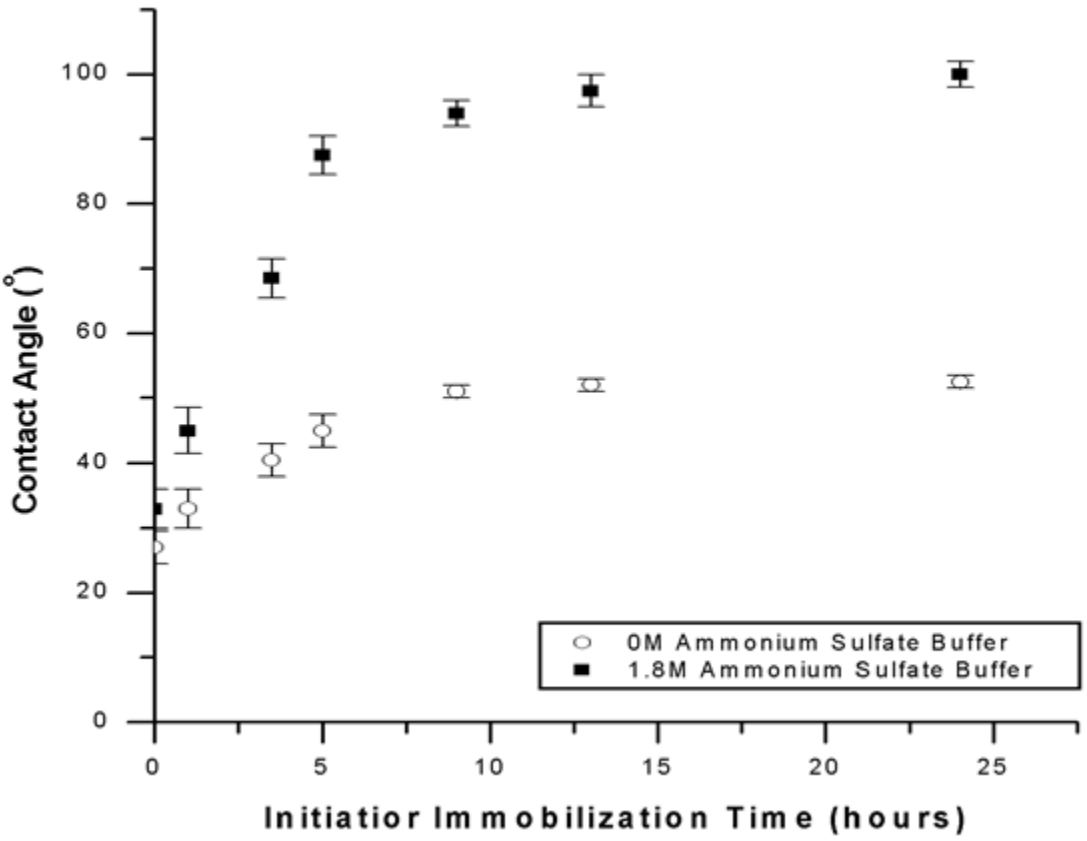

Figure 6.3: Average contact angle as a function of initiator immobilization time for low and high ionic strength buffers

6.4.2 Field Emission Scanning Electron Microscopy (FESEM)

FESEM was used to study the effect of modification on the appearance and structure of the membrane. Figure 6.4(a-b) give images of the top surface of an unmodified regenerated cellulose membrane and membranes modified with 5 hours initiator immobilization. The porous

structure and large void volume of the unmodified membrane is seen. Qualitatively, the effective pore size appears to be on the order of 0.5 μm, in agreement with the manufacturer's designation of 0.45 μm. For the modified membrane the membrane structure is tighter, with less void volume, due to the presence of the grafted PVCL. Importantly, the overall membrane structure and integrity was not damaged by the modification.

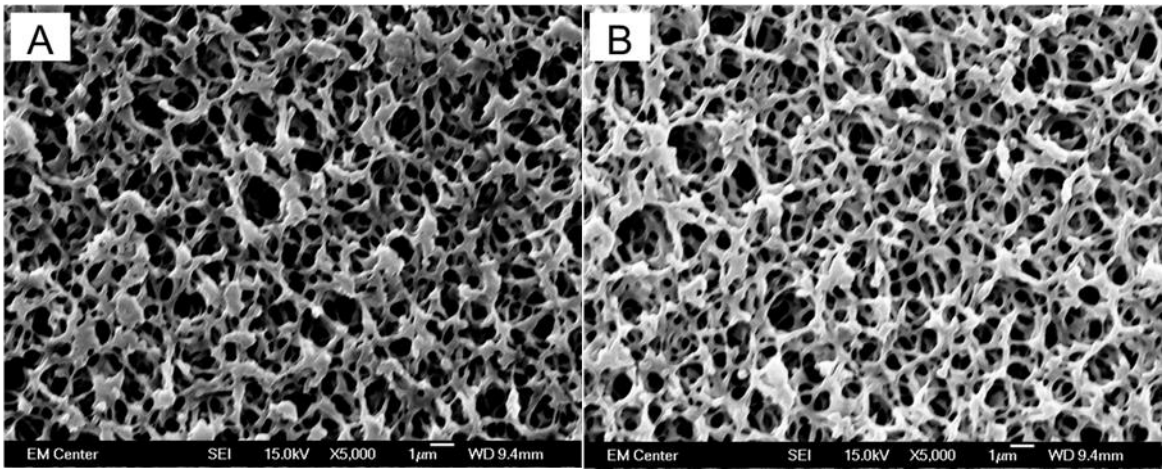

Figure 6.4: FESEM images for (A) unmodified membrane (B) membrane modified using 5 hour initiator immobilization at 5,000x magnification.

6.4.3 Attenuated Total Reflectance Fourier-Transform Infrared Spectroscopy (ATR-FTIR)

The spectra for the unmodified membrane and modified membranes with initiator immobilization times of 5 and 24 hours are shown in Figure 6.5. For the unmodified membrane the largest peak (~3335 cm^{-1}) corresponded to the stretching of C-OH bonds. The spectra for the modified membranes showed some key differences. Primarily, the large peak at ~3335 cm^{-1} associated with the hydroxyl groups was diminished with increasing PVCL DG. Additionally, peaks associated with hydrocarbon bonds increased at ~2900 cm^{-1}. This is consistent with the absence of C-OH groups in PVCL. The amide I peak at 1640-1670 cm^{-1} is seen for modified membranes and increased with increasing PVCL grafting.

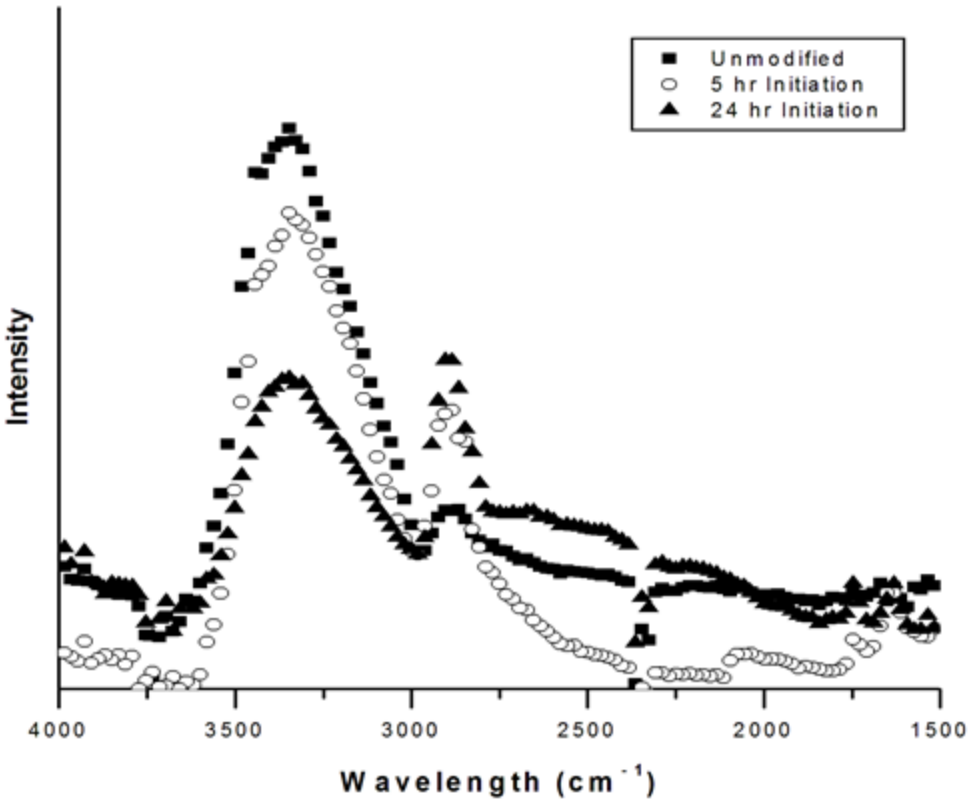

Figure 6.5: ATR-FTIR spectra for an unmodified membrane and membranes modified using 5 and 24 hour initiator immobilization times.

6.4.4 X-ray Photoelectron Spectroscopy (XPS)

The three regions of particular interest are nitrogen, oxygen, and carbon. High-resolution spectra for each of these regions are shown in Figure 6.6(a-c). Results are given for the unmodified membrane as well as membranes modified with initiator immobilization times of 5 and 24 hours. The most straightforward evidence of PVCL grafting is seen in the nitrogen region (Figure 6.6a). No peak was seen for the unmodified regenerated cellulose membrane since it contains no nitrogen. Following ATRP, a pronounced nitrogen peak appeared due to the grafting of PVCL, which contains an amide group. The height of the nitrogen peak increased with increasing initiator immobilization time due to the increased amount of grafted PVCL.

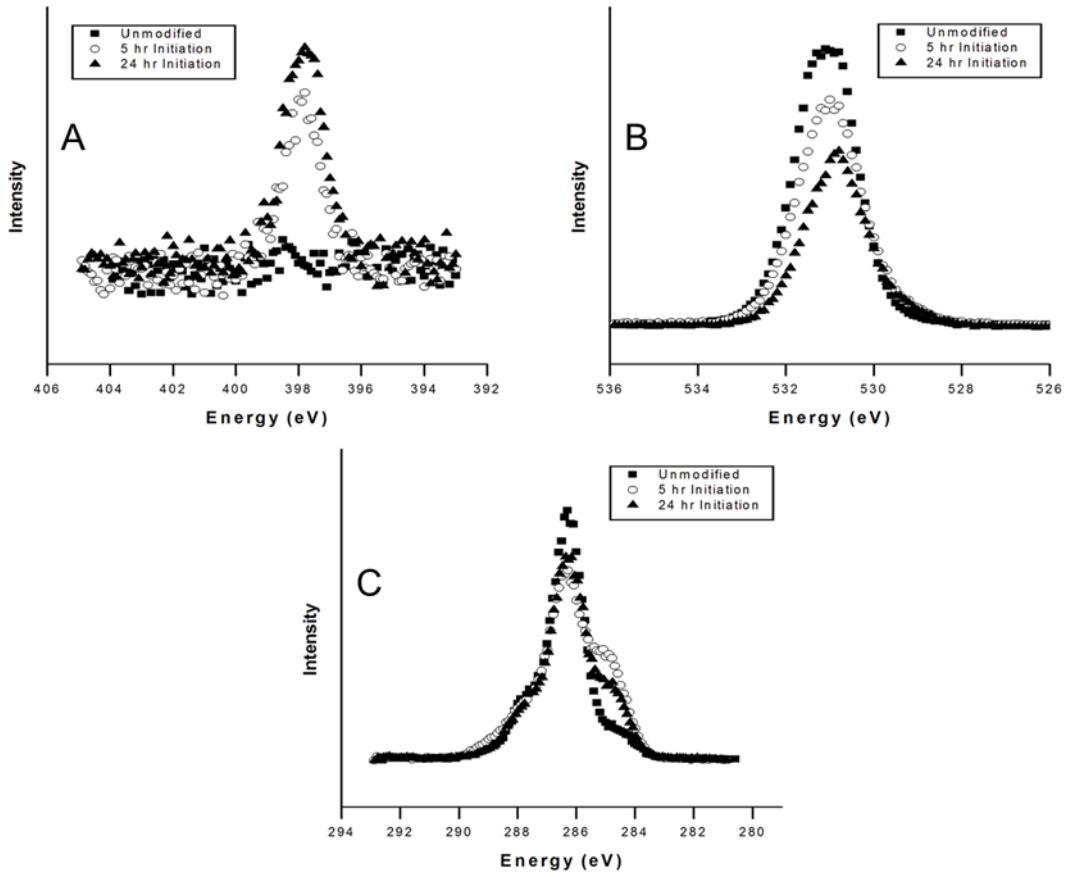

Figure 6.6: XPS spectra for the (A) nitrogen, (B) oxygen, and (C) carbon regions. Spectra are given for unmodified and modified membranes for 5 and 24 hour initiator immobilization times.

The oxygen (Figure 6.6b) and carbon (Figure 6.6c) regions offer additional evidence for the successful grafting of PVCL. The unmodified membranes showed a very strong oxygen peak due to the large number of oxygen atoms in the cellulose matrix. With increasing initiator immobilization time, this peak steadily decreased as the thickness of the grafted PVCL chains increased. The peak also shifted slightly towards lower energy with increasing grafting degree due to the carbonyl oxygen present in the PVCL representing a greater percent of the observed oxygen.

Finally, the carbon region also provides evidence of PVCL grafting. The largest peak (286.3 eV) corresponded to alcohol and ether groups, both present in large numbers in the

unmodified regenerated cellulose membranes. This peak, as with the oxygen region peak, decreased with increasing initiator immobilization time due to the increased thickness of the grafted PVCL nanostructure. A shoulder can be observed at 288 eV for modified membranes. This corresponds to carbonyl groups in the grafted PVCL nanolayer. It can also be seen that the hydrocarbon peak (284.8 eV) increased for modified membranes. This is a result of the fact that the unmodified membrane contains far fewer carbon atoms that are bonded strictly to carbon or hydrogen.

6.4.5 Hydrophobic Interaction Chromatography (HIC)

The flux versus transmembrane pressure was determined before each load cycle. All membranes displayed a linear variation of flux with transmembrane pressure as expected. Further, no statistical difference in the flux as a function of transmembrane pressure was observed for modified and unmodified membranes suggesting that the resistance due to surface modification was minimal. The FESEM results (Figure 6.4) support this observation.

Breakthrough curves for 0.1 mg/mL BSA in phosphate buffer containing 1.8 M ammonium sulfate loaded at 1 mL/min for unmodified membranes and membranes modified with 5 and 24 hours initiator immobilization times are shown in Figure 6.7(a-c). UV absorbance, which is directly proportional to protein concentration, is plotted against the ratio of effluent volume to volume occupied by the membrane stacks (0.0806 mL). The right hand side y-axis gives the variation of conductivity of the mobile phase. For the unmodified membrane Figure 6.7a, the UV absorbance began to increase at about 25 membrane volumes after loading began. This corresponded to immediate breakthrough as the system holdup volume was about 25 membrane volumes (approximately 2 mL). Loading continued for 10 min at 1 mL/min (about 125 membrane volumes). After this washing was conducted using a further 125 membrane

volumes of feed buffer without BSA. The UV absorbance rapidly drops to zero during the washing step. Finally elution buffer, 20 mM phosphate with no ammonium sulfate, was pumped through the membrane. The absence of an elution peak confirmed that there was little nonspecific binding of BSA to the base regenerated cellulose membrane.

As can be seen the conductivity remains constant during loading and washing but drops to a very low value during elution. At the end of the elution cycle, the absorbance drops below zero. This is because the UV absorbance is set to zero before the loading cycle in buffer containing 1.8 M ammonium sulfate. The elution buffer however, contains no ammonium sulfate.

The chromatograms for the two modified membranes (Figure 6.7(b,c)) indicate that breakthrough occurs at about 50 membrane volumes rather than 25 membrane volumes as observed for the unmodified membrane. This longer time to breakthrough indicates adsorption of BSA. Both modified membranes also display a sharp elution peak, suggesting rapid desorption of the adsorbed BSA and the absence of large resistances due to pore diffusion. In fact for flow rates between 0.1 and 10 mL/min, no effect on dynamic capacity was observed. Consequently, all experiments were conducted at a flow rate of 1.0 mL/min. As was the case for the unmodified membrane, the absorbance falls below zero during elution. Again the conductivity remains constant during loading and washing and drops to a very low value during elution.

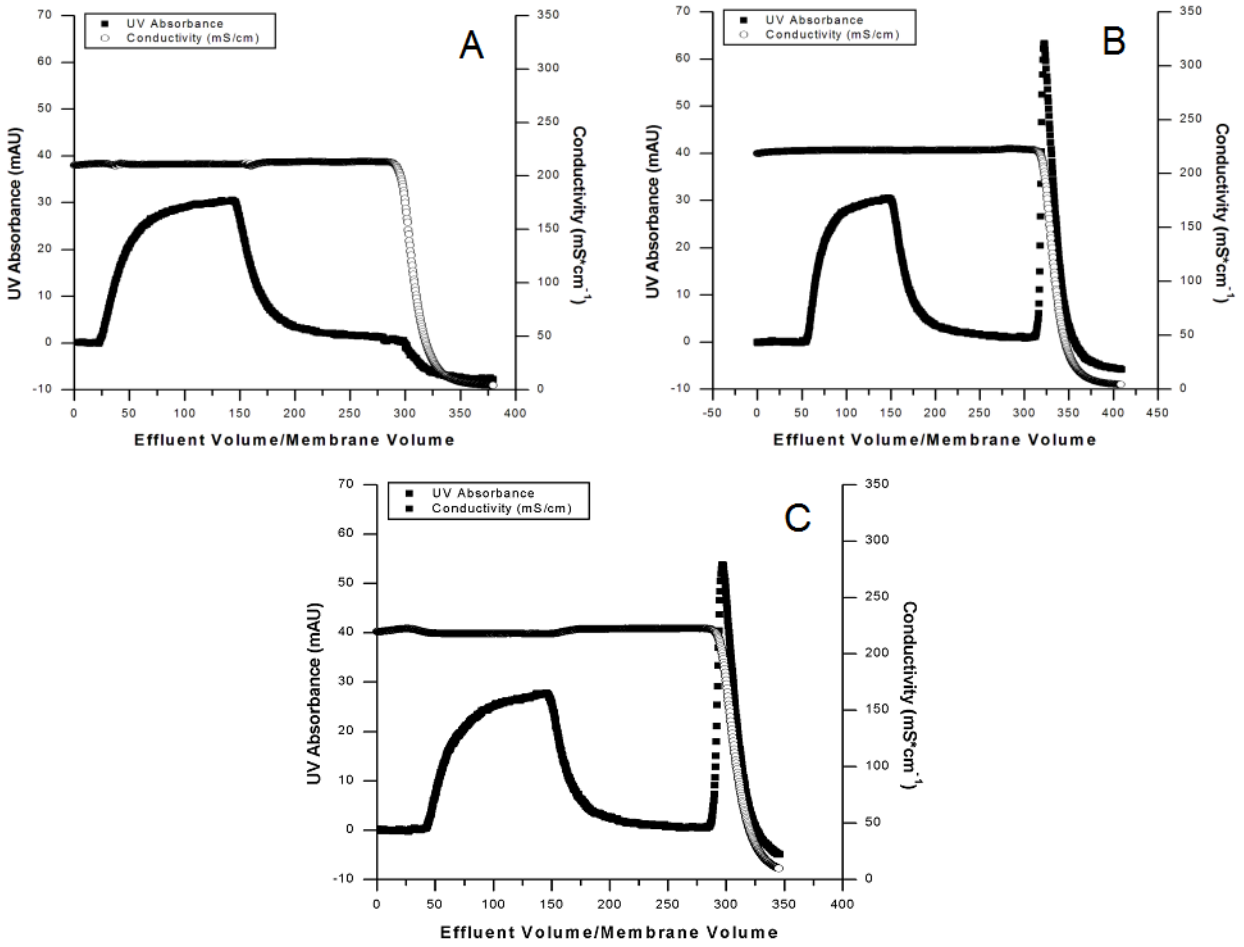

Figure 6.7: HIC chromatographs for the (a) unmodified RC membrane and membranes modified at (b) 5 and (c) 24 hour initiator immobilization time. Loading conditions were 0.1 mg/mL BSA in 1.8 M ammonium sulfate buffer at 1 mL/min.

Based on chromatograms analogous to those in Figure 6.7, BSA binding capacity and recovery were determined for membranes modified with a range of initiator immobilization times. The binding capacity was defined as the capacity at which the concentration in the flow through reached 90% of the feed concentration (90% saturation). Experiments were conducted at least 4 times for each condition and average results are reported. The results are given in Table 6.1. The error values shown give the observed variability.

Table 6.1: Average binding capacity and percent recovery for various membranes modified in this study. Loading conditions were 0.1 mg/mL BSA in phosphate buffer (pH 7.0) containing 1.8 M ammonium sulfate pimped at1 mL/min.

Initiator Immobilization Time (hr)	Recovery (%)	Binding Capacity (mg/mL)
Control	0	0
1	97.6 ± 1	3.3 ± 0.1
3.5	91.0 ± 3	4.3 ± 0.3
5	96.0 ± 1	4.8 ± 0.2
13	72.9 ±3	4.5 ± 0.3
24	70.2 ± 3	4.9 ± 0.2

Table 6.1 indicates that within the observed variability between repeat runs, the overall trend is that the binding capacity increases with increasing DG. However, the increase in capacity decreases for membranes modified with initiator immobilization times above 5 hours. This observation is in agreement with the DG and contact angle data shown in Figures 6.2 and 6.3.

The observed recovery remains very high for initiator immobilization times up to 5 hours and then decreases. At higher chain densities (higher initiator immobilization times) steric hindrance could prevent complete swelling and hydration of the chains at low ammonium sulfate concentrations. This could result in less efficient desorption of adsorbed BSA resulting in the observed lower recovery. Earlier work in the Wickramasinghe lab (Du et al, 2010; Du et al, 2011) and preliminary classical molecular dynamics simulations for poly(N-isopropylacrylamide) (pNIPAM) indicate that the degree of swelling is strongly dependent on the distances between the polymer chains. Even for temperature below its LCST transition, two pNIPAM chain separated by as much as 30 Å are seen to collapse onto each other even though the polymers are in a hydrated extended conformation. High chain density is likely to limit the

degree of hydration of these responsive polymers. Consequently all further testing was conducted using membranes that were modified with 5 hour initiator immobilization.

Figure 6.8 gives some literature data for HIC membranes and resins. Data from Ghosh and Wang (Ghosh et al, 2006) are for 0.1 μm pore size PVDF membranes and a feed stream consisting of 0.5 mg/mL BSA in 20 mM sodium phosphate buffer (pH 6.5). A range of ammonium sulfate concentrations in the feed buffer were investigated. Experiments were conducted in pulse mode at a flow rate of 10 mL/min. Results for the loading buffer containing 1.5 and 1.7 M ammonium sulfate are given in Figure 6.8.

Data from Fraud et al. (Fraud et al, 2009) are for commercially available Sartobind HIC membranes manufactured by Sartorius AG, Göttingen, Germany. Phenyl groups were covalently attached to base regenerated cellulose membranes, pore size about 3 μm. The BSA concentration in the feed stream was 2.0 mg/mL. The feed buffer consisted of 2.0 M ammonium sulfate in 50 mM potassium phosphate buffer (pH 6.0). The feed flow rate was 10 mL/min. Dynamic binding capacities were determined for breakthrough concentrations defined as 10% saturation. No recovery data were provided.

Hahn et al. (Hahn et al, 2003) provide data for various HIC resins. The feed buffer consisted of 20 mM sodium phosphate (pH 7.0) containing 1.75 M ammonium sulfate. The BSA concentration in the feed was 1.0 mg/mL. Dynamic binding capacities were determined for breakthrough defined as 2.5% saturation. A range of feed flow rates from 0.15 to 1.30 mL/min were investigated. Recoveries ranged from 80 to 100% though for most resins recoveries were above 90%.

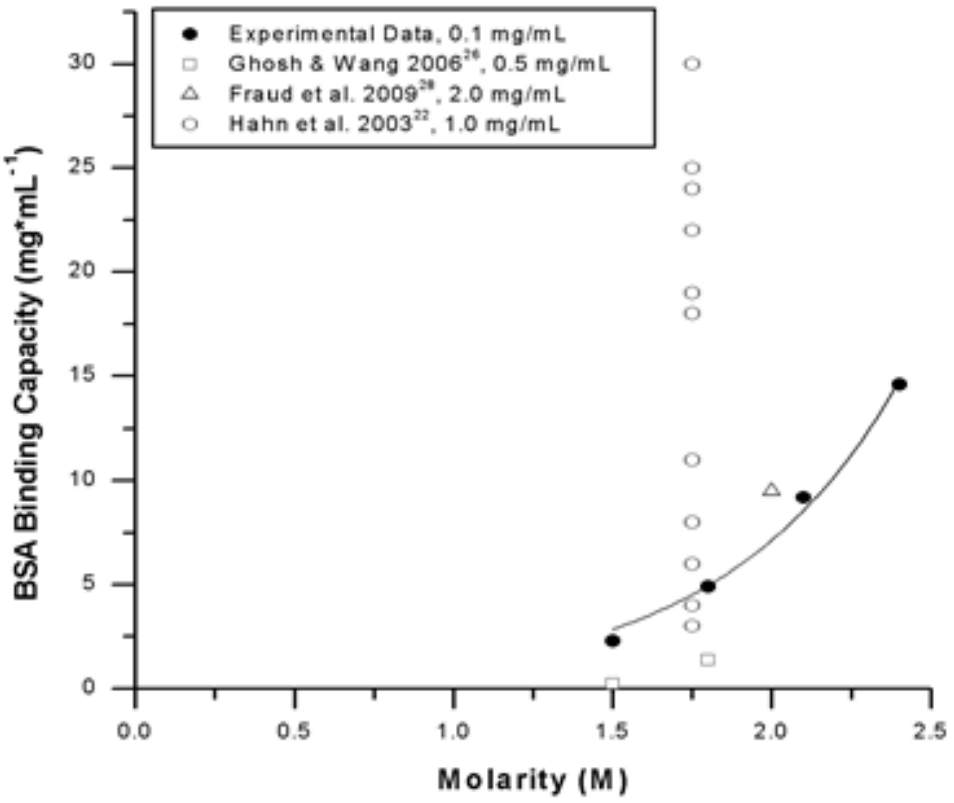

Figure 6.8: BSA binding capacity as a function of ammonium sulfate concentration in the feed buffer. Literature data are for various resins and membranes are compared to the results obtained in this study.

Data for membranes modified in this study with an initiator immobilization time of 5 hours are included in Figure 6.8. The results given in Figure 8 are difficult to compare directly as the experimental conditions are not identical. Comparing results for packed beds and membrane adsorbers is difficult given the different flow geometries and residence times for these devices. Previous studies (Han et al, 2006; Charcosset et al, 1995) have indicated a basis for comparison of membranes and resins based on the Thomas model (Thomas et al, 1944) which assumes a Langmuir adsorption isotherm. Such a comparison is not possible here as there is insufficient information for the previous studies. However Hahn et al. (Hahn et al, 2003) do indicate that the dynamic capacity of the various resins they investigated does depend on feed flow rate. It is

expected that the adsorptive membranes will display a dynamic capacity that is independent of flow rate over a large range of flow rates. The modified membranes in this study displayed a dynamic capacity that was independent of flow rate over the range 0.1 to 10 mL/min.

Figure 6.8 indicates that the dynamic capacity of the resins investigated by Hahn et al. have a significant range. Capacities can be less than the membranes tested in this study; however, capacities can also be 7 times greater than the membranes developed here. The surface area of highly porous chromatographic resins is higher than for membranes. Resin capacities for small proteins are frequently much higher than for adsorptive membranes (Weaver et al, 2013) though the dynamic capacity does decrease with increasing flow rate due to pore diffusional resistances.

The membranes developed here display much higher capacities than those described by Ghosh and Wang (Ghosh et al, 2006). This is not surprising as Ghosh and Wang used PVDF membranes with no surface modification. Attaching hydrophobic polymer chains to the internal pore surface of the membrane will increase the number of binding sites and hence the capacity. As can be seen, the commercially available Sartorius membrane which contains phenyl groups attached to a base regenerated cellulose membrane, does display a much higher capacity than the PVDF membranes tested by Ghosh and Wang. The capacity of the membranes developed here is similar to the commercially available Sartorius membranes.

The responsive membranes developed in this study were tested using a BSA concentration in the feed stream of 0.1 mg/mL much less than the feed concentration used in the earlier studies (Fraud et al (Fraud et al, 2009) 2.0 mg/mL, Ghosh and Wang (Ghosh et al, 2006) 0.5 mg/mL and Hahn et al. (Hahn et al, 2003) 1.0 mg/mL). In the absence of dynamic effects, the adsorption isotherm determines the amount of BSA that binds at a given solution concentration.

The responsive membranes developed here have a much more favorable adsorption isotherm as indicated in Table 6.1 and Figure 6.8. Further, for initiator immobilization times less than 5 hours high BSA recovery is also observed. Finally, as expected, higher ammonium sulfate concentration in the feed buffer yields higher binding capacities.

Additional experiments were conducted to determine the IgG binding capacity of the membrane with 5 hour initiator immobilization in a feed buffer containing 1.8 M ammonium sulfate. An average binding capacity of 21.0 mg/mL was obtained at the same operating conditions we used for BSA. Fraud et al. (Fraud et al, 2009) obtained a capacity of around 12 mg/mL using Sartorius membranes. Since the operating conditions used by Fraud et al. were not identical to the ones used here, direct comparison of the results is difficult. However, the results do highlight the tremendous potential benefit of designing responsive membranes for HIC.

The results obtained here indicate that optimization of the grafted nanolayer will be essential for maximizing both capacity and recovery. In particular, a very high grafting density is likely to limit the ability of the grafted nanolayer to swell below its LCST adversely affecting rapid protein desorption (Du et al, 2010; Du et al 2011). On the other hand a low graft density will lead to low capacity. Previous studies have indicated that a critical ligand hydrophobicity is required to capture and recover a specific protein (Chen et al, 2007). Fractionation of different proteins depends on the hydrophobicity of the proteins. More hydrophobic proteins may be fractionated at low (0.3-0.5 M) ammonium sulfate concentrations. Further, due to the possible loss of protein during adsorption at high salt concentration, there is significant interest in conducting HIC at low salt concentrations.

The relatively high binding capacities at low concentration obtained here could be advantageous for purification of biopharmaceuticals, where the concentration of the target

product is often very low (< 1 mg/mL). Development of responsive ligands offers the potential to tailor ligands for efficient fractionation of proteins. The degree of hydration and dehydration as well as their corresponding response time depends not only on the ionic strength of the buffer solution but also on the specific cations and anions in solution (Du et al, 2010; Du et al, 2011). Our earlier results for PNIPAM in sodium halide salt solutions and more recent results for PNIPAM in different singly-charged alkali and doubly-charged alkaline chloride solutions show that the radius of gyration and the number of water molecules of PNIPAM in the first hydration shell are ion specific at a given temperature. This is likely to be the same for PVCL. Thus it is likely that by carefully choosing the salt used during loading, efficient fractionation of proteins by HIC in low salt concentration feed solutions may be possible.

6.5 Conclusions

Responsive membranes represent a class of multifunctional membranes whose performance can be modified by an external stimulus. Here PVCL chains have been grown from the surface of regenerated cellulose membranes. The PVCL chains display an LCST. Above the LCST the chains adopt a collapsed and dehydrated conformation while below the LCST the chains swell. The value of the LCST may be altered by changing the ionic strength of the buffer solution.

We have shown that BSA may be efficiently adsorbed and desorbed from regenerated cellulose membranes grafted with PVCL. At high grafting densities, recovery of BSA is reduced. This is likely due to the fact that swelling of the grafted polymer chains is restricted due to steric hinder effects. Importantly BSA is efficiently adsorbed at very low feed concentrations.

The use of commercial membrane adsorbers for protein purification is growing. Unlike packed beds, membrane adsorbers display dynamic capacities that are independent of flow rate spanning a large range of flow rates. Development of efficient HIC membrane adsorbers could be of significant benefit in the downstream purification of biopharmaceutical products.

References

Brandt, S., Goffee, RA., Kessler, SB., O'Connor, JL., Zale, SE. 1988. Membrane based affinity technology for commercial scale purifications, *Biotechnology.* 6: 779-782.

Charcosset, C., Su, Z., Karoor, S., Daun, G., Colton, CK. 1995. Protein-A immunoaffinity hollow fiber membranes for immunoglobulin G purification – experimental characterization, *Biotechnol Bioeng.* 48: 415-427.

Chen J., Luo, Q., Breneman, CM., Cramer, SM. 2007. Classification of protein adsorption and recovery at low salt conditions in hydrophobic interaction chromatographic systems, *J Chromatogr A.* 1139: 236-246.

Du, H., Wickramasinghe, SR., Qian, X. 2010. The effects of salt on the lower critical solution temperature of poly (N-isopropylacrylamide), *J Phys Chem B.* 114: 16594-16604.

Du, H., Qian, X. 2011. Molecular Dynamics Simulations of PNIPAM-co-PEGMA Copolymer Hydrophilic to Hydrophobic Transition in NaCl Solution, *J Polym Sci B: Polym. Phys.* 49: 1112-1122.

Endres, HN., Johnson, JAC., Ross, CA., Welp, JK., Etzel, MR. 2003. Evaluation of an ion-exchange membrane for the purification of plasmid DNA, *Biotechnol Appl Biochem.* 37: 259-266.

Fausnaugh, JL., Regnier, FE. 1986. Solute and mobile phase contributions to retention in hydrophobic interaction chromatography of proteins, *J Chromatogr A.* 359: 131-146.

Fraud, N., Faber, R., Kiss, C., Demmer, W., Hoerl, HH., Fischer-Fruehholz, S. 2009. Hydrophobic-interaction membrane chromatography for large-scale purification of biopharmaceuticals, *BioProcess Int.* 7 (S6): 30-35.

Ghosh, R. 2001. Separation of proteins using hydrophobic interaction membrane chromatography, *J Chromatogr A.* 923: 59-64.

Ghosh, R. 2002. Review: protein separation using membrane chromatography: opportunities and challenges, *J Chromatogr A.* 952: 13-27.

Ghosh, R., Wang, L. 2006. Purification of humanized monoclonal antibody by hydrophobic interaction membrane chromatography, *J Chromatogr A.* 1107: 104-109.

Hahn, R., Deinhofer, K., Machold, C., Jungbauer, A. 2003. Hydrophobic interaction chromatography of proteins: II. Binding capacity, recovery and mass transfer properties, *J Chromatogr B.* 790: 99-114.

Han, B., Carvalho, W., Canilha, L., da Silva, SS., Almeida, e Silva JB., McMillan, JD., Wickramasinghe, SR. 2006. Adsorptive membranes vs. resins for acetic acid removal from biomass hydrolysates, *Desalination*, 193: 361-366.

Himstedt, HH., Yang, Q., Qian, X., Wickramasinghe, SR., Ulbricht, M. 2012. Toward remote-controlled valve functions via magnetically responsive capillary pore membranes, *J Membr Sci.* 423–424: 257–266.

Huang, R., Mah, KZ., Malta, M., Kostanski, LK., Filipe, CDM., Ghosh, R. 2009. Chromatographic separation of proteins using hydrophobic membrane shielded with an environment-responsive hydrogel, *J Membr Sci.* 345: 177-182.

Ieong, NS., Hasan, M., Phillips, DJ., Saaka, Y., O'Reilly, RK., Gibson, MI. 2012. Polymers with molecular weight dependent LCSTs are essential for cooperative behaviour, *Polym Chem.* 3: 794-799.

Kanazawa, H., Yamamoto, K., Matsushima, Y., Takai, N., Kikuchi, A., Sakurai, Y., Okano, T. 1996. Temperature responsive chromatography using poly(N-isopropylacrylamide)-modifeid silica, *Anal Chem.* 68: 100-105.

Klein, E. 2000. Affinity membranes: A 10-year review. *J Membr Sci.* 179: 1-27.

Kovvali, AS., Sirkar, KK. 2003. Membrane contactors: recent developments, in New insights into membrane science and technology: polymeric and biofunctional membranes, Ed: Bhattacharyya D., Butterfield D.A., *Membrane Science and Technology.* 8: 147-164.

Kubota, N., Kounosu, M., Saita, K., Sugita, K., Watanabe, K., Sugo, T. 1997. Protein adsorption and elution performances of porous hollow-fiber membranes containing various hydrophobic ligands, *Biotechnol Prog.* 13: 89-95.

Kuczewski, M., Fraud, N., Faber, R., Zarbis-Papastoitsis, G. 2010. Development of a polishing step using a hydrophobic interaction membrane adsorber with PER.C6-derived recombinant antibody, *Biotechnol Bioeng.* 105: 296-305.

Lienqueo, ME., Mahn, A., Salgado, JC., Asenjo, J.A. 2007. Current insights on protein behavior in hydrophobic interaction chromatography, *J Chromatogr B.* 849: 53-68.

Ling, Y., Lu, M. 2009. Thermo and pH dual responsive poly(n-isopropylacrylamide-co-itaconic acid), hydrogels prepared in aqueous NaCl solutions and their characterization, *J Polym Res.* 16: 29-37.

Maeda, Y., Nakmura, T., Ikeda, I. 2002 Hydration and phase behavior of poly(N-vinylcaprolactam) and poly(N-vinylpyrrolidone) in water, *Macromolecules.* 35: 217-222.

Machold, C., Deinhofer, K., Hahn, R., Jungbauer, A. 2002. Hydrophobic interaction chromatography of proteins: I. Comparison of selectivity, *J Chromatogr A.* 972: 3-19.

Mah, KZ., Ghosh, R. 2010. Paper-based composite lyotropic salt-responsive membranes for chromatographic separation of proteins, *J Membr Sci.* 360: 149-154.

Melander, W., Horváth, C. 1977 Salt effects on hydrophobic interactions in precipitation and chromatography of proteins: interpretation of the lyotropic series, *Arch Biochem Biophy.* 183: 200-215.

Melander, WR., El Rassi, Z., Horváth, C. 1989. Interplay of hydrophobic and electrostatic interactions in biopolymer chromatography, Effect of salt on the retention of proteins, *J Chromatogr A.* 469: 3-27.

Miserez, B., Lynen, F., Wright, A., Euerby, M., Sandra, P. 2010. Thermoresponsive poly(N-vinlycaprolactam) as stationary phase for aqueous and green liquid chromatography, *Chromatographia*, 71: 1-6.

Nfor, BK., Hylkema, NN., Wiedhaup, KR., Verhaert, PDEM., van der Wielen, LAM., Ottens, M. 2001. High-throughput protein precipitation and hydrophobic interaction chromatography: salt effects and thermodynamic interrelation, *J Chromatogr A.* 1218: 8958-8973.

Peng, S., Wu, C. 2001. Surfactant effect on pH and temperature sensitivities of poly(N-vinylcaprolactam-co-sodium acrylate) microgels, *Macromolecules.* 34: 568-571.

Porath, J., Sundberg, L., Fornstedt, N., Olsson, I. 1973. Salting out in amphiphilic gels as a new approach to hydrophobic adsorption, *Nature.* 245: 465-466.

Prabaharan, M., Grailer, JJ., Steeber, DA., Gong, S. 2008. Stimuli-responsive chitosan-graft-poly(N-vinylcaprolactam) as a promising material for controlled hydrophobic drug delivery, *Macromol Biosci.* 8: 843-851.

Ramos, J., Imaz, A., Forcada, J. 2012. Temperature-sensitive nanogels: poly(N-vinylcaprolactam) versus poly(N-isopropylacrylamide), *Polym Chem.* 3: 852-856.

Specht, R., Han, B., Wickramasinghe, SR., Carlson, JO., Czermak, P., Wolfe, A., Reif, OW. 2004. Densonucleosis virus purification by ion exchange membranes, *Biotechnol Bioeng.* 88: 465-473.

Teeters, MA., Conrardy, SE., Thomas, BL., Root, TW., Lightfoot, EN. 2003. Adsorptive membrane chromatography for purification of plasmid DNA, *J Chromatogr A.* 989: 165-173.

Thomas, HC. 1944. Heterogeneous Ion Exchange in a Flowing System, *J Am Chem Soc.* 66: 1664-1666.

Thömmes, J., Kula, MR. 1995. Membrane chromatography – An integrative concept in the downstream processing of proteins, *Biotechnol Prog.* 11: 357-367.

Vihola, H., Laukkanen, A., Hirvonen, J., Tenhu, H. 2002. Binding and release of drugs into and from thermosensitive poly (N-vinylcaprolactam) nanoparticles. *Eur J Pharm Sci.* 16: 69-74.

Vogel, J.H., Nguyen, H., Giovannini, R., Ignowski, J., Garger, S., Salgotra, A., Tom, J. 2012. A new large scale manufacturing platform for complex biopharmaceuticals, *Biotechnol Bioeng.* 109: 3049-3058.

Wandera, D., Wickramasinghe, SR., Husson, SM. 2010. Stimuli-responsive membranes, *J Membr Sci.* 357: 6-35.

Weaver, J., Husson, SM., Murphy, L., Wickramasinghe, SR. 2013. Anion exchange membrane adsorbers for flow-through polishing steps: part I. Clearance of minute virus of mice, *Biotechnol Bioeng.* 110: 491–499.

Weaver, J., Husson, SM., Murphy, L., Wickramasinghe, SR. 2013. Anion exchange membrane adsorbers for flow-through polishing steps: part II. Virus, host cell protein, DNA clearance and antibody recovery, *Biotechnol Bioeng.* 110: 500–510.

Wickramasinghe, SR., Carlson, JO., Teske, C., Hubbuch, J., Ulbricht, M. 2006. Characterizing solute binding to macroporous ion exchange membrane adsorbers using confocal laser scanning microscopy, *J Membr Sci.* 281: 609-618.

Yoo, SM., Ghosh, R. 2012. Simultaneous removal of leached protein-A and aggregates form monoclonal antibody using hydrophobic interaction membrane chromatography, *J Membr Sci.* 390-391: 263-269.

Yu, D., Chen, X., Pelton, R., Ghosh, R. 2008. Paper-PEG-Based membranes for hydrophobic interaction chromatography: purification of monoclonal antibody, *Biotechnol Bioeng.* 99: 1434-1442.

Chapter 7

Identification and Characterization of Novel Fc-binding Heptapeptides via Phage Display and ELISA[1]

7.1 Summary

Purification of biologically-derived therapeutics is a major cost contributor to the production of this rapidly growing class of pharmaceuticals. Monoclonal antibodies comprise a large percentage of these products therefore new antibody purification tools are needed. Small peptides, as opposed to traditional antibody affinity ligands such as Protein A, may have advantages in stability and production costs. Multiple heptapeptides that demonstrate Fc binding behavior that have been identified from a combinatorial peptide library using M13 Phage Display are presented herein. Seven unique peptide sequences of diverse hydrophobicity and charge were identified, suggesting multiple sites on the Fc were bound by the peptides. All seven peptides showed strong binding to the four major human IgG isotypes, human IgM, as well as binding to canine, rat, and mouse IgG. These seven peptides were also shown to bind human IgG4 from DMEM cell culture media with 5% FCS and 5 g/L ovalbumin present. These peptides may be useful as surface ligands for antibody detection and purification purposes.

[1]Weaver, J., Wickramasinghe, SR. Identification and Characterization of Novel Fc-binding Heptapeptides via Phage Display and ELISA. (submitted)

7.2 Introduction

Pharmaceutical sales, and in particular biologically derived pharmaceutical sales, are increasing (Merie, 2011). In fact many of the top selling pharmaceuticals are monoclonal antibodies (mAb). However biologically derived pharmaceuticals, including mAbs, are much more expensive than typical small-molecule therapeutics due to the complexity of both the molecule and the production process. Downstream purification of these mAbs can account for almost 80% of the total cost of manufacturing suggesting opportunities for novel antibody purification technology (Gottschalk, 2005). Thus there is a continual need to develop new, more efficient purification processes. Recently, much work has gone into finding possible functional replacements for protein A which is the workhorse affinity technology for mAb purification. Drawbacks of protein A include the fact that it is expensive and unstable under typical column cleaning/sanitization conditions such as 1M NaOH (Costioli et al., 2010; Gagnon, 2012).

Derivatives of protein A have been shown to retain similar binding properties while showing an increase either in binding capacity or stability (Gulich et al., 2002; Linhult et al., 2004). A few alkaline-stabilized protein A derivatives are currently marketed as chromatography resins such as the GE Healthcare (Pittsburgh, PA, USA) MabSelect Sure resin which uses a modified tetrameric B binding domain, protein A ceramic Hyper D F resin from Pall Corporation (Port Washington, NY, USA) and Tosoh Biosciences (South San Francisco, CA, USA) Toyopearl AF-protein A-650F resin which uses a tetrameric derivative of the C binding domain of protein A. However, protein A derivatives still suffer from high costs associated with licensing fees and costs of producing the recombinant protein.

Therefore synthetic ligands that have little or no protein A homology have received a good deal of academic and industrial interest over the past decade. Totally synthetic chemical ligands, such as the multi-modal hydrophobic charge induction MEP Hypercel® ligand from Pall Corporation which displays both charge and hydrophobic binding characteristics, are actively being researched currently. Wang et al showed that by screening parallel small libraries of combinatorial chemical ligands certain ligands could perform chromatographic separation of BSA and avidin (Wang and Li, 2002). Haigh et al identified small molecule immunoaffinity ligands based on a multicomponent Ugi reaction combinatorial library (Haigh et al., 2009). A very interesting study in 2011 by Arnold et al. demonstrated a method for evaluating large libraries of small molecules for Fc binding based on surface plasmon resonance (SPR) analysis of chemical microarrays (Arnold et al., 2011). Several chemical ligands were identified with potential Fc binding properties. While these chemical-based ligands show promise as yet they have generally not shown comparable selectivity to protein A.

Synthetic peptides are also currently being explored as possible antibody purification ligands (Verdoliva et al., 2002). Small peptides have several advantages over both large protein A derivatives and small-molecule chemical affinity ligands. Due to the much smaller size and reduced complexity of peptides as compared large protein A derivatives, peptides may be inherently more stable. Short peptides do not assume complex tertiary structures like that found in protein A but may or may not form helical secondary structure (Finkelstein et al., 1991). Secondary structures such as α-helices and β-sheets are thermodynamically favored. Further, recovery of these structures after denaturation is generally rapid and much more reproducible than recovery of tertiary structures. Therefore recovery of active peptide after exposure to

unfavorable folding conditions is more likely than recovery of large proteins after similar exposure.

There have been multiple peptide-based ligands identified as Fc binders or specific protein binders using various selection methods (Berntzen et al., 2009; DeLano et al., 2000; Gurgel et al., 2001a; Gurgel et al., 2001b; Jeong, 2010; Krook et al., 1998; Sinha et al., 1999). The unusual peptide PAM first described by Fassina et al in 1996, has very promising antibody purification characteristics, producing antibody with greater than 90% purity from clarified cell supernatant. (Dinon et al., 2011; Fassina et al., 1996). Another peptide, HWRGWV, was identified by Yang et al via an elegant radiolabeled target screening method of a solid phase hexapeptide resin library (Yang et al., 2006). The HWRGWV peptide has been shown to demonstrate good performance for purification of hIgG from CHO cell culture media, and Fc binding site data has been obtained (Naik et al., 2011; Yang et al., 2010). Impurity removal was also studied, showing good removal of DNA and host cell proteins. A common method used to identify promising peptides is panning of peptides from phage display libraries. This is the method used in this work.

Phage display is a method for evaluating a very large protein library for specific sequences that bind the desired target. Today the method is used to study molecular biology mechanisms involving protein-protein and protein-non-protein interactions (Gaskin et al., 2001; Hober et al., 2007; Larbanoix et al., 2011; Levine et al., 2013; Mooney et al., 2011; Serizawa et al., 2007; Vodnik et al., 2011b). Protein libraries of varying length, from short peptides to full antibody, are "displayed" on the surface of bacteriophage coat proteins. Since the protein displayed on the surface is coded by the genetic material within the viral genome there is a direct link between the phenotype of the phage and its genotype, thereby allowing DNA sequencing

and identification of the displayed protein. M13 phage is the most common phage currently used, and is the one used in this study in the form of the Ph.D-7 library from New England BioLabs Inc. (Ipswich, MA, USA) (Georgieva and Konthur, 2011; Sidhu, 2001).

In this contribution seven novel heptapeptides have been identified through a series of solution affinity panning experiments that have specific affinity for the Fc region of immunoglobulins. Heptapeptides have been identified as selective binding ligands for other targets, providing assurance small 7-amino acid ligands can be selective (Islam, 2013; Islam et al., 2014; Ng et al., 2012; Pulicherla and Asokan, 2011; Yang et al., 2011). To our knowledge there have not been any previously reported heptapeptide Fc binding ligands in the public literature. Importantly, these peptides may be excellent candidates for either antibody detection or purification ligands. The previously mentioned hexapeptide HWRGWV demonstrates small peptides may show sufficient selectivity and affinity to Fc to act as a purification ligand. Heptapeptides may add some additional selectivity while still retaining the robustness and ease of production of small peptides. To that end binding experiments were conducted via ELISA with hIgG4 coated wells in challenging cell culture media (DMEM with 5% FCS and 5 g/L BSA) to demonstrate specificity. Protein A has known binding tropisms for hIgG1, hIgG2, hIgG4 but is a poor hIgG3 binder (Starovasnik et al., 1999). Therefore binding to various human and non-human antibodies has also been explored.

7.3 Materials and Methods

7.3.1 Reagents

Ph.D.-7 phage-peptide library and F^+ E. Coli strain K12 ER2738 were purchased from New England BioLabs (Ipswich, MA, USA). 2xYT media (powder mix, 31 g/L) was

purchased from Amresco (Solon, OH, USA). Tetracycline hydrochloride (antibiotic), bovine serum albumin (BSA), lactoferrin, and horseradish peroxidase enzyme chromogenic substrate ABTS (2,2'-Azino-bis(3-ethylbenzthiazoline-6-sulfonic acid) diammonium salt) was obtained from Sigma-Aldrich Corp. (St. Louis, MO, USA). High glucose DMEM media and fetal calf serum (FCS) were obtained from HyClone, a division of Thermo Fisher Scientific (Waltham, MA, USA). Human IgG4 was obtained through a generous donation by Eli Lilly (Indianapolis, IN, USA). Human IgG1, IgG2, IgG3, and IgM, canine IgG, murine IgG, and rat IgG were purchased from Athens Research & Technology, Inc. (Athens, GA, USA). Microlon 200 medium-binding, clear, flat-bottomed, polystyrene 96-well plates were purchased from USA Scientific (Ocala, FL, USA). All buffer reagents including mono- and di-basic phosphate, Tris base and Tris hydrochloride, L-Glycine, Hydrochloric Acid, cysteine HCl, EDTA disodium salt, Tween 20, citric acid, glacial acetic acid, sodium hydroxide, glycine, 30% hydrogen peroxide, and NaCl were purchased from JT Baker (Philipsburg, NJ, USA). A Biomax PES 5 kDa MWCO TFF membrane was purchased from EMD Millipore (Billerica, MA, USA). Papain proteolytic enzyme, protein A, streptavidin agarose beads, and EZ-Link Sulfo-NHS -Biotin no weigh format were all purchased from Pierce Biotechnology, Inc. (Rockford, IL, USA). Isopropyl β-D-1-thiogalactopyranoside (IPTG) and 5-bromo-4-chloro-indolyl-β-D-galactopyranoside (X-Gal) were purchased from Fermentas, Inc. (Glen Burnie, MD, USA). Affi-Gel 10 activated immunoaffinity agarose resin was obtained from Bio-Rad (Hercules, CA, USA). Anti-M13 HRP-conjugated antibody was purchased from GE Healthcare (Piscataway, NJ, USA).

7.3.2 Fc target preparation

7.3.2.1 Fc generation

Human IgG4 (hIgG4) monoclonal antibody was digested with papain that had been immobilized on Affi-Gel 10 agarose beads and then purified over a protein A conjugated agarose column to obtain enriched Fc. Originally in citrate buffer pH 6.7, hIgG4 was diafiltered using 10 diavolumes into 20 mM phosphate, 150 mM NaCl, 10 mM EDTA, pH 7.0 (PBES) using a 5 kDa MWCO Biomax TFF membrane module and then concentrated to 20 mg/mL. Papain (5 mg lyophilized) was reconstituted with 1 mL of 20 mM phosphate containing 150 mM NaCl at pH 7.0 (PBS). Next 0.2 mL of 50% slurry of Affi-Gel 10 was transferred to a 1.7 mL centrifuge tube, washed with cold DI water, and equilibrated in PBS according to the product instructions.

The 0.2 mL of equilibrated 50% Affi-Gel 10 slurry (0.1 mL total bead volume) was added to the 1 mL of 5 mg/mL papain solution in a centrifuge tube and allowed to conjugate for 4 hr with agitation at 4 ºC. The effectiveness of conjugation was determined by measuring the absorbance at 280 nm of the reaction supernatant (diluted 1:10 in 0.1 M HCl). Any unreacted sites on the Affi-Gel 10 were quenched by incubation with 0.1 M glycine overnight at 4 ºC with agitation. Then 0.1 mL of the immobilized papain was activated prior to digestion for 30 min at 37 ºC with 1 mL PBES containing 10 mM freshly added cysteine (pH was readjusted to 7.0). The Affi-Gel 10 resin with immobilized papain was pelleted by centrifugation.

The resin was resuspended in 1 mL of hIgG4 solution (prepared by adding 0.5 mL PBES containing 20 mM cysteine to 0.5 mL of 20 mg/mL hIgG4 for final concentration of 10 mg/mL) and allowed to digest at 37 ºC for six hours with agitation. The immobilized papain containing digested hIgG4 mixture was centrifuged to pellet the resin and the supernatant containing hIgG4

fragments was collected, diluted with 9 mL PBS and immediately loaded over 1 mL Affi-Gel Protein A conjugated resin packed in a 5/100 tricorn column (GE Healthcare Pittsburgh, PA, USA) on an AKTA FPLC (GE Healthcare Pittsburgh, PA, USA).

Protein A (5 mg lyophilized) was reconstituted and conjugated to 1 mL Affi-Gel 10 resin following the same procedure for papain conjugation. The immobilized protein A was equilibrated with PBS prior to loading. The column containing resin with immobilized portion A was operated at 0.5 mL/min throughout the run. After loading, the column was washed with 10 column volumes of PBS and the bound material eluted with 0.1 M acetic acid and neutralized to pH 7.0 with 1 M phosphate pH 8.5.

Papain digestion of the antibody in the presence of a mild reducing agent generates Fc and a mixture of Fab and fragments. Protein A resin binds to the Fc fragments strongly while Fab predominantly passes through the column unbound; therefore the eluted fraction is highly enriched in Fc fragments as well as any undigested antibody. Fc enrichment after protein A purification was observed on a non-reducing 12% SDS-PAGE gel.

7.3.2.2 Fc Biotinylation

1 mL of 0.1 mg/mL Fc in acetate/phosphate buffer pH 7.0 (as described in section 2.2.1) was biotinylated using the EZ-Link Sulfo-NHS -Biotin no weigh format at the recommended conditions. Briefly we aimed for a 20-fold excess of sulfo-NHS-biotin reagent. Therefore 4 µL of 10 mM sulfo-NHS-biotin was added to 1mL of 0.1 mg/mL Fc (~50 kDa) solution and incubated for 2 hr on ice. Biotinylated Fc was diluted with 10 mL (of 50 mM Tris containing 150 mM NaCl at pH 7.5 (TBS buffer) and concentrated to 0.1 mg/mL (1mL) using an EMD

Millipore Amicon Ultra-15 5 kDa MWCO spin concentrator in a swing-bucket rotor centrifuge at 3000 rpm for approximately 40 min.

7.3.3 Phage Display Panning

The Ph.D.-7 heptapeptide phage library was supplied at $2x10^{13}$ pfu/mL and had a sequence diversity of approximately $2x10^{9}$ unique codon sequences. The panning experiments generally followed the procedure outlined in the Ph.D. phage display library manual. A 100-fold representation of the sequence diversity, $2x10^{11}$ phage particles, was added to the 1st round panning reaction. Initially, several panning experiments were conducted with Fc (non-biotinylated) being directly adsorbed to the surface of polystyrene dishes. Though these panning experiments yielded clear consensus sequences after 3 rounds of panning, it was subsequently discovered all clones showed appreciable plastic binding and not Fc binding, even with strenuous (1% Tween 20) surfactant washes. Such behavior has been detected before (Adey et al., 1995; Vodnik et al., 2011a). Therefore a solution panning system was employed with no polystyrene present. In the first round of panning $2x10^{11}$ library phage particles were diluted in 200 µL TBS with 0.1% Tween 20 and 2 pmol biotinylated Fc (100 ng or 1 µL of 0.1 mg/mL solution) and incubated at room temperature with agitation for 1 hr. Previously blocked streptavidin agarose beads (blocked with 5 g/L BSA in TBS) were used as an affinity resin to capture the biotinylated Fc, along with phage clones displaying Fc-binding peptides. Phage clones were eluted with 1 mL of 0.2 M glycine pH 2.4 (0.2 M Glycine adjusted to pH 2.4 with HCl). The supernatant was transferred to a separate tube after centrifugation, and neutralized with 150 µL of 1.5 M Tris pH 8.8. Eluted phages were amplified as described in the Ph.D.-7 phage-peptide library manual.

The number of phage particles in the second and third panning rounds were reduced to $2x10^9$ for each round to increase the stringency of selection. The Tween 20 concentration was increased to 0.5% for all binding and washing steps in the second and third rounds to prevent non-specific binding. In order further ensure that we did not select clones due to non-specific binding, negative streptavidin bead selection was performed in the second and third panning cycles. Prior to incubation with the Fc target, the phage particles were incubated with blocked streptavidin beads for 30 min after which the tubes were centrifuged. The supernatant used for panning with Fc, and streptavidin beads with non-Fc binders were discarded. In this way all components of the panning system were controlled to ensure only Fc binders will be present after 3 panning rounds.

Round 2 clones were eluted twice, first with 2 µM protein A (possibly a direct Fc-binding competitor depending on where on the Fc peptides bind) and then with 0.2 M glycine, pH 2.4. Round 3 was performed similarly to round 2 with two simultaneous panning experiments. Phage particles for each panning experiment were previously eluted either using protein A or glycine. After each panning experiment phage particles were again eluted by protein A followed by glycine for a total of 4 distinct phage pools at the end of round 3. Phage pools were titered and plaques picked for confirmation of Fc binding by ELISA.

7.3.4 ELISA binding experiments

7.3.4.1 Initial clone screening

A total of 44 clones were picked from the 4 enriched phage pools for Fc binding confirmation and further analysis by ELISA. The first ELISA plates were intended to demonstrate which clones were positive hIgG4 binders; further selecting against weak binders or

those binding something other than hIgG4. Odd rows (A, C, E, and G) of clear, flat-bottomed 96-well polystyrene plates were coated with 200 µL of 100 µg/mL hIgG4 in TBS for at least 24 hours at 4 ºC with agitation. Even rows (B, D, F, and H) served as negative control rows for each clone as they were filled with TBS only. Plates were blocked with 5 g/L BSA overnight at 4 ºC with agitation prior to use. Clones were screened by adding $2.5x10^{11}$ phage in 100 µL in two wells, one coated with hIgG4 and the other blank and serially diluting each 5-fold for two more wells, giving 6 wells total for each clone. In this way 15 clones could be screened per plate, leaving 6 wells as the plate background.

Phage dilutions in TBS with 0.5% Tween 20 (TBST) were performed on a separate blocked 96-well plate to prevent adsorption during dilution. $2.5x10^{11}$ phage particles in 100 µL is equivalent to only a 4 nM phage concentration; therefore lower binding energy clones would not give a positive signal. An anti-M13 phage HRP-conjugated antibody and ABTS HRP substrate were used as the phage detection system. Criteria for positive clones included a signal of at least 0.3 A.U. and signals from hIgG4 coated wells were at least 3 times higher than the corresponding signal from the negative control uncoated wells. Plates were read at 405 nm (1 sec per well) on a Victor X5 multimode plate reader from Perkin Elmer (Waltham, MA, USA) 40 minutes after ABTS was added to plates.

7.3.4.2 Peptide-phage binding in cell culture conditions

Since these peptides could be used as antibody purification ligands positive clones from the initial ELISA assays were subject to more rigorous testing to confirm binding in conditions resembling cell culture media with other proteins present. Each positive clone from the previous assay (section 2.4.1) was tested further by exploring binding to hIgG4 in DMEM with 5% FCS

and 5 g/L ovalbumin. Plates were coated as in the previous section 2.4.1 and clones were assayed in triplicate ($2.5x10^{11}$ phage particles in 100 µL per well). Instead of no coating, control wells were coated with 200 µL of 100 µg/mL lactoferrin in TBS, again to control for Fc specificity. The original phage library was assayed as well (coated and uncoated wells).

7.3.4.3 Peptide-phage binding to different antibody isotypes

All previous binding assays used the same hIgG4 Fc or full antibody as the target. Peptide binding to multiple antibody types was also investigated. Plates were coated with 7 other types of antibodies, hIgG1, hIgG2, hIgG3, hIgM, canine IgG, murine IgG, and rat IgG. Plates were coated with 200 µL of 100 µg/mL for each antibody with the exception of hIgG1 which was at 20 µg/mL. 2.5×10^{11} phage particles per well were assayed.

7.3.4.4 *Competitive Binding ELISA with Protein A*

A separate plate was again coated with 200 µL of 100 µg/mL hIgG4. ELISA conditions were identical to those in section 2.4.1 except for the addition of 0.2 µM native protein A to one virus-peptide solution (the other did not have protein A present) for each individual peptide clone prior to addition to coated wells.

7.3.5 DNA Sequencing of Positive Clones

DNA from positive Fc-binding clones was purified and sequenced to determine peptide composition. DNA was selectively isolated from viral protein via sodium iodide precipitation. DNA was sequenced on an ABI 3130xL Genetic Analyzer (Life Technologies Corp., Carlsbad, CA, USA) prepared with ABI BigDye Terminator v3.1 sequencing chemistry at the Colorado State University Proteomics and Metabolomics Facility. The sequencing primer used was a

downstream (-96 nt) complimentary strand primer with sequence 5' CCCTCATAGTTAGCGTAACG 3' as suggested in the manual. Therefore sequencing data revealed the anticodon sequence.

7.4 Results

7.4.1 Phage Display Panning Results

In round 1 of panning, phage particles were eluted from Fc bound to streptavidin beads via a biotin linker with a strongly acidic glycine buffer. This resulted in a phage titer of $6.7x10^5$ pfu/mL. This relatively high titer after only one round of enrichment for specific Fc binders most likely indicated numerous non-specific interactions of phage-peptides with other species present such as the streptavidin agarose beads. Negative selection with streptavidin beads and amplified round 1 phage eluate ($2x10^9$ pfu input) prior to panning with the Fc target was successful in reducing non-specific binding of phage particles as shown by the lower titers from both protein A ($5.0x10^4$ pfu/mL) and subsequent acidic glycine ($2.8x10^5$ pfu/mL) eluate pools. This also demonstrates the level of non-specifically interacting peptide-phage in the original library that need to be removed from the panning pool before successful Fc binders can be isolated.

Before switching to a solution phase affinity bead panning system, several attempts were made to isolate Fc binding peptides with Fc coated to a polystyrene plate. High final round panning eluate titers (greater than $1x10^9$ pfu/mL) were observed and consensus sequences were reached however all ELISA binding assays were either negative or showed similar binding to negative control (uncoated) wells as the positive wells indicating polystyrene or, less probably, BSA binding. However, the final round of unamplified eluate titers from the solution panning

was in the $10^5 – 10^6$ pfu/mL range. This, combined with the small amount of target Fc present (2 pmol) and input phage particles (less than $2x10^9$ pfu/mL, after negative selection) during solution panning, gave higher confidence that specific peptide-Fc interactions were dominant.

7.4.2 Confirmation of selected clone binding by ELISA

Previously, non-specific clones had been selected from surface panning experiments; therefore initial binding characterization of selected clones was essential before more detailed binding experiments. As stated in section 2.4.1, 44 total clones were isolated from titer plates and amplified for characterization by ELISA. Of those 44, 15 were from plates eluted with acidic glycine in the 2nd panning cycle and 2 µM protein A in the 3rd panning cycle. Another 15 were from plates eluted with protein A in both the 2nd and 3rd panning cycles. An additional 14 clones were from plates eluted with acidic glycine buffer in both the 2nd and 3rd panning cycles.

Two criteria were used for selecting positive clones. The signal in the hIgG4 coated well with the most phage ($2.5x10^{11}$ particles) had to be at least 0.3 A.U. At such a low concentration (4 nM in 100 µL) of phage particles a positive signal was only possible if the dissociation constant of the peptides was low (less than µM), increasing the selection of peptides with high binding energy. The second criterion was the ratio of the signal from hIgG4 coated wells and uncoated wells (non-specific control) had to be greater than 3. Again, this provided assurance that selected clones were binding to the Fc portion of the antibody and not unblocked portions of the polystyrene well.

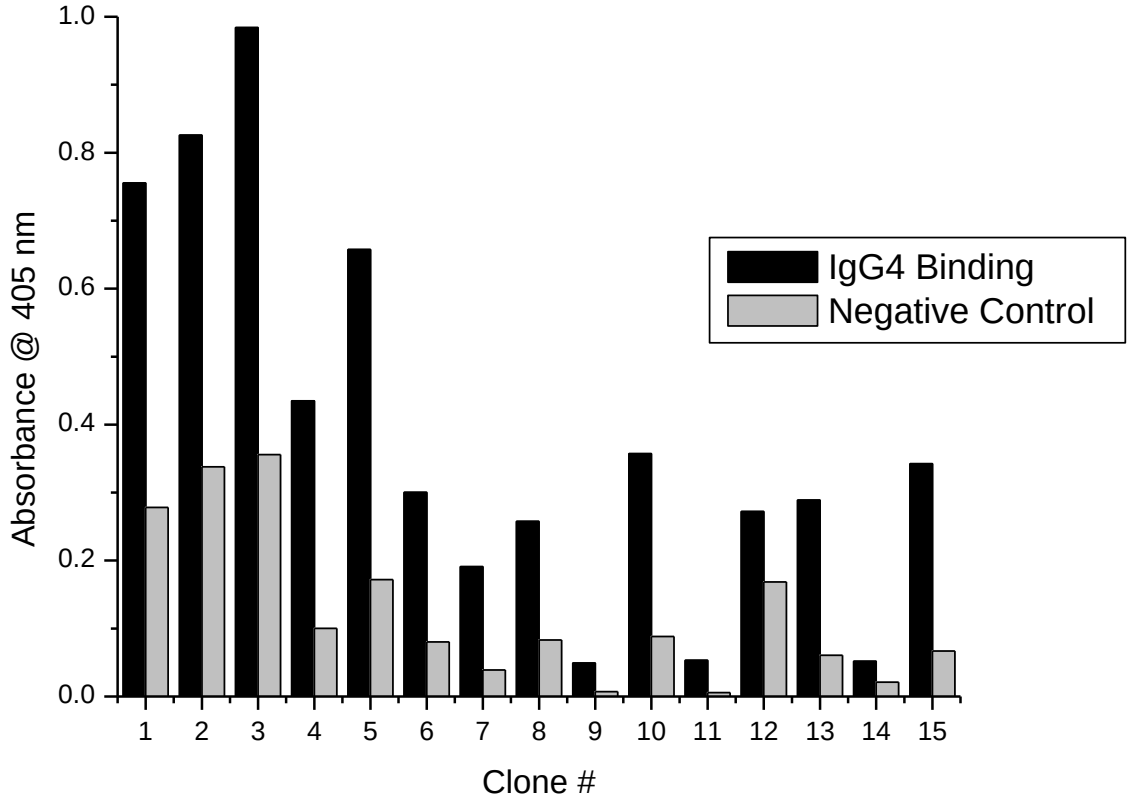

Figure 7.1: ELISA results showing hIgG4 binding by peptide-virus clones eluted with (2nd round) 5 µM Protein A followed by (3rd round) 0.2 M glycine pH 2.4.

Figure 1 shows the binding results for clones eluted with acidic glycine buffer and protein A. Elution conditions for round two and three panning were acidic glycine and protein A, respectively. Three clones (1, 3, and 5) met the selection criteria and further binding studies included these clones. Figure 2 shows binding results from clones eluted with protein A (2nd round) and protein A again (3rd round).

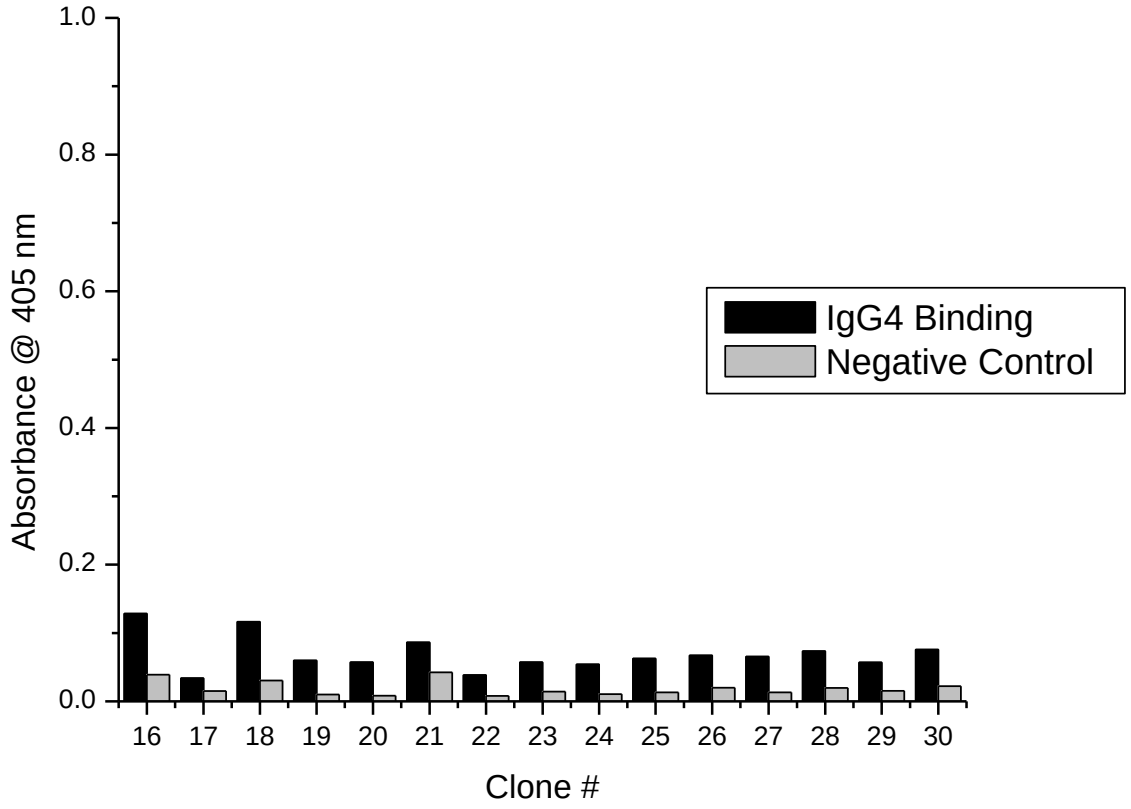

Figure 7.2: ELISA results showing hIgG4 binding by peptide-virus clones eluted with (2nd round) 5 µM Protein A followed by (3rd round) Protein A.

Interestingly none of the clones isolated from these elution conditions showed strong enough binding to evaluate further. Figure 3 presents the binding results from the acidic elution conditions. Clones 31 – 44 were isolated using acid elution conditions in both the 2nd and 3rd rounds. Four clones (34, 36, 40, and 44) satisfied the selection criteria and were further evaluated as well.

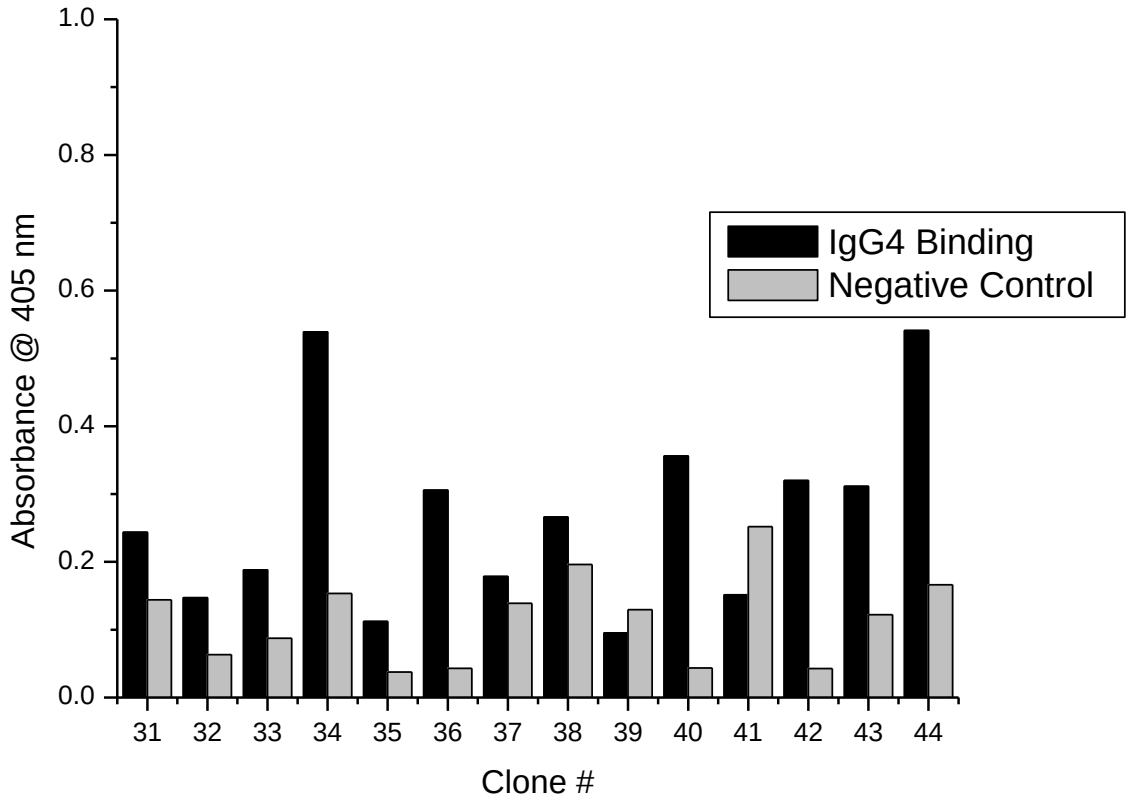

Figure 7.3: ELISA results showing hIgG4 binding by peptide-virus clones eluted with (2nd round) 0.2 M glycine pH 2.4 followed by (3rd round) 0.2 M glycine pH 2.4.

7.4.3 Secondary screening of clones

Seven total clones (1, 3, 5, 34, 36, 40, and 44) were screened further to confirm selective binding to hIgG4. The binding conditions in this round of ELISA were designed to mimic antibody binding from cell supernatant. Therefore binding to hIgG4 was attempted in DMEM cell culture media with 5% FCS and 5 g/L ovalbumin (BSA was present as a blocking agent as well). The presence of ovalbumin at orders of magnitude higher concentration compared to the peptide-virus clones, as well as the proteins and other molecules associated with FCS established a challenging binding environment for the peptides to hIgG4. Figure 4 shows the secondary

selection results. Similar to the uncoated negative control well results during the screening ELISA, all 7 clones showed at least 3-fold greater absorbance in hIgG4-coated wells than in

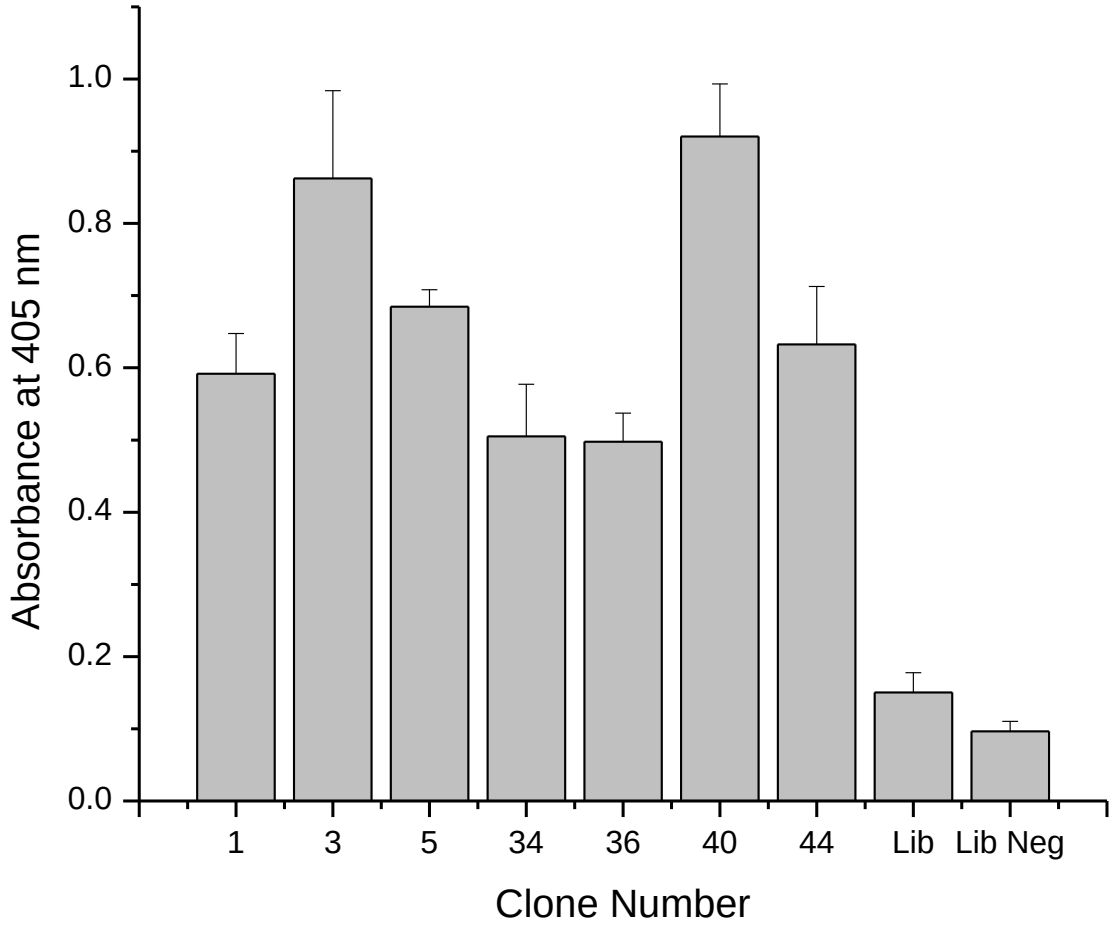

Figure 7.4: ELISA results for peptide binding (in triplicate) to hIgG4 in DMEM, 5% fetal calf serum, and 5 g/L Ovalbumin. Original phage library (Lib) binding to IgG4 coated wells and original library binding to uncoated wells (Lib Neg) are presented as well. Error bars represent standard deviation.

lactoferrin-coated negative control wells (data not shown). All clones also showed greater than 2.5-fold higher absorbance on IgG4-coated wells than the original phage library indicating successful enrichment of IgG_4-binding clones. Binding signal of the original phage library to

IgG4-coated wells was not statistically different from the phage library signal to negative control wells indicating very low positive binding as expected in the non-enriched library. Clones 3 and 40 showed the highest binding with ELISA signals above 0.85 AU, representing over 4-fold enrichments in ELISA signal as compared to the original library. As indicated by the error bars which represent the standard deviation, the results were highly reproducible.

7.4.4 Binding to Multiple Antibody Types

To further characterize the binding of the peptides to antibody Fc ELISA plates were coated with multiple antibody types. Native Protein A has strong affinity for human IgG1, IgG2, and IgG4 antibody isotypes but not IgG3. Therefore peptide binding to all 4 different human IgG isotypes was tested as well as binding to human IgM which has shown variable binding to protein A (Hakoda, 1996). Binding to non-human IgG molecules such as murine IgG, canine IgG, and rat IgG was also investigated. The ELISA binding results from the multiple antibody plate are shown in Figure 5. With the exception of binding to human IgG1, all peptides demonstrated strong binding to all antibody types tested. It was difficult to conclude the peptides do not bind to hIgG1 because the well coating concentration was 5-fold lower than the other antibodies as a result of limited available hIgG1 reagent. Higher ELISA signal was observed for all peptides binding to hIgG1 as compared to uncoated negative control wells, however the signal was not at least 3X higher to match the selection criteria set forth previously. Interestingly, clone 44 showed strong binding to all antibody types with the exception of binding to canine IgG (and hIgG1, previously explained). In general, the peptides bound strongest to both murine IgG and hIgG3, which is particularly interesting given the lack of hIgG3 affinity for Protein A.

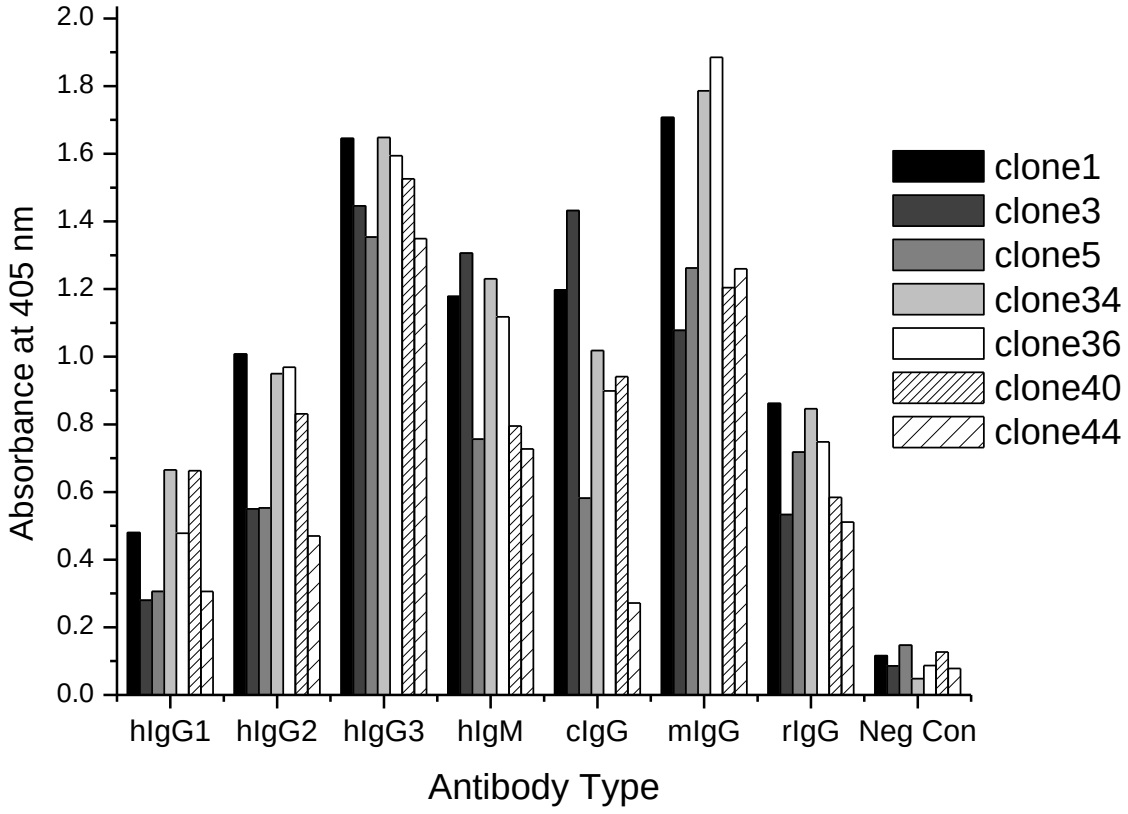

Figure 7.5: Peptide binding to various human antibody isotypes, as well as canine IgG (cIgG), murine IgG (mIgG), and rat IgG (rIgG)

7.4.5 Competitive ELISA with Protein A

To determine whether selected peptides shared portions of the same binding site as Protein A a competitive binding ELISA was conducted. An interesting outcome of the ELISA were all wells wherein Protein A was added showed at least 2X higher signal than non-Protein A wells, which is the opposite of what was expected of a competitive binding assay (results not included). On the surface these data are hard to reconcile until the nature of the Protein A binding protein is considered. Multiple studies have characterized the Protein A binding stoichiometry as greater than 2.4 to 1 referring to the ratio of antibody molecules to Protein A

molecules (Ghose et al., 2007; Jungbauer and Hahn, 2004). When considering the multi-valency of the Protein A ligand it is hypothesized that Protein A is binding to the immobilized hIgG4 and is subsequently sandwiched by a second antibody which is the HRP-conjugated reporter antibody present in the ELISA assay. Therefore high ELISA signal was considered independent of bound peptide-viral particle concentration when Protein A was present.

7.4.6 Sequencing of Selected Peptides

Peptides displayed on selected phage clones were sequenced at the Colorado State University Proteomics and Metabolomics Facility. Sequencing results are presented in Table 1. All seven selected peptides were single heptapeptide displays; previous panning attempts (less stringent) had resulted in a high percentage of multi-heptapeptide constructs which were subsequently shown to bind in a non-specific manner. The unique heptapeptides selected in this work bound specifically to the Fc region of multiple antibody types.

Table 7.1: Sequencing results from clones showing positive Fc binding

Clone	Amino Acid Sequence
1	CPSTHWK
3	NVQYFAV
5	ASHTQKS
34	QPQMSHM
36	TNIESLK
40	NCHKCWN
44	SHLSKNF

7.5 Discussion

This study was successful at identifying seven unique heptapeptides with specific affinity for the Fc region of immunoglobulins. The importance of the phage display selection system and multiple screening and selection rounds were highlighted for effective peptide selection.

Identified peptides were shown to have broader binding tropisms than Protein A as evidenced by peptide binding to all major human IgG isotypes including IgG3, human IgM, and canine, murine, and rat IgG. Binding was shown not to be inhibited by the presence of Fetal Calf Serum, Bovine Serum Albumin, Ovalbumin, or DMEM cell culture medium.

It was interesting that, even after stringent efforts put forth to remove non-specific clones, only 20.5% of the clones were positive Fc and hIgG4 binders. There is the possibility that, because panning was performed with Fc only whereas the ELISA's were all performed with intact antibody, several peptides initially selected may have bound Fc near the N-terminal hinge region normally connected to the Fab portion of the antibody. That would preclude peptide binding of the intact antibody, which was the goal of this study.

The stringent selection conditions, three rounds of phage display panning, as well as the relatively large Fc binding surface, may account for the lack of overall consensus sequence obtained in this study. The screening ELISA and secondary selection ELISA data showed positive clones were present after three rounds of panning and therefore subsequent panning rounds were not undertaken. Four or more rounds of panning may have led to a consensus sequence however further rounds of panning can lead to selection not on the basis of binding but selection by viral reproductive characteristics.

Though each peptide identified was unique they did exhibit some common characteristics. Histidine residues were present in five of the seven peptides selected; Serine and Lysine residues were also present in five of the seven peptides. Histidine, and to a lesser extent Lysine and Serine, are common residues in several previously identified Fc binding peptides such as CHKRSFWADNC from Jeong et al, or the HWRGWV peptide first identified by Yang

et al (Jeong, 2010; Yang et al., 2006). Histidine and Lysine residues are both highly conserved in the 5 homologous Fc binding domains present in native Protein A (NCBI GenBank). Protein BLAST analysis on the NCBI website showed each selected peptide sequence is present in a multitude of different functional and structural proteins however none contain known immunoglobulin binding domains providing further evidence these peptides are novel. Though the binding site(s) of the peptides to the Fc region have not been elucidated in this study it is likely the peptides do not share a common site on the Fc (such as the Protein A groove). The differences in charge and hydrophobicity of the residues found in each of the seven peptides indicate independent Fc binding regions were likely bound by the different peptides.

A library of heptapeptides was chosen to evaluate for Fc binding for several reasons. No heptapeptides specifically binding Fc have been reported in the existing public literature. Existing available heptapeptide libraries enabled relatively quick exploration without the need for library generation. Importantly, these short heptapeptides, as well as other Fc-binding peptides, may show greater chemical stability than native or recombinant Protein A ligands. Their short primary sequence, in this case seven amino acids total, eliminate the need to preserve any tertiary or secondary structures present in larger binding ligands. This may make peptides less susceptible to denaturing or chemical alteration in sanitizing conditions such as 1M NaOH, while current Protein A ligands are highly sensitive to such conditions. Finally, these peptides may prove useful in the purification of Fc-containing immunoglobulins, such as monoclonal antibodies, from serum or cell culture supernatant.

Identification of multiple peptides which specifically bind to a given target (in this case Fc) may be beneficial to engineering ligands with higher specificity. Several peptides or small binding domains joined together have been shown both in natural and engineered ligands to

increase specificity (Heiskanen et al., 2003; Traxlmayra et al., 2011) including protein A itself (Moks et al., 1986). The Fc binding peptides identified in this work are disparate enough in sequence that we speculate the peptides bind to multiple sites on the Fc. Based on the structure of protein A (5 binding domains), MabSelect Sure ligand (4 binding domains), and other successful commercially available Fc binding ligands with 4 binding domains (described in section 1.0) a multi-domain ligand may be desirable to achieve high specificity. To that end identification of multiple sites within a target for peptides to bind can only occur when the target is of sufficient size to allow multiple peptide attachment. The 50 kDa Fc region fits that criterion.

7.6 Conclusion

A stringent solution panning phage display method has been used to identify seven unique heptapeptides that have specific affinity for the Fc region of immunoglobulins. Applying multiple ELISA screening and selection rounds confirmed selective binding of the peptides to Fc. Binding of the peptides to human IgG1, IgG2, IgG3, IgG4, and IgM (Protein A does not bind hIgG3) was demonstrated as well as binding to canine, murine, and rat IgG. Due to selective binding for Fc and ease of production and use, these peptides may be useful in antibody detection and purification applications.

References

Adey, N.B., Mataragnon, A.H., Rider, J.E., Carter, J.M., Kay, B.K. 1995. Characterization of phage that bind plastic from phage-displayed random peptide libraries. *Gene* 156: 27 - 31.

Arnold, M., Bittermann, H., Kalbfuss-Zimmermann, B., Neumann, T., Schmidt, K., Sekul, R., Hilbrig, F., Ludolph, H., Freitag, R. 2011. Antibody purification by affinity chromatography based on small molecule affinity ligands identified by SPR-based screening of chemical microarrays. *J. Chromatogr A* 1218 (29): 4649 - 4659.

Berntzen, G., Andersen, J.T., Ustgard, K., Michaelsen, T.E., Mousavi, S.A., Qian, J.D., Kristiansen, P.E., Lauvrak, V., Sandlie, I. 2009. Identification of a High Affinity FcyRIIA-binding Peptide That Distinguishes FcyRIIA from FcyRIIB and Exploits FcyRIIA-mediated Phagocytosis and Degradation. *J. Biol. Chem.* 284 (2): 1126 - 1135.

Costioli, M., Guillemont-Potelle, C., Mitchell-Logean, C., Broly, H. 2010. Cost of Goods Modeling and Quality by Design for Developing Cost-Effective Processes. *Biopharm International* 23 (6).

DeLano, W.L., Ultsch, M.H., deVos, A.M., Wells, J.A. 2000. Convergent Solutions to Binding at a Protein-Protein Interface. *Science* 287: 1279 - 1283.

Dinon, F., Salvalaglio, M., Gallotta, A., Beneduce, L., Pengo, P., Cavallotti, C., Fassina, G. 2011. Structural refinement of Protein A mimetic peptide. *J. Mol. Recognit.* 24: 1087 - 1094.

Fassina, G., Verdoliva, A., Odierna, M., Ruvo, M., Cassini, G. 1996. Protein A mimetic peptide ligand for affinity purification of antibodies. *J. Mol. Recognit.* 9 (5 - 6): 564 - 569.

Finkelstein, A., Badretdinov, A., Ptitsyn, O. 1991. Physical Reasons for Secondary Structure Stability - Alpha-Helices in Short Peptides. *Proteins: Struct., Funct., Genet.* 10 (4): 287 - 299.

Gagnon, P. 2012. Technology trends in antibody purification. *J. Chromatogr A* 1221: 57 - 70.

Gaskin, D.J.H., Starck, K., Turner, N.A., Vulfson, E.N. 2001. Phage display combinatorial libraries of short peptides: ligand selection for protein purification. *Enzyme Microb Tech* 28: 766 - 772.

Georgieva, Y., Konthur, Z. 2011. Design and Screening of M13 Phage Display cDNA Libraries. *Molecules* 16: 1667 - 1681.

Ghose, S., Hubbard, B., Cramer, S. 2007. Binding Capacity Differences for Antibodes and Fc-fusion Proteins on Protein A Chromatographic Materials. *Biotechnol. Bioeng.* 96 (4): 768 - 779.

Gottschalk, U. 2005. Downstream processing of monoclonal antibodies: From high dilution to high purity. *Biopharm Int.* 18 (6): 42 - 58.

Gulich, S., Linhult, M., Stahl, S., Hober, S. 2002. Engrineering streptococcal protein G for increased alkaline stability. *Protein Eng* 15 (10): 835 - 842.

Gurgel, P.V., Carbonell, R.G., Swaisgood, H.E. 2001a. Fractionation of whey proteins with a hexapeptide ligand affinity resin. *Bioseparation* 9: 385 - 392.

Gurgel, P.V., Carbonell, R.G., Swaisgood, H.E. 2001b. Indentification of Peptide Ligands Generated by Combinatorial Chemistry that Bind alpha-Lactalbumin. *Separ. Sci. Technol.* 36 (11): 2411 - 2431.

Haigh, .J, Hussain, A., Mimmack, M., Lowe, C. 2009. Affinity ligands for immunoglobulins based on the multicomponent Ugi reaction *J. Chromatogr B* 877 (14-15): 1440 - 1452.

Hakoda, M., Kamatani, N., Hayashimoto-Kurumada, S., Silverman, G.J., Yamanaka, H., Terai, C., Kashiwazaki, S. 1996. Differential Binding Avidities of Human IgM for Staplylococcal Protein A Derive From Specific Germ-Line VH3 Gene Usage. *J. Immunol.* 157 (7): 2976 - 2981.

Heiskanen, T., Li, X-D., Hepojoki, J., Gustafsson, E., Lundkvist, A., Vaheri, A., Lankinen, H. 2003. Improvement of binding of Puumala virus neutralization site resembling peptide with a second-generation phage library. *Protein Eng. Des. Sel.* 16 (6): 443 - 450.

Hober, S., Nord, K., Linhult, M. 2007. Protein A Chromatography for antibody purification. *J. Chromatogr B* 848: 40 - 47.

Islam, T. 2013. Selection of Ceramic Fluorapatite-Binding Peptides from a Phage Display Combinatorial Peptide Library: Optimum Affinity Tags for Fluorapatite Chromatography. *Journal of Molecular Recognition* 26 (8): 341-350.

Islam, T., Aguilar-Yanez, J.M., Simental-Martinez, J., Ortiz-Alcaraz, C.I., Rito-Palomares, M., Fernandez-Lahore, M. 2014. A Novel Strategy for the Purification of a Recombinant Protein Using Ceramic Fluorapatite-Binding Peptides as Affinity Tags. *Journal of Chromatography A* 1339: 26-33.

Jeong, Y-j. 2010. Efficient selection of IgG Fc domain-binding peptides fused to fluorescent protein using E. Coli expression system and dot-blotting assay. *Peptides* 31: 202-206.

Jungbauer, A., Hahn, R. 2004. Engineering Protein A Affinity Chromatography. *Curr. Opin. Drug Discovery Dev.* 7 (2): 248 - 256.

Krook, M., Mosbach, K., Ramstrom, O. 1998. Novel peptides binding to the Fc-portion of immunoglobulins obtained from a combinatorial phage display peptide library. *J. Immunol. Methods* 221: 151 - 157.

Larbanoix, L., Burtea, C., Ansciux, E., Laurent, S., Mahieu, I., Elst, L.V., Muller, R.N. 2011. Design and evaluation of a 6-mer amyloid-beta protein derived phage display library for molecular targeting of amyloid plaques in Alzheimer's disease: Comparison with two cyclic heptapeptides derived from randomized phage display library. *Peptides* 32: 1243.

Levine, R.M., Scott, C.M., Kokkoli, E. 2013. Peptide functionalized nanoparticles for nonviral gene delivery. *Soft Matter* 9: 985 - 1004.

Linhult, M., Gulich, S., Graslund, T., Simon, A., Karlsson, M., Sjoberg, A., Nord, K., Hober, S. 2004. Improving the tolerance of a protein a analogue to repeated alkaline exposures using a bypass mutagenesis approach. *Proteins* 55 (2): 407 - 416.

Merie, L. 2011. Biologics Sales in 2010 exceeded US$ 100 bln. www.pipelinereview.com/index.php/2011030740651/Financials/Biologics-Sales-in-2010-exceeded-US$-100-bln.html

Moks, T., Abrahmsen, L., Nilsson, B., Hellman, U., Sjoquist, J., Uhlen, M. 1986. Staphylococcal protein A consists of five IgG-binding domains. *Eur. J. Biochem.* 156: 637 - 643.

Mooney, J.T., Fredericks, D., Hearn, M.T.W. 2011. Use of phage display methods to identify heptapeptide sequences for use as affinity purification 'tags' with novel chelating ligands in immobilized metal ion affinity chromatography. *J. Chromatogr A* 1218: 92 - 99.

Naik, A.D., Menegatti, S., Gurgel, P.V., Carbonell, R.G. 2011. Performance of hexamer peptide ligands for affinity purification of immunglobulin G from commercial cell culture media. *J. Chromatogr A* 1218: 1691 - 1700.

Ng, M.Y.T., Tan, W.S., Tey, B.T. 2012. Purification of Recombinant Hepatitis B Core Antigen from Unclarified Escherichia Coli Feedstock using Phage-Immoblizied Expanded Bed Adsorption Chromatography. *Journal of Chromatography B* 903: 60-67.

Pulicherla, N., Asokan, A. 2011. Peptide Affinity Reagents for AAV Capsid Recognition and Purification. *Gene Therapy* 18: 1020-1024.

Serizawa, T., Iida, K., Matsuno, H., Kurita, K. 2007. Cellulose-binding heptapeptides identified by phage display methods. *Chemistry letters* 36: 988 - 989.

Sidhu, S. 2001. Engineering M13 for phage display. *Biomol. Eng* 18 (2): 57 - 63.

Sinha, P., Sengupta, J., Ray, P.K. 1999. A Minimized Fc Binding Peptide from Protein A Induces Immunocyte Proliferation and Evokes Th1-Type Response in Mice. *Biochem. Biophys. Res. Commun.* 258: 141 - 147.

Starovasnik, M., O'Connell, M., Fairbrother, W., Kelley, R. 1999. Antibody variable region binding by Staphylococcal protein A: Thermodynamic analysis and location of the Fv binding site on E-domain. *Protein Sci.* 8: 1423 - 1431.

Traxlmayra, M.W., Wozniak-Knoppa, G., Antesd, B., Stadlmayra, G., Rükera, F., Obingera, C. 2011. Integrin binding human antibody constant domains—Probing the C-terminal structural loops for grafting the RGD motif. *J Biotech* 155: 193 - 202.

Verdoliva, A., Pannone, F., Rossi, M., Catello, S., Manfredi, V. 2002. Affinity purification of polyclonal antibodies using a new all-D synthetic peptide ligand: comparison with protein A and protein G. *J. Immunol. Methods* 271: 77 - 88.

Vodnik, M., Zager, U., Strukelj, B., Lunder, M. 2011a. Phage Display: Selecting Straws Instead of a Needle from a Haystack. *Molecules* 16: 790 - 817.

Wang, Y., Li, T. 2002. Identification of Affinity Ligands for Protein Purification from Synthetic Chemical Combinatorial Libraries. *Biotechnol. Prog.* 18: 524 - 529.

Yang, H., Gurgel, P.V., Carbonell, R.G. 2006. Hexamer peptide affinity resins that bind the Fc region of human immunoglobulin G. *J. Pept. Res.* 66: 120 - 137.

Yang, H., Gurgel, P.V., Williams Jr, D.K., Bobay, B.G., Cavanagh, J., Muddiman, D.C., Carbonell, R.G. 2010. Binding site on human immunoglobulin G for the affinity ligand HWRGWV. *J. Mol. Recognit.* 23: 271 - 282.

Yang, H., Liu, Z., Zhang, L., Wang, J., Yang, H., Qin, L., Jin, R., Feng, Y., Cui, Z., Zheng, R. and others. 2011. Selection and Application of Peptide Mimotopes of MPT64 Protein in Mycobacterium Tuberculosis. *Journal of Medical Microbiology* 60: 69-74.

Chapter 8

Conclusions and Suggested Future Work

8.1 Conclusions

This thesis presents the development and application of adsorptive membranes for recombinant protein, specifically monoclonal antibody, purification as well as identification of novel peptide affinity ligands, also for antibody purification. Commercially available anion-exchange membrane adsorbers were investigated for trace impurity removal, specifically virus, host cell protein, and DNA which are all major contaminants in industrial processes. Novel anion-exchange membranes, constructed by our collaborators at Clemson University, were also evaluated for binding capacity as well as DNA and virus removal. and novel heptapeptides were identified with binding affinity and selectivity similar to protein A; a gold standard in monoclonal antibody purification processes. Commercially available anion-exchange membrane adsorbers including the quaternary amine-containing Sartobind® Q and Mustang Q® from Sartorius and Pall, respectively, as well as the primary amine ligand membrane ChromaSorb® sold by Millipore were evaluated. Removal of minute virus of mice (MVM), host cell proteins, and DNA was demonstrated across a wide range of solution variables including pH, conductivity, mono- and multi-valent anionic buffer species, and flow rate. In addition to commercially available membranes, novel strong anion-exchange membranes constructed by Dr. Bharat Bhut in the Husson group at Clemson University were evaluated as well. Both the commercially available membranes, in particular the ChromaSorb due to its multi-modal binding

potential, and the novel membranes were proven to have distinct advantages over traditional porous bead packed-bed anion-exchange columns commonly used in the biopharmaceutical industry.

In addition to anion-exchange chromatography investigations and improvements, small peptides displaying binding behavior similar to protein A were identified and characterized. The peptides were shown to bind specifically to the Fc region of immunoglobulins, particularly human IgG's. Binding of the peptides was not inhibited by cell culture media or the presence of 5g/L BSA or ovalbumin.

Chapter 2 presented the work associated with completing research aim one of this thesis as outlined in section 1.7. Here a comprehensive evaluation of how solution properties and membrane properties affected the binding of MVM. Two of the membranes investigated, Sartobind Q and Mustang Q, have strong anion-exchange quaternary amine ligands which were capable of electrostatic interactions only. Both membranes showed 4 log removal of virus (LRV) or 99.99% binding at pH 9.0 and 0 - 50 mM NaCl, which was consistent with the few papers published on membrane virus removal. However MVM binding was severely compromised at 200 mM NaCl over a pH range of 6 - 9 with the Mustang Q, whereas binding was maintained at pH 9 on the Sartobind Q. Further analysis proved the difference may be explained by differences in the ligand density on the membrane pore surface. In contrast membranes with primary amine weak anion-exchange ligands such as the ChromaSorb make use of both electrostatic and secondary H-bond stabilizing interactions which contribute to a high MVM removal over the entire pH (6-9) and NaCl (0 - 200 mM) range explored. Competing anionic species with H-bonding capability such as phosphate have a detrimental affect on MVM removal with primary amine ligands; the detrimental affect is minimal over strong quaternary amine ligands.

Maximizing the ligand density on the membrane pore surface, while having a positive binding affect, alone will not maximize capacity. Because virus particles are large compared with other contaminants membrane pore structure and 3-D spacial arrangements of binding ions will need to be optimized for maximal virus binding over the largest solution range.

In chapter 3 trace impurity binding to the three anion-exchange membrane adsorbers was investigated further by evaluating more complex impurity solutions, thereby satisfying research aim number two in this thesis. MVM removal was shown to be minimally affected by concurrent host cell protein and DNA binding; however removal in the presence of 5 g/L monoclonal antibody was significantly reduced across all three membranes due to competitive antibody binding to the membranes. The combination of low NaCl/high pH resulted in excellent removal of MVM and DNA over the quaternary amine membranes (Sartobind Q and Mustang Q) however 100 - 200 mM NaCl at pH below 9.0 showed reduced removal, especially of host cell protein. This is further evidence of the predominantly coulombic nature of the binding interactions on the Q membranes. Continuing the trend demonstrated in chapter 2, the ChromaSorb showed greater than limit of detection MVM removal for all buffer conditions not containing phosphate. Phosphate containing buffers (25 - 50 mM) contributed to a substantial loss of MVM removal; this affect was more pronounced at higher pH where the divalent form of phosphate is dominant suggesting mutli-charged/H-bond capable anionic species are especially detrimental to impurity binding on primary amine ligands. Host cell protein, a heterogeneous population of positive and negatively-charged proteins, removal was to limit of quantification for all buffer conditions, excluding phosphate, over the ChromaSorb. This supplied additional evidence secondary H-bonding interactions were stabilizing the binding of anionic, neutral, and even overall positively charged impurities. DNA binding was generally high across all buffer

conditions owing to the strong negative charge in all pH conditions evaluated. Monoclonal antibody recovery was poor in all cases indicating excessive binding to the membranes; this was most likely due to the low pI of the mAb evaluated. Lowest recovery was encountered on the ChromaSorb, indicating both increased ligand density and secondary non-electrostatic interactions are a contributing factor. Overall, prediction of trace removal is much simpler over purely electrostatic ligands such as the quaternary amine ligands on the Sartobind Q and Mustang Q. However, impurity binding decreases rapidly in solutions outside of the favorable low NaCl/high pH conditions. Primary amine ligands, such as those on the ChromaSorb, overcome those solution limitations as impurity removal was demonstrated across a wide range of pH and NaCl concentrations; however, the presence of competing multi-valent anion species such as phosphate severely impedes impurity binding. Finally binding was shown to be independent of flow rate, proving convectively driven transport of impurities to all binding sites on the membrane.

Chapters 4 and 5 present the work completed to evaluate ligand chain length and density on novel anion-exchange membrane adsorbers fulfilling research aim three. This work was completed in collaboration with the Husson group at Clemson University, specifically with Dr Bharat Bhut who designed and constructed the novel ligands on regenerated cellulose membranes. It was shown that IgG, DNA, and virus binding capacity increased with both chain length and chain density. Binding capacity for IgG but especially for larger impurities like MVM was not impeded at high ligand density suggesting the spacing between ligands was still great enough to allow efficient transport of all impurity species to the majority of binding sites. The IgG dynamic binding capacities achieved on these membranes was higher than current

commercially available membrane adsorbers further proving the utility of three-dimensional anion-exchange ligands.

In chapter 6 protein purification using membrane adsorbers was further explored with a different mechanism of binding, hydrophobic interaction. Similar to chapters 4 and 5, three-dimensional binding ligands were grafted from the pore surface of regenerated cellulose membranes. Poly N-vinylcaprolactam, which has the advantageous property of dehydrating and becoming more hydrophobic at high ionic strength, yet transitions to a hydrated, more hydrophilic ligand at low ionic strength due to changes in the LCST with ionic strength, was used as the binding ligand. Varying the initiator immobilization time, and therefore the ligand density across the pore surface and overall degree of grafting, increased the BSA binding capacity. As indicated in Chapter 1, one issue with hydrophobic interaction chromatography for protein purification is recovery off the hydrophobic media, without the use of denaturing organic solvents, is low compared to ion exchange media. However the novel hydrophobic interaction membranes discussed in Chapter 6 showed excellent recovery even at high binding capacities. This is reflective of the change in hydrophobic properties of the N-VCL in response to solutions properties, in this case ionic strength.

Finally, monoclonal antibody purification was explored from a different perspective than membrane adsorbers; small peptides were investigated for activity similar to protein A which is a monoclonal antibody gold standard. Chapter 7 discusses the work performed on this topic, satisfying research aim number four. A solution phase phage display method was developed with high target stringency and low non-specific binding. An ELISA assay was developed to assay for and confirm specific binding to the immunoglobulin targets. Multiple rounds of ELISA confirmed specific binding of peptides to the Fc region of Ig's. Binding was demonstrated not

only to the original target, human IgG4 Fc, but to human IgG1, IgG2, and IgG3 as well as human IgM and murine, rat, and canine IgG. Sequencing results showed different amino acid sequences suggesting multiple binding sites on the Fc are being utilized. The selectivity demonstrated as well as required affinity for phage display suggest these peptides may be useful alternatives to protein A for monoclonal antibody purification.

8.2 Suggested Future Work

Though much has been accomplished towards the goal of increasing productivity or reducing the cost of monoclonal antibody production through anion-exchange or hydrophobic interaction membrane adsorber use or identifying small peptides with protein A-like functionality more still needs to be researched in order to fully realize the benefits of these technologies.

Virus breakthrough behavior analysis was attempted through fractionation of membrane effluent however binding site saturation at the 500 membrane volumes per load was not accomplished. Construction of binding isotherms of MVM binding to anion-exchange membrane media in varying solutions of pH/NaCl/phosphate would give a more thorough understanding of MVM equilibrium binding behavior. Though, as noted in chapter 3, competitive binding of protein of interest (in this thesis IgG) may present more of a challenge to robust virus binding. Competitive binding experiments are complicated, requiring different protein of interest with differing binding properties to compete with the virus particles. For a given solution condition (constant pH/NaCl/phosphate), different proteins will bind to the anion-exchange media with varying binding constants; comparing the binding of proteins with that of virus could perhaps

lead to a more predictive model for virus binding. If successful this would negate the need for many expensive virus removal experiments in the biopharmaceutical industry.

A different approach to use of anion-exchange, or any type, membrane adsorbers would be to re-use them for multiple cycles during protein purification processes. The economics of membrane adsorbers are generally very favorable as compared to traditional packed-bed column processes; however membranes have been designed for single-use only. Membrane regeneration and cleaning experiments with both commercial and the novel membranes developed in this thesis (chapters 4, 5, and 6) will need to be performed. Parameters to monitor after each protein run, and subsequent cleaning with 1N NaOH, include binding capacity, recovery, and flow/pressure behavior. Surface characterization techniques like those employed in chapters 2, 3, and 6 (FTIR, XPS, and contact angle) could also be used to confirm ligand stability (or instability) under such harsh cleaning conditions.

The novel HIC membranes developed herein represent a step forward in three-dimensional and environmentally responsive HIC membranes. Further studies with proteins other than BSA (almost always the proof of concept model protein of choice) such as IgG would provide additional evidence of the benefits of these membranes to industrial applications. Application of these 3-D ligands to traditional chromatography beads with larger pore sizes (> 50 nm) to accommodate the polymer brush structure would also be a very interesting series of experiments. Similar to the novel anion-exchange membranes developed in chapters 4 and 5, the three-dimensional nature of the binding ligand may result in significantly higher binding capacities in traditional chromatography beads as well. This would overcome a disadvantage of HIC in industry in that binding capacities are typically much lower for HIC than observed in ion

exchangers. And again the environmentally responsive nature of the N-VCL ligands may prove highly beneficial in obtaining higher protein recovery even at high binding capacities.

Finally logical next steps need to follow the identification of these novel heptapeptide Fc-binding ligands. This thesis deals with the identification of and binding tropism of the peptides. The peptides could then be ordered in bulk and attached to either membrane or resin chromatography media to show how these peptides could be applied to industrial antibody separations. The peptides would be much cheaper than the current Protein A ligands currently marketed attached to chromatography media. In addition, because of their small size these peptides may be grafted to a three-dimensional binding matrix instead of the membrane/bead pore surface; thereby increasing ligand density and theoretically increasing binding capacity, which currently is a major economical and logistical bottleneck in the production of antibodies. Further, due to the lack of tertiary/quaternary structure of the peptides they are inherently more stable than the larger Protein A molecule; studies could be performed similar to those described above with the anion-exchange membranes evaluating cleanability/stability in harsh conditions (1N NaOH).

Appendix

A.1 QPCR Assay Parameters

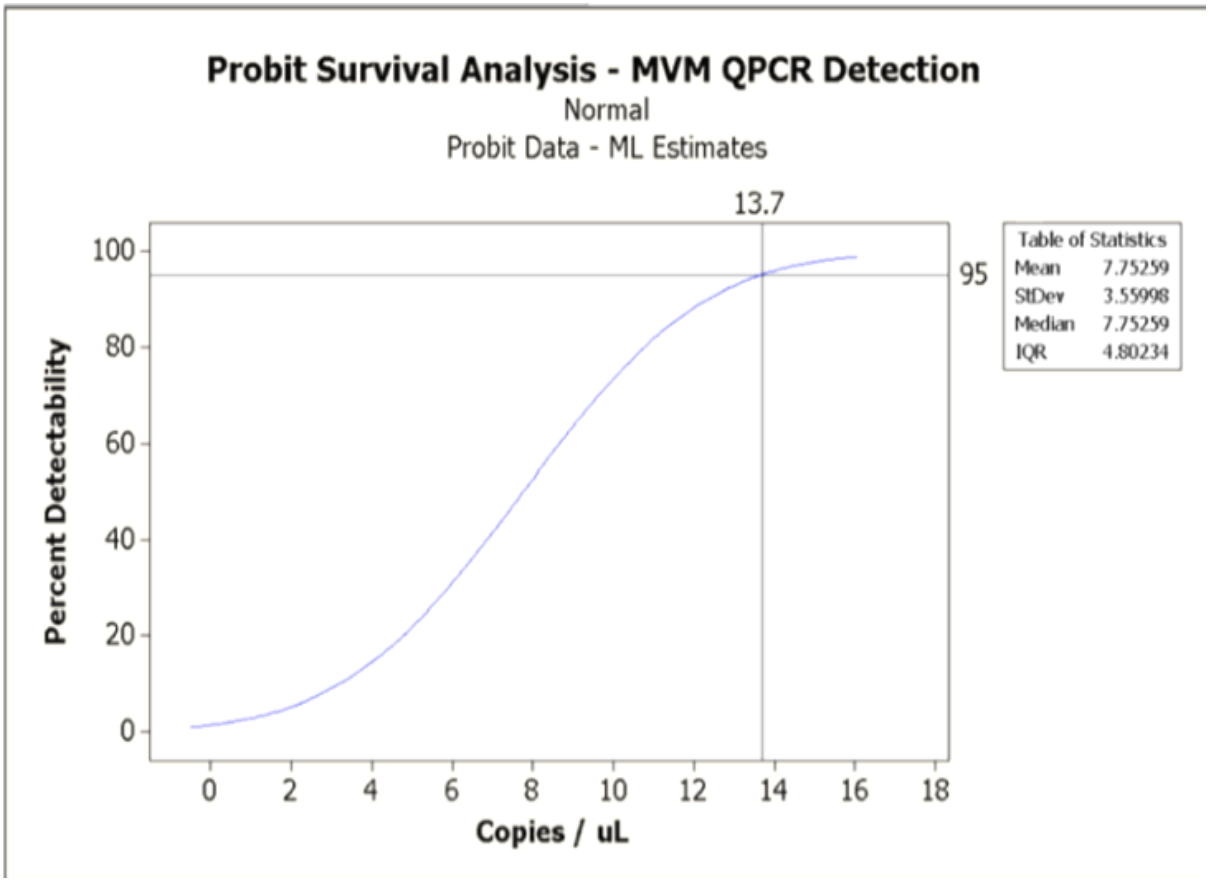

Figure A.1: MVM QPCR limit of detection at 95% confidence. LOD = 14 copies / µL

Table A.1: MVM QPCR assay variability

Copies / µL	Coefficient of Variation (%)
1×10^9	5.59
1×10^8	9.32
1×10^7	17.10
1×10^5	5.51
1×10^4	8.61
1×10^3	19.15
1×10^2	27.43
1.4×10^1	66.43

A.2 Publications, Manuscripts, Presentations, and Posters

The following is a list of the publications, manuscripts, presentations, and posters I generated or contributed significantly to during my graduate work at Colorado State University.

A.2.1 Publications and Manuscripts

Weaver, J., Wickramasinghe, SR. 2014. Identification and Characterization of Novel Fc-binding Heptapeptides via Phage Display and ELISA. (submitted)

Himstedt, HH., Qian, X., Weaver, J., Wickramasinghe, SR. 2013. Responsive membranes for high-performance hydrophobic interaction chromatography. *J Membr Sci.* 447: 335-344.

Weaver, J., Husson, SM., Murphy, L., Wickramasinghe, SR. 2013. Anion Exchange Membrane Adsorbers for Flow-through Polishing Steps: Part II. Virus, Host Cell Protein, DNA Clearance and Antibody Recovery, *Biotechnol Bioeng.* 110(2): 500-510.

Weaver, J., Husson, SM, Murphy, L., Wickramasinghe, SR. 2013. Anion Exchange Membrane Adsorbers for Flow-through Polishing Steps: Part I. Clearance of Minute Virus of Mice, *Biotechnol Bioeng.* 110(2): 491-499.

Ruckh, T., Carroll, D., Weaver, J., Popat, K. 2012. Mineralization content alters osteogenic responses of bone marrow stromal cells on hydroxyapatite/polycaprolactone composite nanofiber scaffolds. *J Funct Biomater.* 3(4): 776-798.

Bhut, BV., Weaver, J., Carter, AR., Wickramasinghe, SR., Husson, SM. 2011. The Role of Polymer Nanolayer Architecture on the Separation Performance of Anion-Exchange Membrane Adsorbers: Part II. DNA and Virus Separations, *Biotechnol Bioeng.* 108(11): 2654 – 2660.

Bhut, BV., Weaver, J., Carter, AR., Wickramasinghe, SR., Husson, SM. 2011. The Role of Polymer Nanolayer Architecture on the Separation Performance of Anion-Exchange Membrane Adsorbers: I. Protein Separations, *Biotechnol Bioeng.* 108(11): 2645 – 2653.

A.2.2 Select Presentations and Posters

Weaver, J., Wickramasinghe, S.R. 2011, Development of a Semi-Synthetic Antibody Binding Protein using Phage Display and Directed Evolution. Poster presentation at PREP 2011, Boston, MA.

Weaver, J., Husson, S.M., Wickramasinghe, S.R. 2011, Examination of Commercial Anion-Exchange Membrane Adsorbers for Use in Biopharmaceutical Drug Purification. Poster presentation at PREP 2011, Boston, MA.

Weaver, J., Murphy, L., Husson, S.M., Wickramasinghe, S.R. 2009, Evaluation of Anion Exchange Membranes for the Removal of Trace Impurities from Mammalian Cell Culture-derived Protein Solutions. Oral presentation at 2009 North American Membrane Society annual meeting, Charleston, SC.

Weaver, J., Husson, S.M., Wickramasinghe, S.R. 2008, Evaluation of Anion Exchange Membranes for the Removal of Trace Impurities from Mammalian Cell Culture Derived Protein Solutions. Oral presentation at 2008 AIChe annual meeting, Philadelphia, PA.